Graduate Theses and Dissertations   Graduate School

January 2014

Forecasting Corrosion of Steel in Concrete Introducing Chloride Threshold Dependence on Steel Potential

Andrea Nathalie Sanchez
University of South Florida, asanchez1@mail.usf.edu

Forecasting Corrosion of Steel in Concrete

Introducing Chloride Threshold Dependence on Steel Potential

by

Andrea Nathalie Sánchez

A dissertation submitted in partial fulfillment
of the requirements for the degree of
Doctor of Philosophy
Department of Civil and Environmental Engineering
College of Engineering
University of South Florida

Major Professor: Alberto Sagüés, Ph.D.
Nathan Crane, Ph.D.
Xiao Li, Ph.D.
Gray Mullins, Ph.D.
Daniel Simkins, Ph.D.

Date of Approval:
July 8, 2014

Keywords: Marine, Forecast, Modeling,
Macrocell, Durability

DEDICATION

This dissertation is dedicated to four exceptional individuals who showed me since little how anything in life can be achieved with God, love, hard work, humbleness and sacrifice. These individuals are: my Father, Miguel Antonio, my Mother, Miriam Iraida, my oldest sister Erika Maria and my middle sister Kiki. Thank you for all your amazing support and prayers during these years. I could have not done it without you. I love you. God bless you always.

ACKNOWLEDGMENTS

TABLE OF CONTENTS

LIST OF TABLES

LIST OF FIGURES

ABSTRACT

Corrosion initiates in reinforced concrete structures exposed to marine environments when the chloride ion concentration at the surface of an embedded steel reinforcing bar exceeds the chloride corrosion threshold (C_T) value. The value of C_T is generally assumed to have a conservative fixed value ranging from 0.2% to - 0.5 % of chloride ions by weight of cement. However, extensive experimental investigations confirmed that C_T is not a fixed value and that the value of C_T depends on many variables. Among those, the potential of passive steel embedded in concrete is a key influential factor on the value of C_T and has received little attention in the literature. The phenomenon of a potential-dependent threshold (PDT) permits accounting for corrosion macrocell coupling between active and passive steel assembly components in corrosion forecast models, avoiding overly conservative long-term damage projections and leading to more efficient design. The objectives of this investigation was to 1) expand by a systematic experimental assessment the knowledge and data base on how dependent the chloride threshold is on the potential of the steel embedded in concrete and 2) introduce the chloride threshold dependence on steel potential as an integral part of corrosion-related service life prediction of reinforced concrete structures. Experimental assessments on PDT were found in the literature but for a limited set of conditions. Therefore, experiments were conducted with mortar and concrete specimens and exposed to conditions more representative of the field than those previously available. The experimental results confirmed the presence of the PDT effect

and provided supporting information to use a value of -550 mV per decade of Cl⁻ for the cathodic prevention slope β_{CT}, a critical quantitative input for implementation in a practical model. A refinement of a previous corrosion initiation-propagation model that incorporated PDT in a partially submerged reinforced concrete column in sea water was developed. Corrosion was assumed to start when the chloride corrosion threshold was reached in an active steel zone of a given size, followed by recalculating the potential distribution and update threshold values over the entire system at each time step. Notably, results of this work indicated that when PDT is ignored, as is the case in present forecasting model practice, the corrosion damage prediction can be overly conservative which could lead to structural overdesign or misguided future damage management planning. Implementation of PDT in next-generation models is therefore highly desirable. However, developing a mathematical model that forecasts the corrosion damage of an entire marine structure with a fully implemented PDT module can result in excessive computational complexity. Hence, a provisional simplified approach for incorporating the effect of PDT was developed. The approach uses a correction function to be applied to projections that have been computed using the traditional procedures.

CHAPTER 1: INTRODUCTION

1.1 Background

Corrosion of steel in concrete is a major limitation to the durability of bridges, especially for those in marine service. The following is a summarized description of the main issues leading to the objective of this dissertation; the reader is referred to Appendix B for a detailed treatment of the fundamentals of corrosion processes in concrete. The corrosion is principally attributable to the chloride ion penetration through the concrete cover. The chloride ions build up at the surface of the embedded steel until reaching a critical chloride threshold level (designated C_T) which causes breakdown of the protective passive film previously present at the steel surface due to the high alkalinity of the concrete. Passivity breakdown results in the onset of rapid steel corrosion with accumulation of expansive corrosion products. The accumulation of corrosion products at the surface of the rebar results in an expansive force on the surrounding concrete causing tensile stresses to form in the concrete. As a result of the concrete's low tensile strength, the concrete subject to the previous conditions often cracks and spalls under those induced tensile stresses. Expensive maintenance repair and subsequent corrosion control is then necessary to extend the design service life.

Corrosion prevention practices include the use of a very low permeability concrete in combination with a thicker concrete cover to retard the chloride ion penetration. Within the United States, the above preventative measures are

1

implemented by private and by public transportation agencies. However, corrosion protection design methods represent an increased initial cost. Thus, an accurate projection of the durability gains that may be obtained for a given initial investment is important to tailor design for the environmental conditions present at the site of a bridge, and to determine the requirements to meet the specified service life for that bridge. It is also often necessary to obtain a quantitative projection of the remaining corrosion-related service life of a structure for decision making on whether to build a new structure or maintain an existing one, or to project future maintenance needs. The projections should be sophisticated enough to estimate not only the structure's age when substantial damage will appear but also the rate at which subsequent corrosion damage would develop.

Durability models available at present (LIFE 365™, DARTS™, and fib (Fédération internationale du béton / International Federation for Structural Concrete) calculate first the time for initiation of corrosion based on how rapidly the transport of chloride ions (measured by the diffusion coefficient D) takes place through the concrete cover, thus establishing the amount of time needed to reach C_T (usually assumed to be time-invariant) at the steel position. A separate estimate is made for the time of propagation involving how long after the corrosion initiation will the expansive product accumulate enough to induce cracking or spalling in the concrete. The sum of both periods (time of initiation and time of propagation) yields the time to appearance of corrosion damage.[1] In a reinforced structure, the concrete cover thickness X_C, diffusion coefficient D, surface chloride content C_S, and even the threshold C_T vary from point to point in a bridge, and therefore damage appears earlier in some locations while

2

in others the damage develops gradually. In a mathematical model, a statistical treatment based on the variability of the data can be used to predict the cumulative progression of that damage, called the "damage function" of the structure.

Although corrosion-related predictive models have significantly advanced in the last three decades, there is still significant room for improvement. Important challenges to wider application remain, stemming primarily from uncertainty or inadequacy in: (i) the values of the input parameters and, equally important their variability and the adequacy of means to measure those parameters (ii) the physical model assumptions and computational methods used, (iii) the degree to which interactions between different parts of the system mutually affect their corrosion progression, (iv) the limited amount of actual field data that may provide model validation, (v) the optimal balance between model complexity and reliability of input data and mechanistic understanding. [2, 3]

One modeling input parameter that has wide scatter of data in the literature is C_T. This is a key parameter for long term prediction of reinforced concrete structures.[4] As mentioned earlier, in predictive models the value of C_T is assumed to be a time-invariant and fixed which selection typically ranges between 0.2-0.5% of chloride ions by weight of cement. The value of C_T depends on many variables such as the condition of the steel surface and concrete properties, as well as the potential of the steel while in the passive state.[5] Examination of the technical literature indicated that a critical feature not available in practical predictive models at the beginning of this investigation, concerns the mutual corrosion aggravation and corrosion protection effects due to existing macrocell coupling between active and passive steel assembly components. Recent work has shown that macrocell effects can greatly affect the projected damage

3

function for a reinforced concrete bridge.[4, 6, 7] However, the issue was until recently largely ignored because a sufficiently simplified approach had yet to be developed, but still accurate enough for use in practical models. Moreover, there has been a shortage of data on the C_T variation with potential. Characterization of the Potential-Dependent Threshold (PDT) is a key item in resolving this missing feature.[8] Consequently, an experimental and modeling thrust in this investigation was directed to provide the necessary data, which was then incorporated into the predictive model prototype produced in the subsequent approach item.

A literature review by Presuel-Moreno et al. on the relationship between C_T and steel potential (E) is shown in Figure 1.[9] Despite the scatter, Presuel-Moreno et al. noted that the general trends from a broad set of data from multiple studies followed an envelope approaching the pattern recognized in the initial investigations by Alonso et al. (blue-dashed line in Figure 1) whereby C_T increases when potentials were more cathodic than the typical open circuit potential of passive steel versus Saturated Calomel Electrode (SCE), and is relatively independent of the potential when it is more anodic than that value.[9, 10] The increase in C_T resulting from cathodic polarization followed an exponential dependence that may be described in general terms by [9,11]

$$log_{10}\left(\frac{C_T}{C_{To}}\right) \sim \frac{E_{To} - E}{|\beta_{C_T}|} \tag{1}$$

where C_T is the threshold expressed as percentage of cement content in the concrete, C_{T0} is the chloride threshold value at a baseline potential E_{T0}, E is the potential of the steel bar (while still in the passive condition), β_{CT} (named here the cathodic prevention

4

slope), is the slope of the straight line corresponding to Equation. (1) when plotted in an E-logC_T representation (negative of the inverse of the slope of the dashed line in Figure 1). The latter has been chosen here to be -100 mV in the SCE scale, which is the one used throughout this investigation. This chloride threshold-changing effect is the basis of the cathodic prevention method, whereby reinforcing steel is cathodically polarized while still in the passive condition to delay or prevent corrosion due to the elevation of the chloride threshold. [12, 13] The redundant 3-parameter line formulation was chosen for convenience to match the form of other ruling equations in electrochemical systems. [14]

At the beginning of this investigation, the work by Alonso et al. was to the author's knowledge the only experimental assessment that focused on determining the chloride corrosion threshold dependence on potential.[10] However, those experiments used small specimens with shallow mortar cover, potentially introducing uncertainties which were subsequently addressed. An experimental work by Li et al. found that the surface area of the steel is an influential parameter on the chloride corrosion threshold, whereby the greater the surface area, the smaller the obtained value of C_T tended to be.[15] Those authors strongly suggested preparing test specimens that have the largest practical steel surface area possible. Moreover, at shallow concrete layers, chloride ion penetration tends to be governed mainly by rapid permeation rather than slower diffusion, which is the usually prevalent transport mechanism of chloride ions ingress in the systems of interest.[16] Corrosion initiation may in that case happen very fast while the chloride content of the cover layer is still evolving, leading to uncertainty in the value of chloride content determined by autopsy tests. Furthermore, leaching of the

5

thin mortar cover into the surrounding medium could introduce significant alterations in the region near the steel, possibly rendering the outcome different from that which would have been obtained with a thicker cover more representatives of field conditions. In view of those possible uncertainties and on the scarcity of data in general, a more systematic and sophisticated experimental assessment was deemed necessary to better quantify the chloride corrosion threshold dependence on steel potential.

In addition to the experimental shortages noted above, implementation of PDT in predictive models had been the subject of preliminary work but some key issues needed further attention. A previous investigation [4] incorporated PDT in a one-dimensional finite difference deterministic model of a partially submerged reinforced concrete column by introducing Equation (1)) with the following parameter values: C_{T0}: 0.2% Cl⁻ by weight of cement, E_{T0}: 100 mV (SCE), and β_{CT}: - 400 mV per decade of Cl⁻ (roughly approaching the dependence given by the dashed line in Figure 1).[4, 6]

In that preliminary model, corrosion was assumed to start when C_T was reached in a steel zone (or node) of a given size. That event resulted in activation of that zone and the creation of a macrocell corrosion pattern where that zone was anodic while the rest of the steel in the column remained passive, namely a cathodic zone. The corrosion macrocell pattern for that configuration was then calculated to obtain the value of the steel potential E at every zone in the system. The steel zones that were still passive, near that first activated site developed a significantly more negative value of E than the potential present before the first activation event. Hence, those zones were assigned per Equation (1)) a correspondingly larger value of C_T than before. Consequently, corrosion initiation in those regions was delayed. As the new C_T value was eventually

6

reached in other zones, the macrocell pattern was affected accordingly and corrosion development was delayed in nearby regions as well. The overall result was a much slower progression of corrosion damage in the system than if the C_T would have been value, potential-independent value (β_{CT} = -∞). The effect, illustrated in Figure 2, was found to be a dramatic decrease in the predicted amount of corrosion damage when β_{CT} was a finite value compared to the case of a potential-independent threshold β_{CT} = -∞.
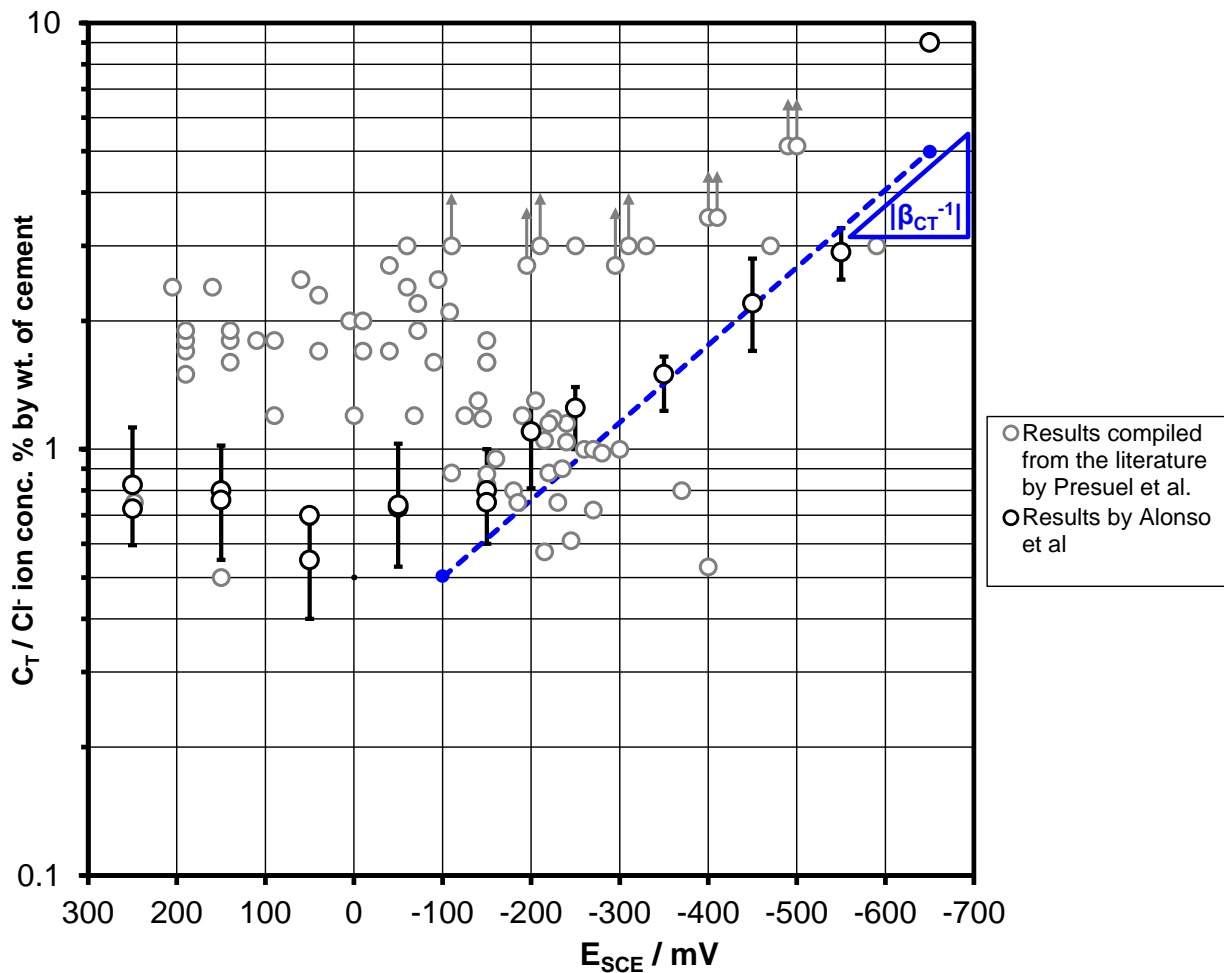
Figure 1 Chloride threshold dependence on steel potential compilation from the literature by Presuel et al. and updated by Sánchez et al.

Moreover, Figure 2 shows that the amount of projected damage can be quite sensitive to the value of β_{CT}, where the corrosion damage was evaluated using values

7

of $|\beta_{CT}| = -100, -200$ and -400 mV/ per decade of Cl$^-$. Thus, for engineering forecasting purposes, more accurate parameter choices (especially for β_{CT}) were desired for a better representation of a marine structure, further justifying the need for the additional experimental work indicated above.
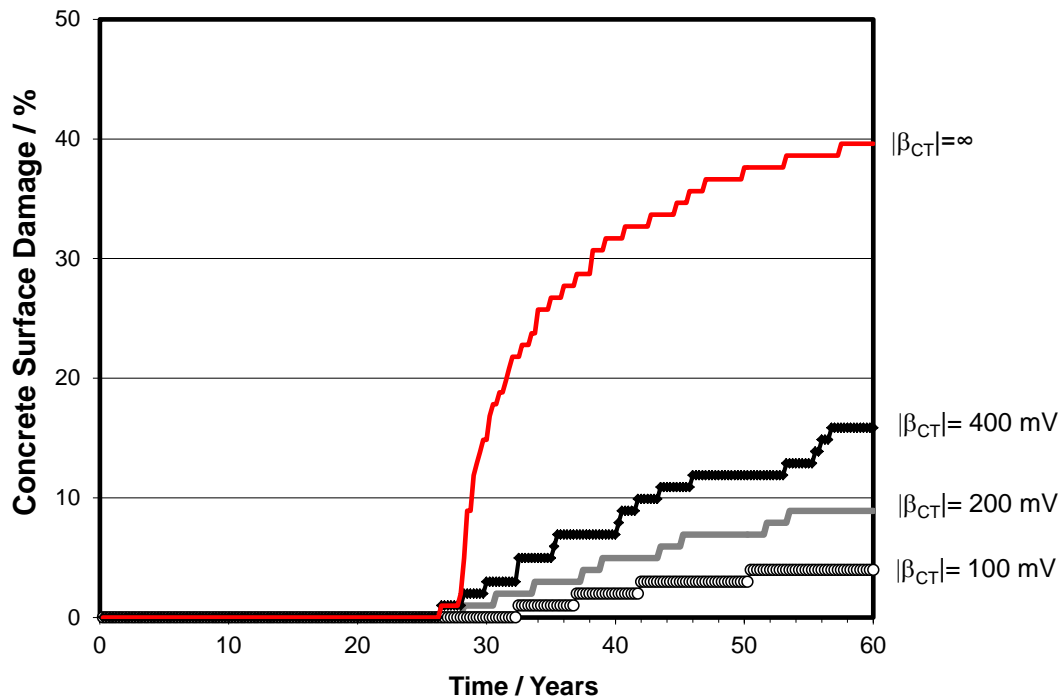
Figure 2 Damage projections in previous model calculations showing strong decrease in projected damage at age=60 years when comparing the case of a potential independent threshold ($\beta_{CT} = -\infty$) and cases where C_T depended on potential of the passive steel

The initial predictive model incorporating PDT served to demonstrate the feasibility of the concept; however, in addition to the dependence on β_{CT} the damage prediction was found to be highly sensitive to the assumed size of the corrosion activation zone (or node). As the size of the activation zones (nodes) was made smaller, the total predicted amount of damage at a given age decreased toward a zero limit value.

8

As explained in Reference [4], that result was not consistent with the trends expected from basic considerations on the behavior of the system, and resolution of the major issue needed to be cleared before further developing the concept. Examination of the model assumptions suggested that the problem stemmed from neglecting the local resistance of the concrete around the steel bars. As a result, the macrocell coupling effect was inappropriately exaggerated as node spacing decreased leading to an erroneous limit condition. A solution the model was formulated by accounting for the local resistance polarization consistent with the size of activation zone and it is addressed in the following section.

1.2 Problem Statement and Research Objectives

Summarizing the issues discussed above, chloride corrosion threshold dependence on potential (PDT) has received little attention in the literature. Available data are scarce and subject to much experimental scatter, and restricted to a limited set of condition involving small steel specimens in thin mortar cover. There is the need for more developed and systematic experimental assessments to address and resolve the uncertainties introduced by other influencing parameters on C_T, especially steel specimen size, thicker cementitious cover, actual concrete embedment, and chloride exposure better resembling actual service regimes, so as to obtain a more solid indication of the value of β_{CT} under experimental assessments, and reduce the extent of uncertainty with regards to incorporating PDT in a corrosion-related predictive model prepared under this investigation.

Current service life predictive models oriented to the practitioner do not account for mutual corrosion aggravation and corrosion protection effects due to macrocell coupling between active and passive steel assembly components. This is a critical modeling feature that may be solved by the incorporation of PDT in corrosion prediction calculations and result in substantially improved damage forecasts, as addressed in this investigation.

Per the discussion above, the objectives of this investigation were the following:

1) Expand by a systematic experimental assessment the knowledge and data base on how dependent the chloride threshold is on the potential of the steel embedded in concrete. Apply the findings toward a more solid indication of the value of β_{CT}.

2) Introduce the chloride threshold dependence on steel potential as an integral part of corrosion-related service life prediction of reinforced concrete structures. By changing model input parameters determine how macrocell coupling between anodic and passive regions in a marine reinforced concrete system affects durability projections in comparison with the traditional potential-independent chloride threshold treatment.

1.3 Research Approach

The following research approach (keyed to Chapters in this dissertation) with related tasks was designed to achieve the objectives.

1.3.1 Addressing Objective 1

1.3.1.2 Chapter 2: Experimental Assessment

- First Stage: conduct an initial set of experiments using specimens with moderate steel surface area embedded in a thick mortar cover and in a continuous immersion regime.

- Second Stage: conduct an advanced set of experiments using concrete specimens with large steel surface area and an alternating wet-dry exposure.

- Evaluate findings of both Stages together with previous literature data to obtain an updated indication of the value of β_{CT}.

1.3.2 Addressing Objective 2

1.3.2.1 Chapter 3: Introducing Potential Dependent Threshold in Corrosion Modeling of Reinforced Concrete

- Develop an advanced potential-dependent threshold model of corrosion damage of a reinforced concrete structure. The model focuses on the case of a partially submerged marine column and incorporates a formulation that accounts for the local resistance polarization consistent with the size of activation zone. The model parameters include the value of β_{CT} determined as part of Objective 1.

- Determine the sensitivity of the model output to the value of β_{CT}, as well as to the size of the steel activation zone and to the fineness of the computational grid, to establish applicability of the model for insight in forecasting and research.

11

- Compare results with those from the traditional potential-independent chloride threshold treatment and establish importance of including potential-dependent threshold in next generation models.

1.3.2.2 Chapter 4: Effect of Variation in System Parameters on Corrosion Damage Forecast with Potential Dependent Threshold

- Simulate the partially submerged reinforced concrete column modeled in Chapter 3 by decreasing the values of the following elevation-invariant input parameters: concrete resistivity, surface concentration, oxygen diffusivity and chloride diffusivity; to establish the sensitivity of the model output under those uniform conditions.

- Establish the relevance of the results on corrosion forecasting of marine substructure.

1.3.2.3 Chapter 5: Probabilistic Corrosion Forecast with Potential Dependent Threshold

- Explore the potential-dependent threshold effect in a reinforced concrete column atmospherically exposed with random variations of the surface chloride concentration and concrete cover profiles; to expand previous systematic modeling approach (Chapter 4)

- Compare with similar random distributed cases with traditional potential-independent chloride threshold treatment. Evaluate the relative degree of conservativeness in each case with a view to establish the advantage of introducing potential-dependent threshold feature in regular modelling practice.

12

1.3.2.4 Chapter 6: Practical Approach to Introduce a Correction for Potential Dependent Threshold in a Practitioner-Oriented Predictive Model

- Develop an approach for incorporating the effect of potential dependent threshold, by the use of a correction function to be applied to projections that have been computed using the traditional procedures.

CHAPTER 2: EXPERIMENTAL ASSESSMENT[1]

Per the Research Approach detailed in Chapter 1, experimental tasks were implemented in two stages. The First Stage consisted of preliminary tests using specimens with moderate steel surface area embedded in mortar and in a continuous immersion regime.[17] The Second Stage involved concrete specimens with large steel surface area and an alternating wet-dry exposure regime more representative of actual service conditions.[18] Both stages, each with its specific methodology, are described in the next sections followed by a discussion leading to the overall findings.

2.1 First Stage – Mortar Test with Moderate Steel Surface Area

2.1.1 Materials and Experimental Setup

Cylindrical mortar specimens with an embedded type #5 rebar were submerged in a saturated NaCl (~5.33 M) solution, as shown in Figure 3.[19] Plain A-615 rebar with high temperature mill scale on the surface was used.[20] The top and bottom of the rebar was coated with an epoxy resin, to prevent corrosion initiation in these areas. Ordinary Portland Cement Type I/II was used with a water-to-cement ratio (w/c) of 0.6 and a cement-sand ratio (c/s) of 1/3. The cement factor (CF) was 488 kg/m^3. The average mortar cover thickness of the rebar was 1.6 cm and it had an exposed area of 32 cm^2. An embedded activated titanium reference electrode (RE), periodically

---

calibrated with respect to SCE, was used for potential control in each specimen.[21] The top and the bottom of the mortar specimens were also covered with a layer of epoxy to avoid chloride ingress in those mortar regions. The specimens were cured for 7 days at high humidity before being placed in the exposure container.
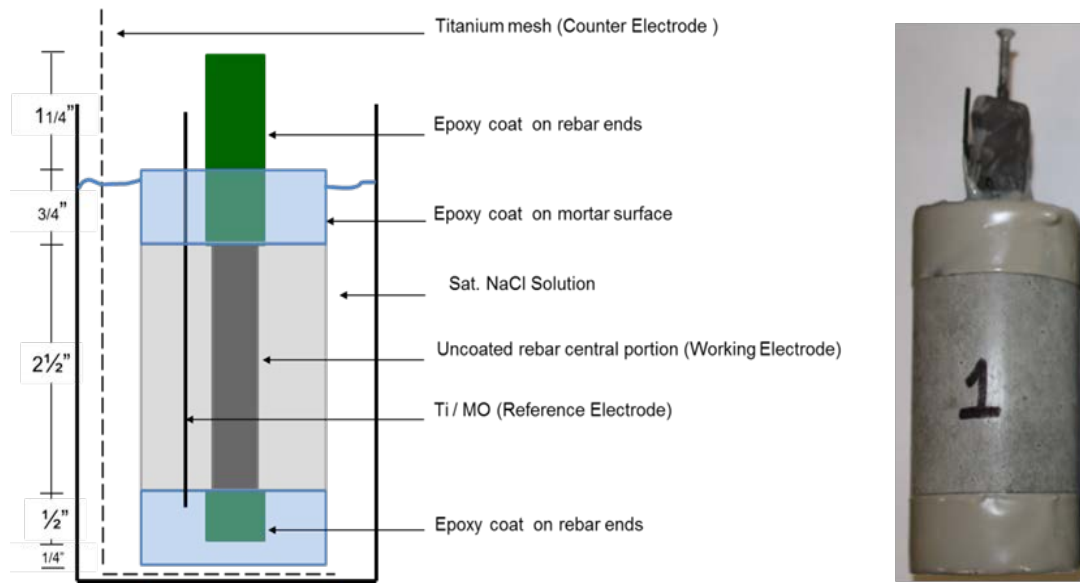
Figure 3 First stage experiment specimen layout

One set of duplicate specimens was exposed at the open circuit potential (OCP) and three other sets were cathodically polarized at -200, -400 and -600 mV (SCE), respectively, representing potentials of passive steel in string macrocell contact with adjacent fully corroding steel. The solution had also addition of $Ca(OH)_2$ in excess of its solubility limit to maintain an average pH of ~>12 and minimize alkaline leaching from the mortar. A counter electrode (CE), mixed metal oxide (MMO) deposited in a titanium mesh, was placed under the submerged specimens. A tight lid minimized access of external air and CO_2 to the solution, but sufficient oxygen existed in the container for the solution to be considered as being naturally aerated. A multiple potentiostat was used to adjust the potential for the polarized specimens and periodically corrected with a SCE

15

as needed to stay within ±10 mV of the target value. The experiment was conducted in a climate controlled laboratory with an average temperature of 21ºC. While developing the First Stage experiment procedure, additional supplemental tests were conducted with a limited number of specimens made with 0.5 w/c mortar and a CF=513 kg/m^3, and exposed to a solution with NaCl content changed stepwise from 0.5 M (day 0) to 1 M (day 36 on). Methodology was otherwise similar to that used for the other specimens. Four of the supplemental specimens experienced activation during the test period and the results are noted together with those of the First Stage experiments.

2.1.2 First Stage Results

2.1.2.1 Open Circuit Specimens

Time of activation t_A or time when corrosion starts was estimated by observation of the potential evolution measurements and through electrochemical impedance spectroscopy (EIS) trends. The Nyquist plots (Figure 4a and Figure 4b) suggest that the interfacial EIS behavior approximated that a simple constant phase element (CPE) – polarization resistance (R_p) parallel combination. At short exposure times, the value of R_p was large but later on there was a sharp transition to smaller values indicative of the onset of active corrosion.

The potential drop progression of the OCP specimens was consistent with that behavior. From observation of Figure 4c, the transitions took place at around the time that the OCP reached -300 mV (SCE), so that exposure duration (13 and 24 days for specimens 7 and 8, respectively) was declared to correspond to the corrosion initiation event for the present purposes.

16

2.1.2.2 Cathodically Polarized Specimens

The polarized specimens initially demanded cathodic currents commensurate with the extent of cathodic polarization imposed as shown in Figure 5. As time progressed, the absolute value of the cathodic current in the -200 and -400 mV (SCE) specimens decreased appreciably, indicative of the onset of diffusion-polarized regimes for those cases.
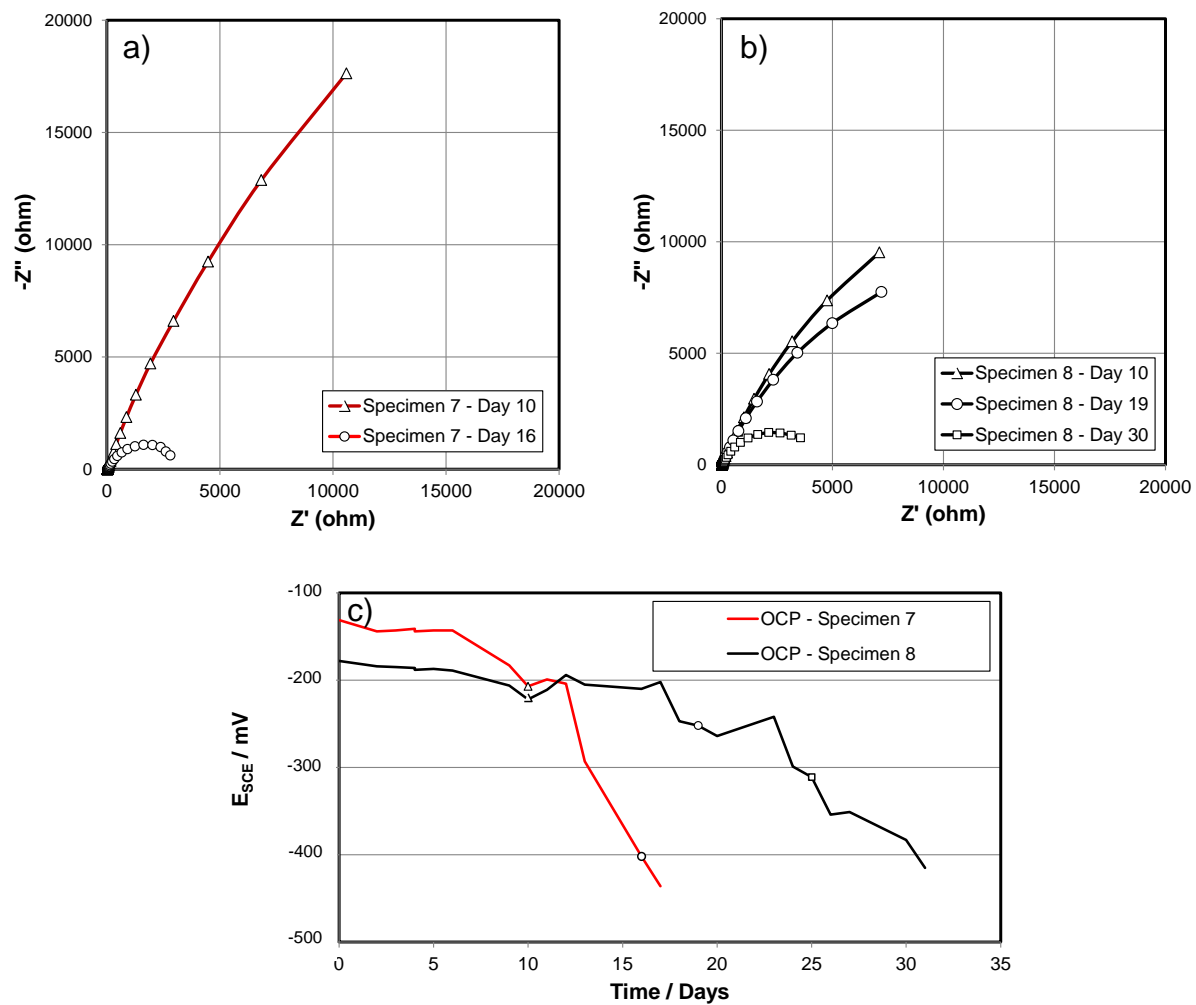
Figure 4 Time trends for OCP specimens. a),b): Nyquist diagrams (lowest frequency shown 1 mHz; 5 data points per frequency decade) keyed to symbols in OCP graphs. c): Potential evolution.

17

Current demand was very small for the specimens polarized to -200 mV (SCE), which are likely to have remained near activation-polarized conditions for the cathodic reaction. Activation was manifested for the polarized specimens by a shift in the polarizing current from a cathodic to an anodic regime. Reaching an anodic current greater than 0.2 µA/cm^2 was chosen as the criterion for the onset of the active regime, following the criterion used by Alonso et al.[10] The transitions for the polarized specimens that experienced activation during the exposure period are shown in Figure 5.
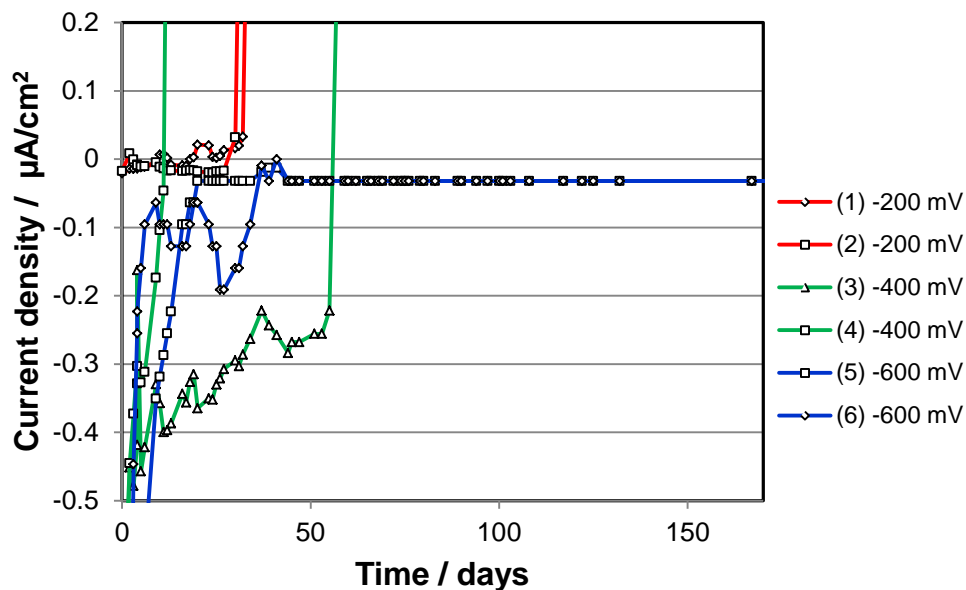
Figure 5 Applied current density (anodic is >0) vs time for each polarized specimen at the indicated potential

2.1.2.3 Estimation of Chloride Content at the Rebar at the Time of Corrosion Initiation

After demolition, a 1 cm masonry drill was used to obtain mortar samples with no corrosion products at the rebar trace for chloride analysis Acid-soluble chloride concentration of 1-gram mortar powder samples duplicates for each specimen was

18

determined following the "Florida Method of Test for Determining Low-Levels of Chloride in Concrete and Raw Materials".[22] The chloride concentration values were expressed in the form of total chloride content by weight of cement. Because of the confirmatory time lag between the time of specimen activation and that of extraction, the chloride content at the time of sampling of the rebar trace was usually greater than that upon activation. A correction procedure was developed by assuming on first approximation simple cylindrical diffusion governed by Equation (2), an expression of simple Fickian one-dimensional diffusion in cylindrical coordinates[23]:

$$\frac{\partial C}{\partial t} = \frac{1}{r}\frac{\partial}{\partial r}\left(rD\frac{\partial C}{\partial r}\right) \qquad (2)$$

where D is the apparent chloride diffusion coefficient, which is time and space invariant, r is the radial dimension, and t is time. The boundary conditions assumed a constant surface chloride concentration (C_S) at the outer cylinder wall and a zero-flux condition at the rebar surface, thus accounting for the rebar obstruction effect for chloride accumulation at the rebar trace.[24] The solution of Equation (2) was solved by the Finite Difference Method (FDM). The equation was formulated in terms of dimensionless expressions: $P = Dt/\alpha^2$, C_{TR}/C_S and r/α; where C_{TR} and α are chloride concentration at the rebar trace at a specific time and radius of the specimen, respectively. The output to the problem was the numerical functional relationship between C_{TR}/C_S and P. A representative value of C_S was obtained following a similar procedure as for the rebar trace, but instead sampling the outer cylinder surface. The chloride content measured by chemical analysis at the rebar trace (C_{TR}) at the time of removal (t_R) was then divided by C_S to obtain C_{TR}/C_S, which in turn yielded $P(t_R)$ (P at

19

the t_R) per the functional relationship determined above. With the values of t_R, $P(t_R)$, and a, an estimate of D was obtained, which was then used to obtain $P(t_A)$ and from similarly obtain an estimate of C_T, the concentration at time of activation, which is the reported threshold value. Samples of the outer surface of specimens 5 and 6 (see Table 1 for specimen condition) that were analyzed to determine C_S yielding values respectively of 41 kg/m^3 and 40 kg/m^3, respectively, with an average of 40.5 kg/m^3. This value is generally consistent with the expected high porosity of the mortar, given its high w/c ratio and an assumption of pores near the surface filled with the saturated NaCl solution plus some extent of chloride binding by the surrounding matrix.[25, 26] For specimens 5 and 6, as of day >170 no activation events were observed. A lower bound for rebar trace chloride concentration was estimated by assuming that the value of D was the same as the average D_{AVG1}, 2.43 ×10^{-7} cm^2/s, of the rest of the specimens and using the C_{TR}/C_S – P relationship to estimate C_T at the latest exposure time. For that long exposure, the resulting C_T value was nearly equal to the C_S value.

For the specimens from the supplemental tests (S2, S4, S7, S8), only activation time data were available. A rough estimate of C_T was made nevertheless in those cases by a similar procedure as used for specimens 5 and 6. Nominal values of C_S and D were assigned as follows. The surface concentration was assumed for simplicity (neglecting adjustments for porosity and chloride binding differences) as being directly proportional to the solution chloride content, prorating directly from the C_S value used for the First Stage tests, and further using a constant nominal weighted value based on the fraction of t_A spent in the 0.5 M and 1 M regimes. Since in the supplemental tests a 0.5 w/c mixture had been used, the corresponding value of D was estimated from the

average value from the main test sequence, and multiplying it by the average ratio of D (0.5 w/c) to D (0.6 w/c) obtained from work by previous authors resulting in D_{AVGS1}.[27-29]

2.1.2.4 First Stage Potential-Dependent Threshold Findings

Table 1 summarizes the results and calculations of each test condition. The values for D estimated from the First Stage test sequence were generally high, consistent with those expected for high w/c mortar in a wet environment. [27-29] It is noted that the estimated value of D for specimen 4 was significantly higher than for the others, reflecting the high chloride content measured at the rebar trace of that specimen after a relatively short exposure period and the consequent early activation as well. It is speculated that mortar consolidation may have been poorer in that sample, although there was no readily visible sign of deficiency. Regardless of the early chloride buildup, the results for this specimen nevertheless followed the same overall trends discussed next. It is recognized that the results from the supplemental tests represent only rough estimates, provided here primarily for completeness.

Table 1 Calculations and results for each first stage test condition.

Specimen	Potential (mV)	t_A (day)	t_R (day)	C_{TR} (kg m^{-3})	D (cm^2 s^{-1})	C_T (kg m^{-3})	C_T (% by wt. of cement)
1	-200	34	45	9.47	1.37×10^{-7}	5.4*	1.10*
2	-200	31	31	4.00	1.35×10^{-7}	4.0*	0.83*
3	-400	59	60	15.31	1.40×10^{-7}	15*	3.06*
4	-400	12	13	14.03	6.09×10^{-7}	13*	2.62*
5	-600	>170	>170	-	D_{AVG1}	>40**	>8.1**
6	-600	>170	>170	-	D_{AVG1}	>40**	>8.1**

21

Table 1 (Continued)

7	-150	13	17	5.34	2.75×10^{-7}	2.5*	0.52*
8	-190	24	31	6.68	1.66×10^{-7}	3.4*	0.69*
S2	-200	117	-	-	D_{AVGS1}	5**	1**
S4	-400	152	-	-	D_{AVGS1}	6**	1.1**
S7	-120	51	-	-	D_{AVGS1}	1.7**	0.3**
S8	-90	63	-	-	D_{AVGS1}	2.5**	0.5**

Notes:

D_{AVG1}: Estimated diffusion coefficient 2.43×10^{-7} cm^2/s = average of values from specimens 1-3 and 7-8.

D_{AVGS1}: Estimated diffusion coefficient 1.56×10^{-7} cm^2/s = value obtained from the conversion of D at w/c 0.6 to D w/c 0.5, as described in text.

* Corrected from direct measurement to account for time lag between activation and extraction.

** Lower bound values of C_T estimated for non-activated specimens

Roundoff applied to finished values; internal table computations conducted with additional digits.

2.2 Second Stage - Concrete Tests with Large Steel Surface Area

2.2.1 Materials and Experimental Setup

A modified version of the ASTM G109 "Standard Test Method for Determining Effects of Chemical Admixtures on Corrosion of Embedded Steel Reinforcement in Concrete Exposed to Chloride Environments"[30] was used as a basis to prepare a set of twelve reinforced concrete slabs 66 cm long, 10.16 cm wide and 6.35 cm high, exposed to a ponding regime while under potentiostatic control. Layout of the side and top view of the modified standard version is shown in Figure 6

The concrete cover thickness X_C of the embedded steel rebar was 2 cm. A single rebar was used, size #5 plain steel ASTM A-615-09B Grade 60 with an undisturbed gray mill scale. A stainless steel bolt screw, with two washers and a nut were tapped to one end of the steel bars to later connect the steel to the potentiostat after casting and curing. Next, the steel bar ends (5 cm) were also coated with epoxy, similar to the First

22

Stage tests, to prevent corrosion in these regions. The uncoated steel area was ~300 cm^2, approximately an order of magnitude greater than in the First Stage.
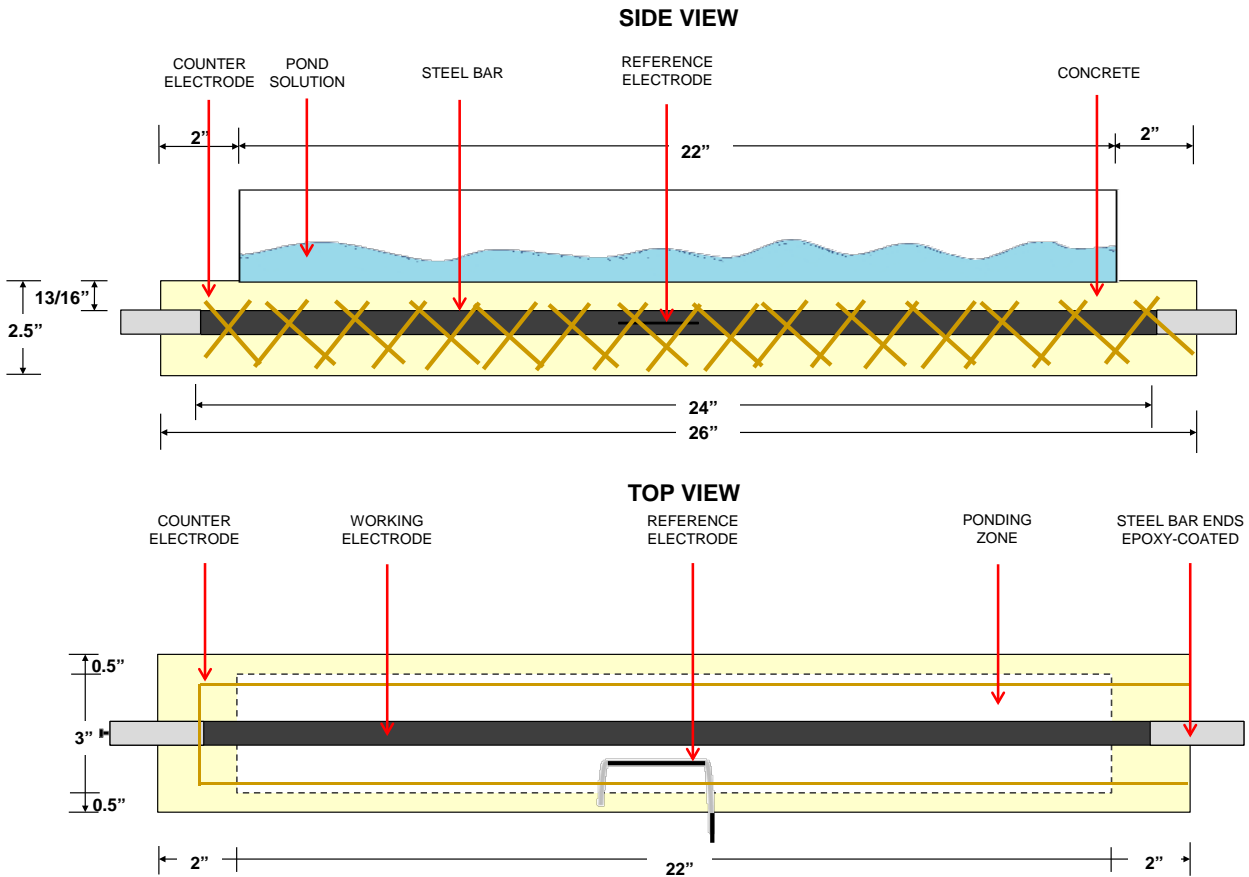
Figure 6 Side and top view of the reinforced concrete specimens

Unlike the specimen configuration in ASTM G-109, the steel bar embedded in each specimen was intended to be cathodically polarized (except those at the OCP condition) with a potentiostat, as mentioned above. For that reason, a 5 cm embedded activated titanium RE, frequently calibrated with respect to an external SCE, was placed parallel to the steel bar. The CE, same material used as in the First Stage as well, was placed on either side parallel to the length of the steel bar. The CE was held to Plexiglass rods to prevent any contact with the working electrode.

23

A 2D model was developed using Comsol Multiphysics® to find optimal position for the CE placement by minimizing the variability of the potential at the steel surface between the upper and lower arrowed points as illustrated in Figure 7. The modeling results showed that the configuration on the left-hand side of the figure, CE placed under the steel bar, resulted in a larger electric potential (red font numbers) difference between the arrowed points, compared to the CE configuration on the right hand side. In the latter, the CE placed in a position parallel to the embedded steel bar yielded an electric potential difference as little as ~0.003 V, indicating a uniform current flow along the steel bar. Hence, the right hand side configuration in Figure 7 was used to build the specimens.
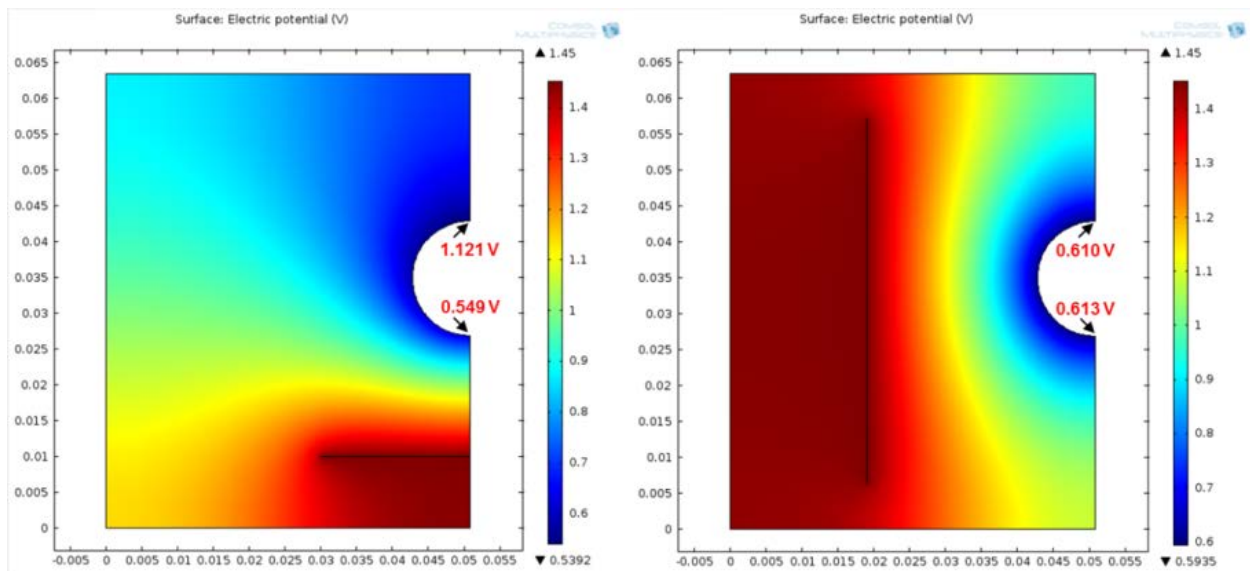
Figure 7 Modeling results to find optimal position for counter electrode placement

Casting molds were built out of wood as shown in Figure 8. Prior to casting, the electrodes were placed in the molds and the interior wood was covered with mineral oil, assuring no contact with the soon-to-be embedded electrodes. Ordinary Portland Cement Type I/II was used with a water-to-cement ratio (w/c) of 0.6 and a cement-to-

24

sand ratio (c/s) of 2.2. The coarse aggregate used was #89 limestone. The cement factor (CF) was 455 kg/m³.

The reinforced concrete specimens were cured for 32 days at high humidity. After curing, a pond built with Plexiglass and sealed with marine adhesive was placed on top of each slab (similarly as in Ref.[17]) to recreate wet and dry regimes. Fresh water was ponded continuously during the first 17 days for leak proofing and stabilization. During this period, the exterior faces of the specimens were coated with epoxy as shown in Figure 9, leaving the bottom region uncovered. Stainless steel bolt screws were attached to the two outer ends of the CE to subsequently connect the two embedded meshes with a wire. Afterwards, regular wet-dry ponding took place; during the wet cycle (3.5-day period) a solution of 4 M NaCl was placed in the pond, a lid was placed on top of the pond to prevent evaporation. The solution was removed for the dry cycle (3.5-days too).
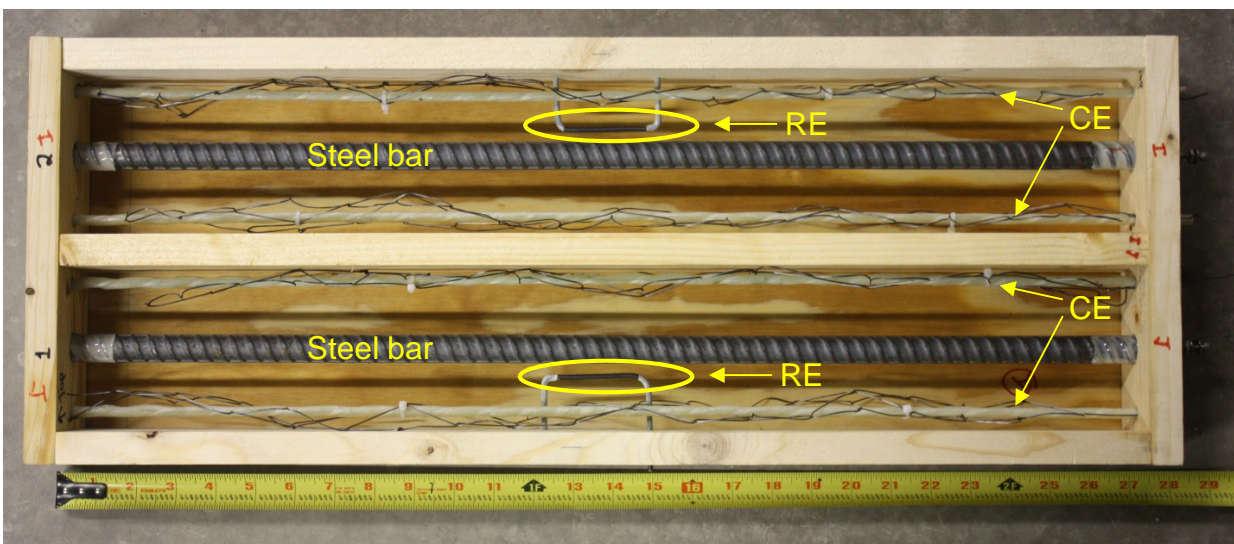
Figure 8 Second stage specimens prior to concrete casting. RE: reference electrode. CE: counter electrode
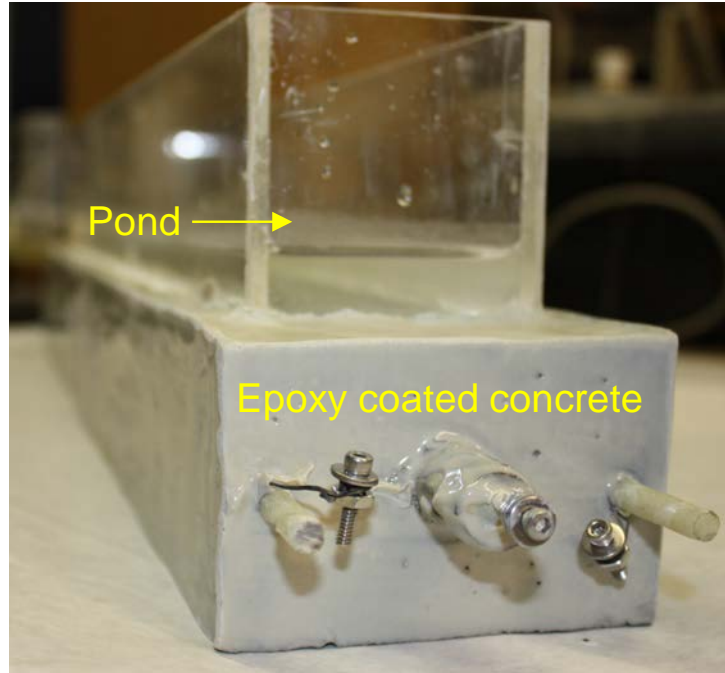
Figure 9 Specimen after applying a layer of epoxy and placing the pond

A set of triplicate specimens were tested at the open circuit potential (OCP) and three additional triplicate sets were cathodically polarized at -200, -400 and -600 mV (SCE), respectively, as shown in Figure 10.

The evolution of the steel potential was measured periodically for all the specimens using the embedded RE and a SCE. EIS tests were performed periodically as well, for the OCP specimens only. A frequency range of 1 mHz to 1 MHz with an amplitude of 0.010 V rms was used. The Echem Analyst software by Gamry Instruments was used to model and estimate the Polarization Resistance (R_p) value of the embedded steel bar. The R_p value was calculated assuming a circuit that has a solution resistance, a non-ideal interfacial capacitance and polarization resistance parallel combination.
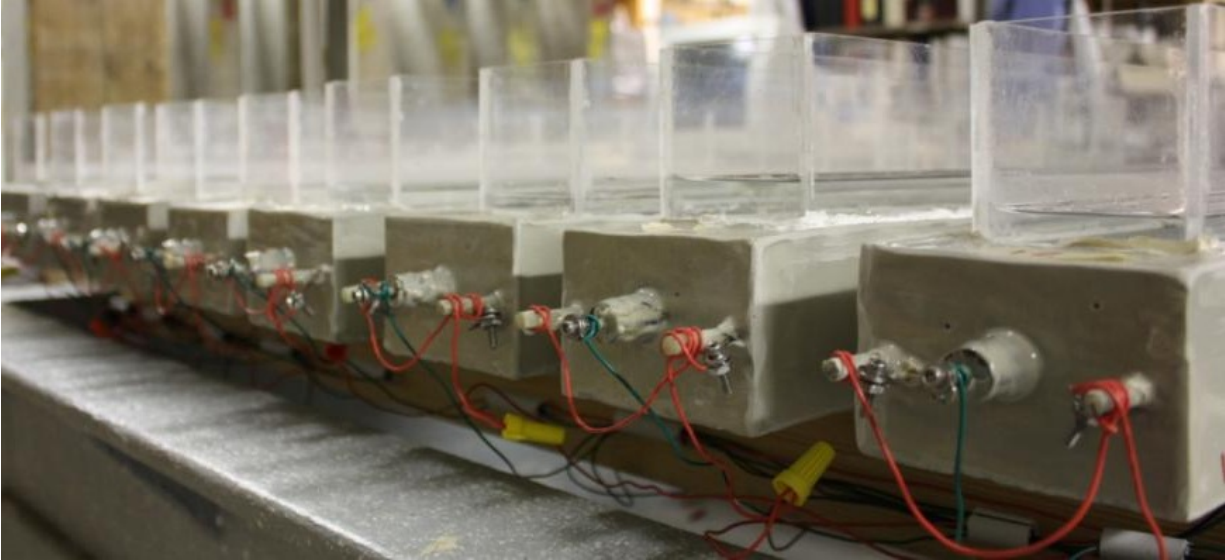
Figure 10 Cathodically polarized specimens

2.2.2 Second Stage Results

2.2.2.1 Open Circuit Specimens

When the salt water ponding regime exposure was initiated (day zero) the steel potential readings were around -80 mV (SCE) and remained so for about 150 days as it is shown in Figure 11. Approximating the usage for the First Stage experiments, the time of corrosion initiation (or activation) t_A for the Second Stage experiments was deemed to be confirmed when a steel potential < -200 mV (SCE) was reached. As a secondary confirmation of steel activation, the value of R_p was observed to have exhibited about one order of magnitude decrease compared to the value when the embedded steel was in the passive condition.

The activation events for the OCP specimens are indicated by the arrows in Figure 11. The average activation time for the triplicate set was 235 days. The specimens were retained sometime after the activation events occurred to validate

27

corrosion initiation through EIS tests. An example of Nyquist plot results is shown for specimen 1 in Figure 12. During the first 150 days the embedded steel bar maintained an R_p value of ~20,000 ohms. Twenty days later, a potential drop to -170 mV vs SCE was measured and a pronounced reduction of the semi-circle diameter on the Nyquist plot was observed with an R_p value of ~4,000 ohms. The activation time was declared on day 161, when the steel potential passed the -200 mV mark with a reading of -220 mV (SCE). EIS test resulted in an R_p of ~2,000 ohms, validating the time of activation estimated from OCP measurements. After confirmation of the time of initiation, the specimen was removed from the experimental set up and the methodology described in section 2.2.2.3 was followed.
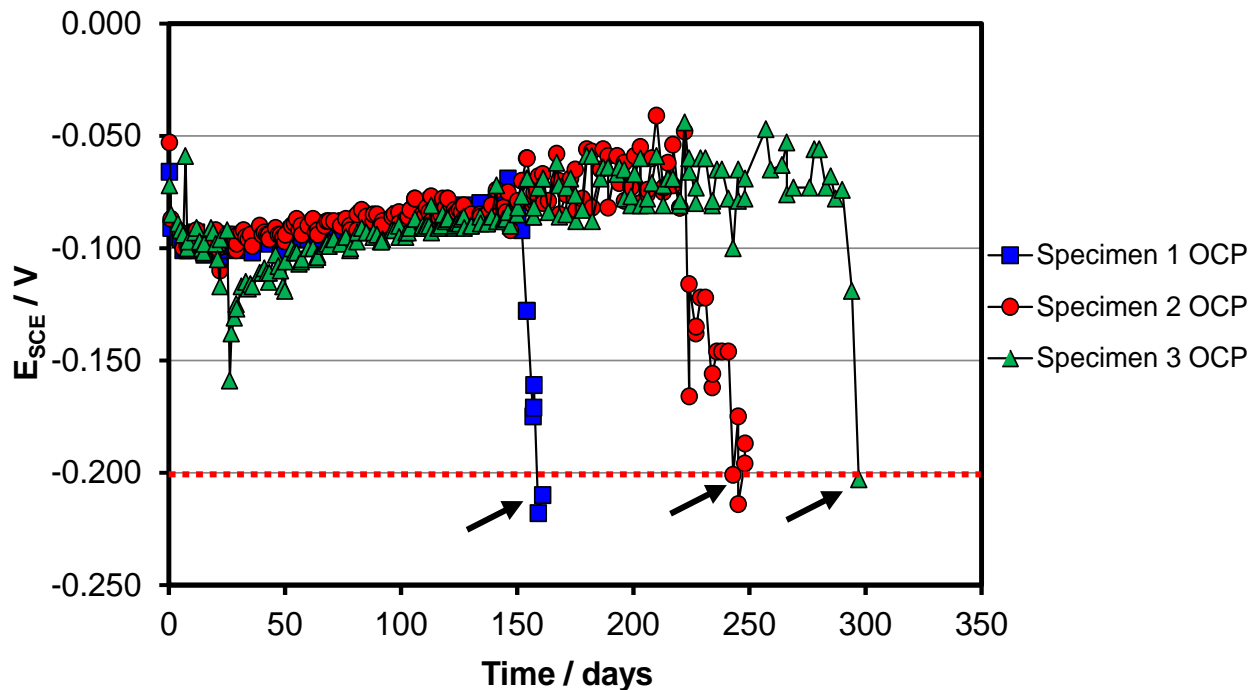
Figure 11 Evolution of the steel potential for the second stage OCP specimens. Arrows indicate activation event declaration.
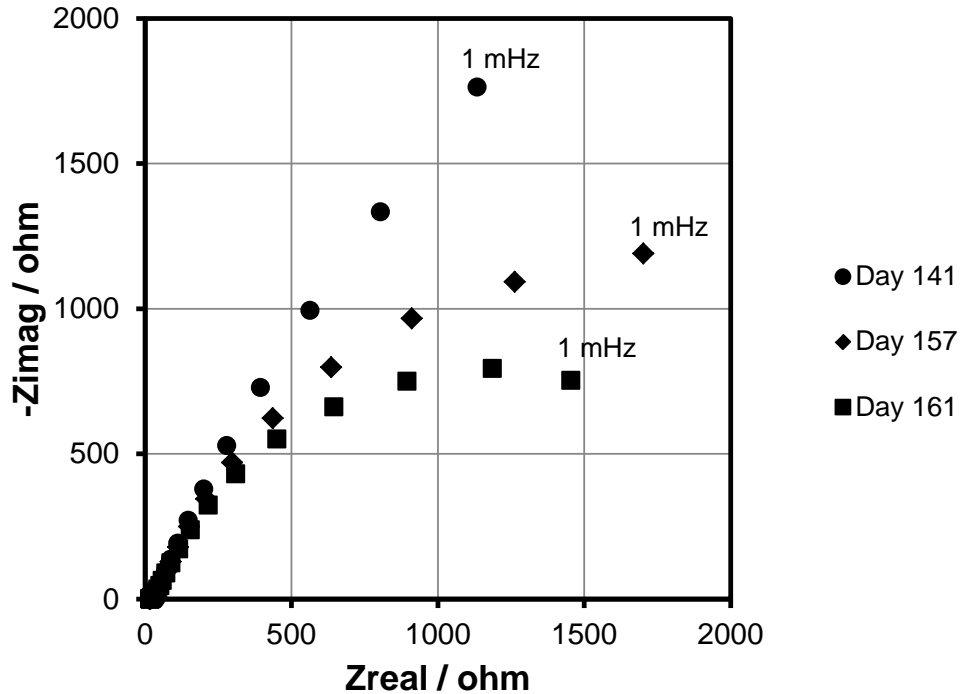
Figure 12 Time progression of EIS for specimen 1 at OCP condition, indicating marked reduction in R_P on activation at day 161. Nyquist representation; 5 data points per frequency decade.

2.2.2.2 Cathodically Polarized Specimens

The current demanded by the polarized specimens was initially negative (cathodic) when the embedded steel bar potential was set towards negative values (-200, -.400 and -600 mV (SCE)). Following the methodology of the First Stage, the moment of activation was declared when the demanding current density reached a value greater than +0.2 $\mu A/cm^2$. An example of this procedure for specimen 6, polarized at -200 mV (SCE) is shown in Figure 13. The red dashed line and the black arrow corresponds to the activation criterion and event, respectively. Fluctuations were observed during the cathodic-anodic current transition as shown in Figure 13, thus specimens were kept polarized for a period afterwards to confirm activation.

29
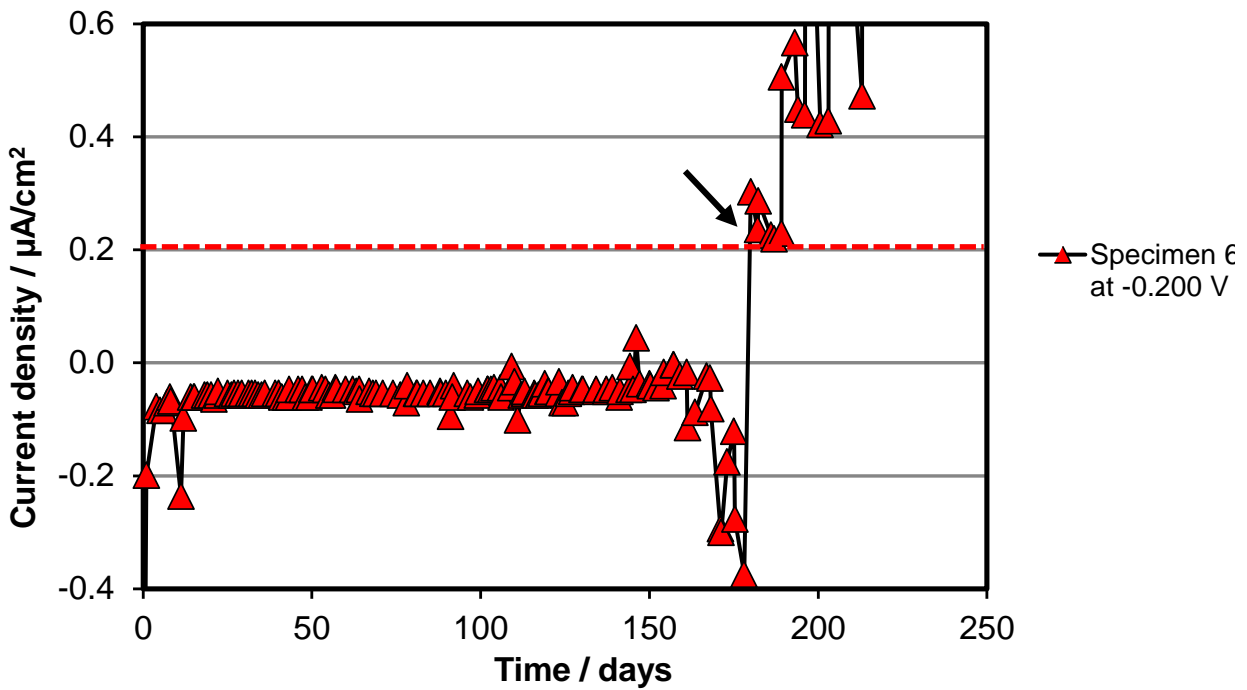
Figure 13 Current density with respect to time for a specimen cathodically polarized at -200 mV

2.2.2.3 Estimation of Chloride Content at the Rebar at the Time of Corrosion

Once activation was confirmed, the specimen was removed from the experimental setup and sliced with a masonry saw on the sides until reaching approximately ~3 mm away from the rebar. A chisel and hammer were then used to break the specimen into two halves. The top part of the specimen was then wedged away from the rebar exposing the rebar trace for the concrete-rebar interface closest to the pond (see Figure 14). The rebar trace was milled using a masonry drill 1 cm diameter similar to the procedure described in the First Stage specimens. The milling depth was ≤ 2 mm, and normally 9 grams of concrete powder were collected avoiding regions where corrosion products were observed. Triplicates of 3-gram concrete powder sample were analyzed for chloride ion concentration following the same procedure as

30

mentioned in the First Stage methodology, the results averaged for a reported result (Table 2).[22]

When specimen 7 was processed, large amounts of corrosion products were observed along the concrete rebar trace; and as a result, an insufficient amount of concrete powder (only about 1/3) was collected to meet the recommendation given in the FDOT FM5-516.[22] Consequently, the reported result for that specimen was for a single (not average of triplicate tests) value and subject to corresponding uncertainty. That value was unusually large and suggestive of an artifact. The chloride content at the concrete ponding surface C_S was determined for selected specimens following a similar procedure as that indicated above for the trace. The results were 20.2 kg/m^3 and 22.4 kg/m^3 for specimens 2 and 3, respectively. The average value, 20.2 kg/m^3, was used as the fixed C_S value for all specimens in the calculations explained in the next section.
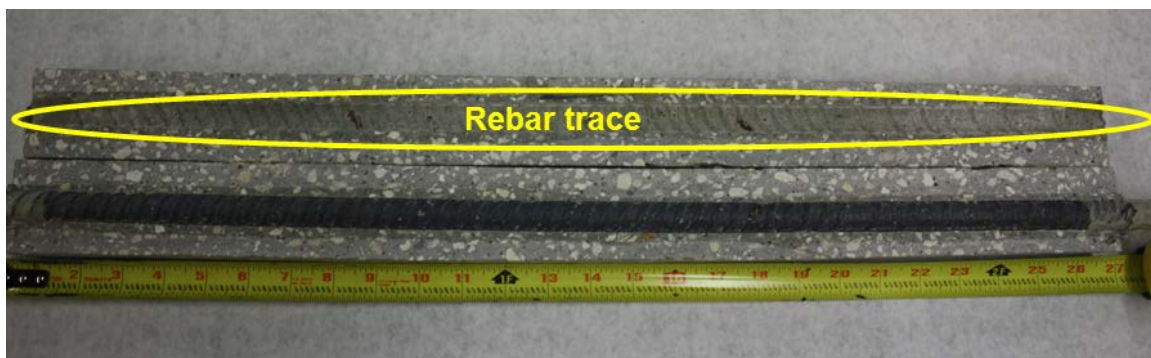
Figure 14 Reinforced concrete specimen after autopsy.

The procedure yielded the chloride ion concentration C_{TR} at the time of specimen removal t_R. An adjustment for time delay was conducted to estimate the concentration C_T at the declared time of activation (t_A). The adjustment was calculated assuming simple diffusion in a semi-infinite plane sheet with invariant C_S, C_0 and D (Equation (3)),

but correcting for the presence of the steel bar (diameter Φ_r) with clear cover X_C as described in a computational investigation by Kranc et al.[24] The domain is actually of finite thickness, but since it is about 3 times greater than X_C, the behavior at the relatively early stages considered here approximates conditions in a semi-infinite domain. Work by Kranc et al.[24] shows that for the above conditions the concentration C after a time of exposure t at the point of the rebar surface, closest to the external surface is given by

$$C = C_S \left(1 - erf \frac{X_C}{2\sqrt{Dt/Tf}} \right) \tag{3}$$

where Tf is a derating factor that is a function of the ratios Φ_r / X_C and C/C_S (note the formulation as expressed in Equation (3) is implicit on C). For the present case Φ_r/ X_C = 0.77, a fixed value. Processing accordingly the graphic solutions to Equation (4) given by Kranc for that ratio value shows that Tf can be approximated by: [24]

$$Tf = -0.65 \frac{C}{C_S} + 0.792 \tag{4}$$

Using the global values of C_S and X_C and taking for each specimen C=C_{TR} and t=t$_R$, the corresponding value of D was calculated by clearing it from Equation (4), with results shown in Table 2.

2.2.2.4 Second Stage Potential-Dependent Threshold Findings

Table 2 shows the results of the Second Stage experiments. Results for specimens 1-6 were quite consistent with each other (average 5.14×10^{-8} cm^2/s,

32

standard deviation 1×10^{-8} cm^2/s) and in the expected range for a highly permeable concrete as used here. Due to the uncertainty associated with the chloride content of specimen 7 as mentioned earlier, two alternative values of C_T were presented as a range in Table 2. The first value was calculated using and average value of D (D_{AVG2}) obtained for specimens 1-6 together with Equation (3) and Equation (4) to obtain a numerical estimate of C_T. The second value involves no adjustment procedure, so C_T was taken to be nominally equal to C_{TR}. Five of the cathodically polarized specimens did not experience corrosion activation up to day 600, as mentioned earlier. Exposure continues, but a nominal bounding lower value of C_T was obtained following the same method as that used to obtain the second alternative for specimen 7.

Table 2 Calculations and results for each second stage test condition.

Specimen	Potential (mV)	t_A (day)	t_R (day)	C_{TR} (kg m^{-3})	D (cm^2 s^{-1})	C_T (kg m^{-3})	C_T (% by wt. of cement)
1	-100	161	180	4.10	5.38×10^{-8}	3.45	0.76
2	-100	243	250	6.20	5.34×10^{-8}	6.01	1.32
3	-100	297	327	6.02	3.98×10^{-8}	5.37	1.18
4	-200	335	347	6.06	3.77×10^{-8}	5.82	1.28
5	-200	213	222	6.64	6.40×10^{-8}	6.35	1.39
6	-200	189	222	6.18	5.99×10^{-8}	5.09	1.12
7	-400	320	347	20.6	-	7.7*-20.6	1.7*-4.5
8	-400	900	-	-	D_{AVG2}	14.1**	3.09**
9	-400	900	-	-	D_{AVG2}	14.1**	3.09**
10	-600	900	-	-	D_{AVG2}	14.1**	3.09**
11	-600	900	-	-	D_{AVG2}	14.1**	3.09**
12	-600	900	-	-	D_{AVG2}	14.1**	3.09**

Notes:
D_{AVG2}: estimated average chloride diffusion coefficient obtained from specimens 1-6
*Value of C_T estimated using average value of D from specimens 1 to 6 (D_{AVG2}=5.14 $\times 10^{-8}$ cm^2/s)
**Lower bound values of C_T estimated with D_{AVG} for specimens non-activated specimens
Roundoff applied to finished values; internal table computations conducted with additional digits.

2.3 Discussion of First and Second Stage Experimental Findings

The experimental results from the First and Second Stage are represented by the red symbols in Figure 15. The C_T values are expressed in total chloride content by weight of cement in the y-axis, and the potential E of the steel is expressed in mV in the x-axis.

Data previously presented in Figure 1 from other sources are reproduced here as well and represented by the open gray circle symbols. The open and red circles symbols correspond to the First Stage and Second Stage C_T results, respectively, for those specimens that reached a confirmed corrosion activation condition during the duration of the tests.

The results of the First Stage and Second Stage specimens that did not reach activation during the tests are indicated by the open and solid red diamonds symbols with an upward pointing arrow. The results for specimen 7 (Second Stage) are shown as a range, which were affected by added uncertainty as noted earlier.

The present findings of both experimental stages are generally consistent with the overall body of evidence, and support the expectation of a substantial increase in threshold as the impressed potential becomes more negative.

The obtained results, considered together with those from earlier sources still support a lower bound of the beneficial effect of cathodic polarization consistent with that identified in previous work, and summarized by the dashed blue line starting at E=-100 mV for C_T=0.5% and β_{CT} of ~ -550 mV/decade of Cl$^-$.[1, 11] Those parameter values will consequently be used as the main base for the PDT model calculations

34

presented later in this investigation. However, it is noted that several values from the present experiments and other sources are present as a lower chloride concentration bound (especially at the more negative potentials around -400 mV to -600 mV SCE). Hence, it is possible that future experiments may provide the foundation for justifying a somewhat more optimistic β_{CT} slope (e.g, in the order of ~400 mV/decade of Cl$^-$), which may serve as a basis for more refined calculations in follow-up work.

It is also noted that the potential effect on C_T implied by Figure 15 has been figured generally on the actual concentration of chloride ions at the steel-concrete interface at the time of activation. Additional benefit could be derived from any migration effect that the electric field used to apply cathodic polarization through the concrete may have in slowing down chloride ion buildup at the steel surface.[30]

For a given steel polarization level that extrinsic effect would vary depending on factors such as the electric conductivity of the concrete, and should be evaluated separately. Similarly, the cathodic reaction increases local alkalinity at the steel surface, which is expected to be a factor in elevating the effective value of the threshold.[31]

The extent to which these factors may be responsible for the overall increase in threshold is likely to depend on cement composition and electrokinetic effects, and is currently being investigated in Florida Department of Transportation (FDOT) project BDV25 977-10 also for possible future refinement of model projections.

It is noted in closing that the procedures used here to correct for the time lag between activation and rebar trace chloride analysis in the specimens tested ignored, for simplicity, any electrokinetic effects during the time lag. While the resulting

35

inaccuracy in the C_T estimate is expected to be of secondary importance given the relatively short period involved, future analyses of the data may benefit from a refined treatment that would include that feature.
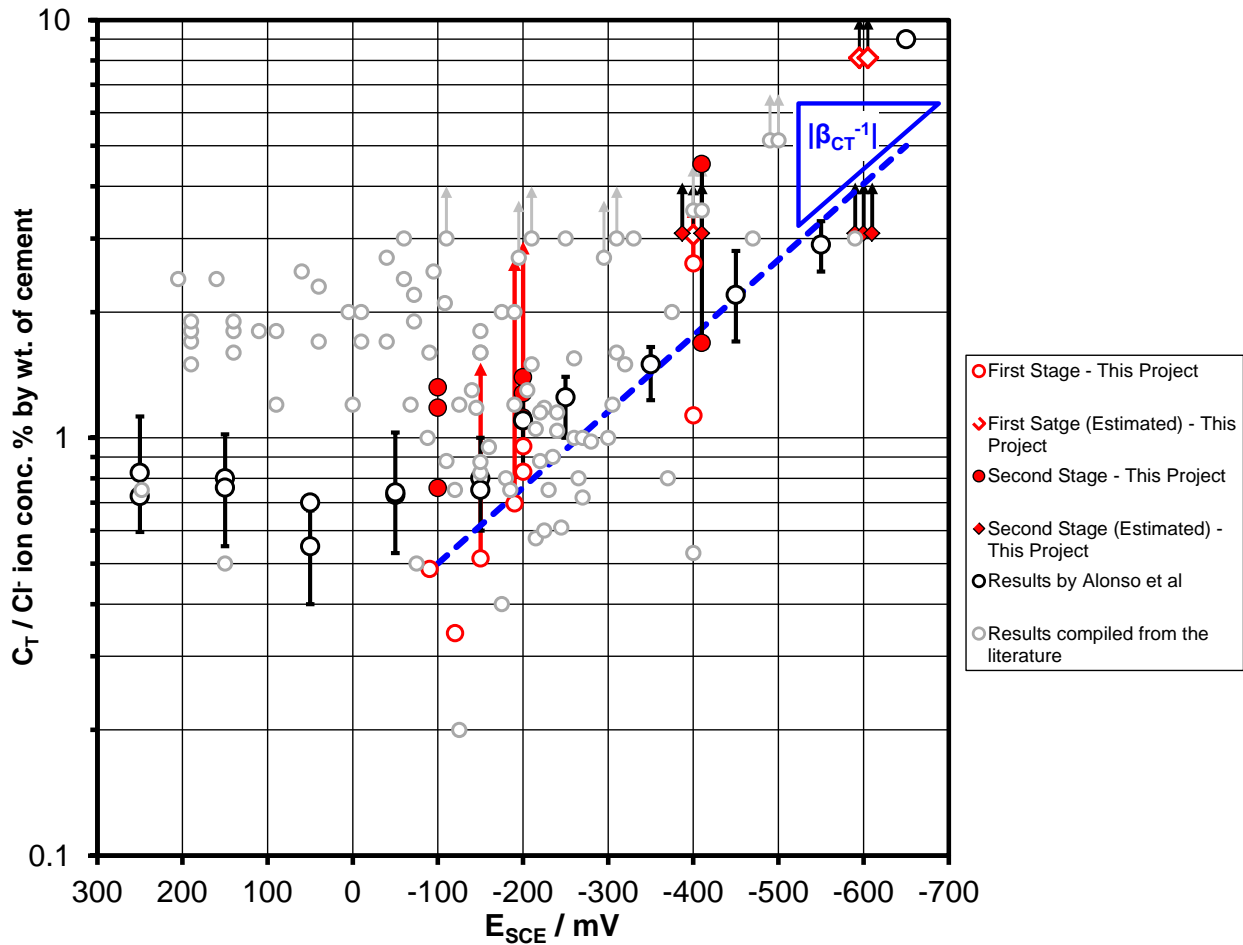
Figure 15 Chloride threshold vs steel potential. Initial compilation by Presuel-Moreno et al. [9]; updated by Sánchez and Sagüés (gray symbols). [7] This project: red symbols. See text for further details. Some symbols are slightly offset for clarity.

2.4 Conclusions of First Stage and Second Stage Experimental Tests Findings

- The present results tend to agree with those of previous investigations showing that negative polarization of several hundred mV may be needed to attain an increase in corrosion initiation threshold of about one order of magnitude.

36

- The updated survey of the literature is consistent with the lower bound of that beneficial effect being approximately described by a threshold value in the order of 0.5% by weight of cement at E=-100 mV (SCE), with a β_{CT} of ~-550 mV/decade of Cl⁻ (dashed blue line in Figure 15) of chloride content, possibly revisable to a less pronounced value. Extrinsic effects, such as an electro kinetic slowdown of chloride buildup at the steel upon cathodic polarization will require separate consideration in follow-up work.

- Because of the nature of lower bound estimates with high C_T values at the more negative potentials, and per the other considerations noted above, the use of a more optimistic slope (e.g. β_{CT} = ~- 400 mV) may merit future consideration but in the meanwhile the value of -550 mV has been adopted for general use in the models detailed later in this investigation (Chapter 3 to Chapter 5).

CHAPTER 3: INTRODUCING POTENTIAL DEPENDENT THRESHOLD IN CORROSION MODELING OF REINFORCED CONCRETE[2]

3.1 General Approach

This modeling approach is described for a situation of chloride-induced concrete reinforcement corrosion. That application is not restrictive however, and a comparable treatment could be made for e.g., carbonation induced corrosion if adequate information on governing parameters were available. For a tractable formulation of the problem, the external surface of a reinforced concrete structure at corrosion risk from environmental attack is divided into small elements, for simplicity taken to be of equal size. All dimensional and material properties as well as other corrosion process ruling parameters are assumed to be uniform within each of those small individual elements, but can vary from element to element. Beneath each surface element there is concrete with embedded reinforcing steel bars (rebars) placed under the clear concrete cover specific for that element. The concrete at each element has likewise individual values of chloride ion surface concentration and effective chloride ion diffusivity that govern the transport of chloride ions penetrating through the pore network towards the rebar. The concrete at each element also has individual values of effective oxygen diffusivity and electric resistivity. If the structure including the steel assembly were to extend

---

[2] This chapter includes previously published material from publications of which the author of this dissertation is the lead author or a principal author [7,39]. Some of that material had also appeared in earlier sources [4,6]. Permissions for all sources are included in Appendix F.
.

significantly further beneath each surface element, a more detailed spatial assignment of concrete properties and steel distribution could be made depending on the degree of geometric complexity.

The portion of steel beneath each surface element (assuming a simple single-mat rebar configuration) is named the corresponding steel element; all steel elements are assumed to be electrically continuous forming a structure-wide rebar assembly. The steel in the assembly is assumed to be initially in the passive state, undergoing anodic dissolution at a small current density dictated by the corrosion kinetic parameters for each element. Once a steel element becomes active (when the chloride content of the concrete at the steel depth reaches the value of C_T corresponding to that element, which is also dependent on the steel potential just before activation), anodic dissolution is declared to proceed at that steel element at a rate that is determined by the corrosion kinetic parameter values ascribed to that element and on the local post-activation steel potential. The cathodic reaction, assumed to be oxygen reduction, is likewise assumed to proceed at rates also determined by the local potential and kinetic parameters, and the local oxygen concentration at the steel surface which is in turn affected by the overall oxygen transport parameters.

Structure service time, starting at the moment of placement in service, is discretized into small equal size consecutive steps. The model consists of modules that calculate the system condition at each consecutive time step. Those modules are broadly described next; simplified implementation for a specific system is presented afterwards.

39

For each time step, a *corrosion distribution module* computes the potential and corrosion rate of the steel elements based on their passive/active condition as determined in the previous time step, and solving the system of polarization equations and electrolyte conduction equations for the array.[31, 32] The resulting steel potential at each point is used to calculate an updated value of C_T for each steel element, based on a chloride threshold dependence on steel potential function having parameters that are part of the model inputs.[9, 10]

A *chloride transport module* calculates for the same time step the updated chloride concentration at the depth corresponding to each steel element, and compares the result with the updated value of C_T just calculated with the corrosion distribution module. If the updated local concentration is found to exceed the updated value of C_T, the steel element is declared to be active effective on the next time step (for which the age is recorded as t_i for the element), and treated accordingly when applying the corrosion distribution module during the next time step.

A *surface damage evaluation module* integrates over the length of the time step the local corrosion rate calculated by the corrosion distribution module, and adds the value to the local integration for all previous time steps. The result is an updated value of the local corrosion penetration P for each steel element. This module also compares P with the value P_{crit} that is assumed to result in concrete cover cracking/spalling for the geometric and environmental conditions corresponding to each element.[33, 34] When P_{crit} is exceeded at a given steel element, the corresponding element external concrete surface area is declared to be damaged and the corresponding age of the element is recorded at its value of ts. The module keeps track of the number of elements that have

40

reached that condition. The sum of damaged concrete area for the entire system as a function of time, expressed as a fraction or percentage of the total external concrete area, was defined as the *damage function* of the system.

The model includes not only the effect of the regions already undergoing corrosion in delaying corrosion initiation elsewhere (through the effect of potential on C_T), but also the later effect of macrocell development in accelerating/slowing corrosion propagation after activation of different zones of the steel assembly, thus successfully integrating the initiation and propagation stages in one single predictive model.

For simplicity, on damage declaration the entire external surface of the concrete for that element is assumed here to exhibit corrosion-induced distress such as cracking, delamination or spalling. That election is not restrictive and alternative scenarios (e.g. spalling affecting only a portion of the element commensurate with the steel placement density and the rebar cover, or the introduction of an additional period of time between cracking and spalling) could be implemented instead if more precise information on the damage modality were available.[35]

3.2 System Chosen and Main Assumptions

The modeling approach indicated above can be implemented in a broad range of applications. For simplicity, demonstration of the concept is limited here to the idealized representation of a partially submerged, reinforced concrete marine substructure column (Figure 16). The surface of the column is divided into stacked ring-shaped elements each of height ΔZ. Additional simplification for corrosion distribution calculations is made by using a straightforward one-dimensional column model,

41

comparable to that employed in related work.[12,18] As shown in that investigation, the one-dimensional approach captures many of the features of interest of such system with minimum computational effort. However, the system chosen for representation could be fully implemented in two or three dimensions if more detail were desired.[4, 6, 36, 37] Furthermore, only systematic spatial variability of system parameters is used in this example, leading to a distributed but deterministic model forecast. Again, that choice is not limiting and the approach is equally suitable to stochastically varying input parameter distributions if so desired.
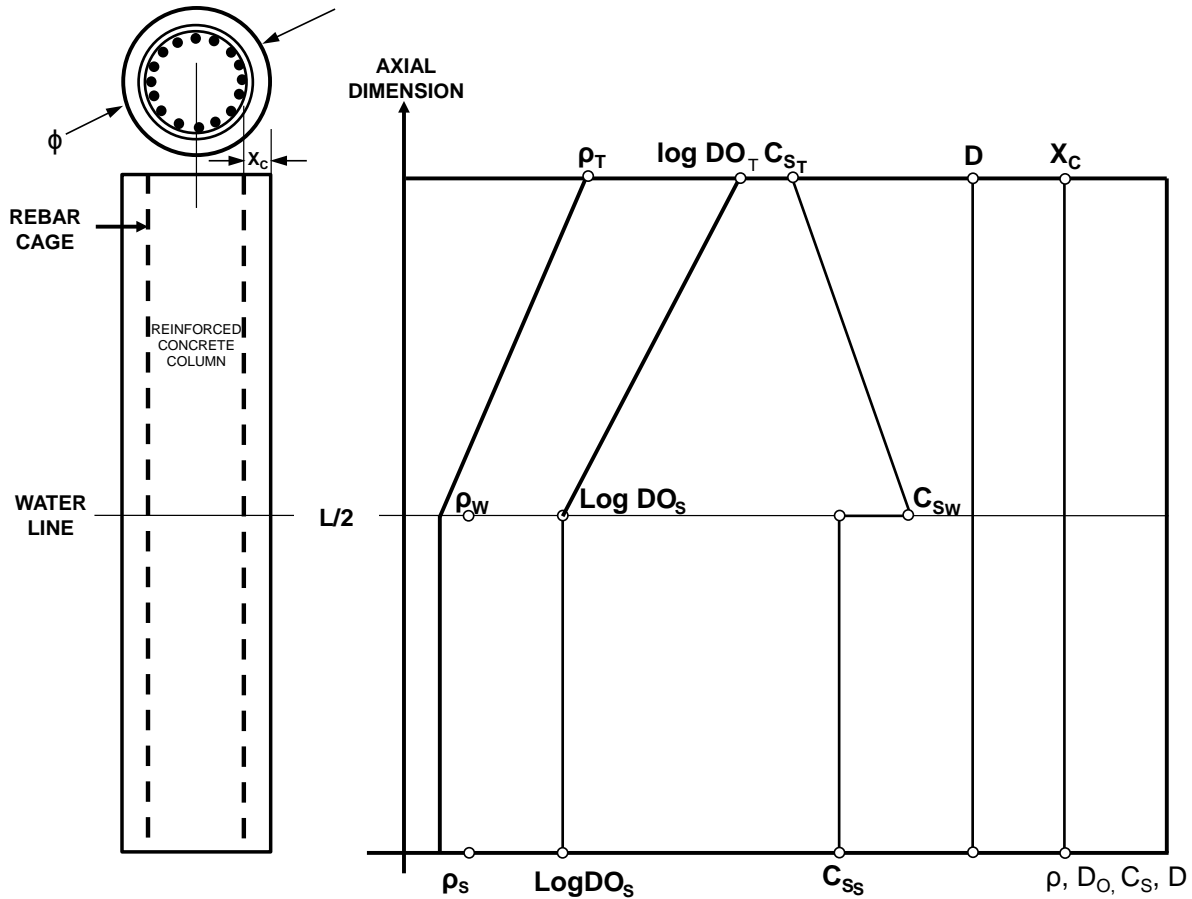
Figure 16 System modeled. Left hand side: sketch represents the front and top view of the reinforced concrete column used to model. Right hand side: a plot indicating the variation with elevation of the resistivity ρ, oxygen diffusivity DO, and chloride ion surface concentration Cs. Chloride ion diffusivity D and concrete cover X_C are invariant with elevation

42

The column has a total height L, diameter Φ, and a single rebar mat, treated for simplicity as a relatively fine mesh, placed at a cover depth X_C from the surface. The rebar mat has a total surface area of steel exposed to concrete equal to the external lateral column surface area multiplied by a Steel Placement Factor S_F, which in typical construction may be in the order of 1. The ends of the cylindrical column are considered to be isolated electrically and from the surrounding environment, and with no reinforcement. The column is assumed to be immersed in seawater to half its height (L/2). Tidal variations are considered to be negligible for simplicity in this example.

The concrete is approximated as an effectively homogeneous electrolytic medium of resistivity ρ, and effective oxygen diffusivity DO, both functions of elevation, and an effective chloride ion diffusivity D treated here for simplicity as a constant value, but again this choice is not limiting. Concrete on the lateral surface of the column is assumed to have developed very early a time-invariant chloride ion concentration C_S that is a function of elevation, and a time-invariant effective oxygen concentration C_{SO}. C_{SO} is treated as being constant with elevation, as reflecting equilibrium between atmospheric oxygen and the pore water at the surface of the concrete (as well as with seawater). However, the effect of salinity variations on C_{SO} is ignored for simplicity. All oxygen concentrations are given as those in the pore water, and the values of representative oxygen diffusivities were converted to be consistent with that choice.[31, 38]

The reinforcing steel is assumed to be the locus of an anodic metal loss reaction,

$$Fe \rightarrow Fe^{2+} + 2e^- \tag{5}$$

43

with a corresponding current density i_a, under two modalities: passive dissolution at a fixed small current density i_p, or active dissolution at a potential-dependent current density i_{aa} so that

$$i_a = i_p \quad \text{(passive)} \tag{6a}$$

$$i_a = i_{aa} = i_{0a} 10^{\frac{(E_s - E_{0a})}{\beta_a}} \text{ (active)} \tag{6b}$$

where i_{0a} is the nominal exchange current density, E_{0a} is the nominal equilibrium potential and β_a is the anodic Tafel slope. The steel is also assumed to support a single cathodic reaction i_c, oxygen reduction:

$$O_2 + 2H_2O + 4e^- \rightarrow 4OH^- \tag{7}$$

which is considered for simplicity to occur under either a fully activation-controlled or a fully diffusion-limited condition. Under full activation control the current density i_{ca} is

$$i_c = i_{ca} = i_{0c} 10^{\frac{(E_{0c} - E_s)}{\beta_c}} \tag{8}$$

where i_{oc} is the nominal exchange current density, E_{0c} is the nominal equilibrium potential and β_c is the cathodic Tafel slope. Under full diffusional control and with $X_C \ll \Phi$ and S_F not far from unity, the current density i_{cd} may be approximated by

44

$$i_{cd} = i_c = 4FC_{SO}D_oS_FX_c \tag{9}$$

where 4 is the number of electrons to reduce O_2 and F = 96.5 10^3 coul/equiv is Faraday's constant. The value of i_c is made to switch from i_{ca} to i_{cd} when the former exceeds the latter, creating a working approximation in lieu of the more computationally intensive mixed polarization function.[12] However, there is no limitation in implementing the latter if desired.

For both anodic and cathodic reactions the corresponding reverse reactions are ignored as the potentials of interest are assumed to be far away from the respective actual equilibrium potentials.

3.2.1 Corrosion Distribution Module

Calling z the distance along the column axis (elevation, with z=0 at the waterline), and treating the problem with a one-dimensional approximation in a manner similar to that used by Presuel-Moreno et al, the charge conservation condition implies that [12]:

$$i_s = \left(\frac{\emptyset}{4\,S_F}\right)\left(\frac{1}{\rho}\frac{d^2E_c}{dz^2} + \frac{d\rho^{-1}}{dz}\frac{dE_c}{dz}\right) \tag{10}$$

where E_C is the steel potential with respect to point in the concrete representative of the bulk of the column at position z; $i_S = i_a - i_c$ is the net current density on the steel surface at elevation z, with i_a being equal to i_{aa} or i_p depending on whether the local steel surface was declared active or passive if the value of C was respectively above or below the value of C_T. The form of the equation results from the one-dimensional approximation

45

used, whereby the corrosion macrocell current travels through the concrete along the z axis and is progressively increased or decreased as it sinks or is sourced at the steel surface. The column concrete cross sectional area is $\pi\Phi^2/4$, and each interval dz of the length encloses a steel surface area of value $S_F\pi\Phi dz$, hence resulting in the $\Phi/(4\,S_F)$ factor. The reader is referred to Presuel-Moreno et al. for further details.[12] As shown there, the formulation can be expressed equivalently in discretized electric circuit form as shown in Figure 17, where each column segment (indexed i) is of uniform length Δz, has a longitudinal concrete resistance R_{Li} related to the local resistivity ρ_i by Equation (11):

$$R_{Li} = \frac{\rho_i \Delta z}{\left(\pi \frac{\emptyset^2}{4}\right)} \tag{11}$$

and where the potential E_{Si} is the local value of E_S which is related to $i_{si} = i_{ai}-i_{ci}$ via polarization equations (6a), (6b), (8) and (9).

Seawater has resistivity that is orders of magnitude smaller than that of concrete; in the below water segments it is then realistic to take the potential distribution at the external submerged portion of the column as space-invariant.[12] For the one-dimensional model used here, all steel elements for the submerged portion of the column were thus assumed to share a common potential, acting in unison and thus behaving as if connected to the waterline steel element by a radial resistance factor R_r of value determined by the resistivity assumed for the waterline level and the column

46

dimensions and internodal spacing. To capture any local current concentration effect a local resistance term R_S was also introduced.
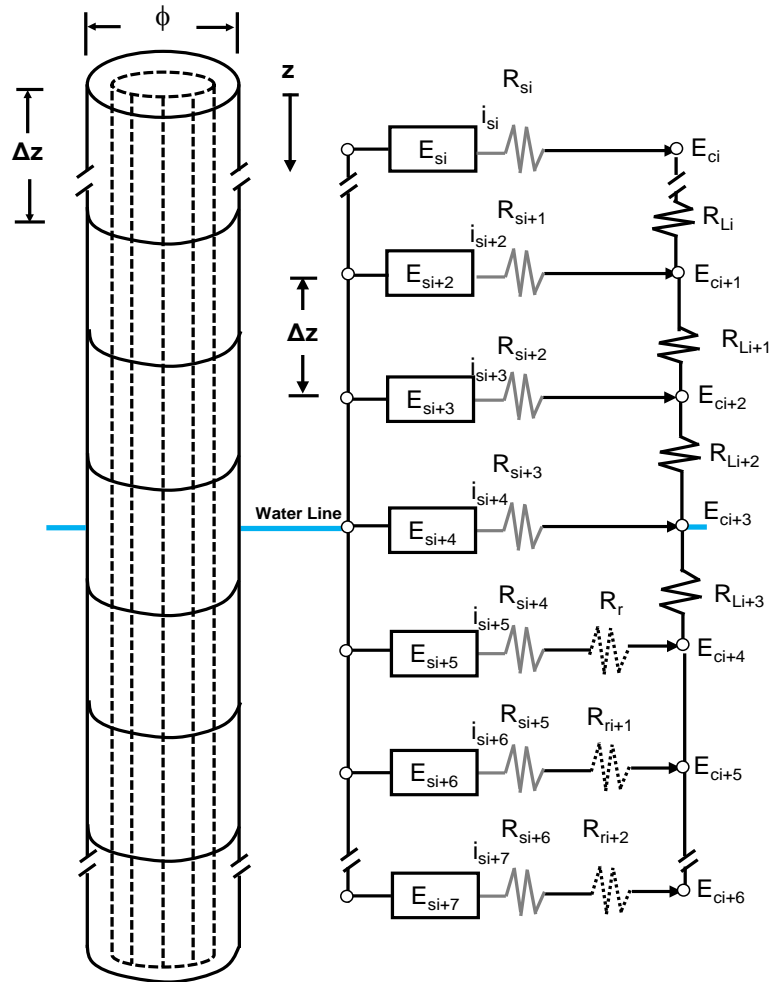
Figure 17 Left hand side: system discretization. Right hand side: symbols representing the types of resistances used in the system showing a portion of the column near the waterline, starting at element i. Black resistor symbol: longitudinal resistance. Dashed resistor symbol: radial resistance. Gray resistor symbol: steel resistance.

The potential-C_T function chosen was that of Equation (1). The declaration of whether a steel element is in the active or passive condition is made using the value of the chloride ion concentration $C(t)$ at the rebar depth X_C at the step time t (see chloride transport module next) per Equation (3), and the local value of C_T calculated at each steel element per Equation (1) using the value of E obtained at the end of the iterative

47

solution process conducted in the previous time step. The array of values of C_T remains unchanged during the iteration process. After iteration is complete the potential array is used as seed for the next time step potential calculations. It is noted that once the steel element is declared active, it is declared to remain so for all subsequent time steps. This is only a simplifying assumption that may be refined in future implementations of the modeling concept.

3.2.1.1 Accounting for Local Resistance Polarization

In a crude approximation both E_{Ci} and E_{Si} in Figure 17 could be treated as being equal, but such simplification would ignore the ohmic resistance associated with geometric current constriction around the rebar, which has a radius much smaller than that of the column.

Recent work [4] showed that neglecting that resistance led to an exaggeration of macrocell coupling between active and passive rebar zones and to unrealistic limit behavior. Consequently, a local resistance term R_{Si} was introduced by treating the rebar as a narrow cylindrical electrode of diameter Φ_r in a cylindrical medium that extended to an influence radius assumed to be in the order of $\Phi/4$.

This choice is a working assumption to capture a dimension representative of the radial distance between a rebar and a point halfway to other macrocell sink or source components. Because of the logarithmic dependence in Equation (12) the precise value of this choice is not critical to the overall result and it was not subject to further refinement. Using the equation for the resistance between concentric cylinders the value of R_{Si} is given by [31, 39]

48

$$R_{Si} = \frac{\rho_i \, \phi_r}{2\pi S_F \emptyset \Delta z} \; ln\left(\frac{\phi}{2\phi_r}\right) \tag{12}$$

The effect of R_{Si} is then accounted by considering it as a resistive element between the bulk of the concrete and the surface of the steel, so consequently

$$E_s = E_c - i_s R_s \tag{13}$$

For the examples presented here, solution of Equation (10) to obtain i_S and E_C as function of z was conducted iteratively for each time t using a finite differences method formulation equivalent to the circuit approach shown in Figure 17. An equispaced node array, of 101 nodes for the base case, was used along the elevation direction of the column. Each node corresponds effectively to one column segment containing the corresponding steel element. The odd number of nodes was selected so that the waterline location could be centrally placed and correspond to only one steel element. As a check of solution convergence the percent difference between total anodic and cathodic currents in the column was calculated, and verified to be normally substantially less than 0.5% except for brief transients immediately following some of the steel activation events. Those transients rapidly dissipated in subsequent time steps.

3.2.2 Chloride Transport Module

The chloride ion concentration C at the rebar depth X_C is calculated for regularly spaced times counting from the moment the structure is put in service. It is assumed for simplicity that diffusion behavior is ideally Fickian (no chloride binding or other

49

complications), initial bulk chloride contamination is zero, and cover values are chosen so that $X_C \ll \Phi$ is approximately satisfied (nearly flat wall diffusional condition), so at a moment t follows Equation (3). Possible macroscopic effects on chloride ion transport from electric fields inside the concrete associated with macrocell formation are ignored for simplicity.

3.2.3 Surface Damage Evaluation Module

The value of i_a calculated by the corrosion distribution module is integrated over time for each steel element, to obtain a cumulative anodic charge density (q_a) array. The anodic charge density at each steel element is Faradically converted into a corrosion penetration depth P_C

$$P_C = \frac{A_{WFe} q_a}{2 F \rho_{Fe}} \tag{14}$$

where A_{WFe} = 55.85 g/mol is the atomic weight of Fe and ρ_{Fe} = 7.8 g/cm^3 is the density of atomic iron (Fe).

For each time t and at each steel element, the value of P_C is compared with the critical penetration depth P_{CRIT} that results in appearance of a crack/spall at the external surface of the concrete for the conditions encountered.[40] If $P_C > P_{CRIT}$ the external concrete surface over the steel element is declared damaged. For the present simplified model, possible effects of the appearance of cracks on subsequent corrosion development in the column are not addressed. Importantly, the present model (as well as an earlier rotational-symmetry 2-dimensional approach [36]) is limited to treat all

50

points at a given elevation equally so lateral corrosion macrocells are not addressed either. The crack is assumed to be associated with simultaneous delamination of size comparable to the steel element area projected on the external concrete surface. The term "spall" is used here broadly to designate a delamination or the loss of concrete that would result if the delaminated portion were to fall off.

3.3 Summary of Model Inputs and Outputs

Per the discussion above, the model inputs for this application example consist of the column dimensions; rebar mat depth and steel factor; concrete resistivity, oxygen diffusivity and chloride diffusivity elevation profiles; steel electrochemical kinetic parameters; surface chloride and oxygen concentration profiles; and value of critical corrosion penetration. Basic model outputs as function of time are the chloride content at the rebar depth and the steel potential elevation profile. From those are derived the reaction current density profiles; corresponding declarations of active/passive steel condition profiles, and cumulative damage profile as well as integrated column damage. In the terminology of Tuutti's initial corrosion damage concepts [1], the corrosion initiation stage at local element ends with the declaration of active condition, and the propagation stage starts with the activation declaration and ends with the damage declaration when P_{CRIT} is exceeded. The duration of both stages varies from steel element to element.[40]

3.4 Model Parameters

The model input parameter values are listed in Table 3, corresponding to a base case with variations for some of the parameters whenever indicated. The corresponding

51

parameter distribution as function of elevation is shown in Figure 16. The dimensions chosen for the column, concrete cover and steel placement density are typical of those encountered in marine substructures.

3.4.1 Elevation Profiles for D, ρ, DO and C$_S$

The elevation profiles of these parameters chosen for this application are graphically described in Figure 16. Chloride diffusivity, elevation-independent for simplicity as noted earlier, was assigned a value representative of a somewhat permeable concrete so as to result, when combined with the concrete cover used, in appreciable damage development during a 75-year evaluation period.

The other parameters are considered to have elevation trends representative of those observed in typical marine substructure conditions.[42] Concrete resistivity was assumed to be constant below water, with value consistent also with a somewhat permeable concrete, and linearly increasing with elevation above the waterline reflecting the expected drier conditions there.

Oxygen diffusivity was assumed to increase exponentially with elevation above water, to reflect the pronounced increase in oxygen transport in concrete that takes place once the pore network is no longer saturated with pore water.

Chloride surface concentration was assumed to be greatest just above the waterline, where evaporative chloride accumulation on the concrete surface would be greatest, and to decrease linearly with elevation as seawater spray becomes less important.[42]

52

Table 3 Model parameters for base case and variations (refer to Figure 16 for key)

Steel Cover	$X_C =$	7.5 cm
Column diameter	$\Phi=$	105 cm
Column Length	$L=$	1200 cm
Concrete Resistivity	$\rho_T=$	$7.5\ 10^4$ ohm-cm
	$\rho_W, \rho_S=$	$1.5\ 10^4$ ohm-cm
Oxygen Diffusivity*	$DO_T=$	10^{-3} cm^2/sec
	$DO_S =$	10^{-5} cm^2/sec
Chloride Diffusivity	$D=$	$2.5\ 10^{-8}$ cm^2/sec
O_2 Surface Concentration	$C_{SO}=$	$2.5\ 10^{-7}$ mol/cm^3 (in pore water)
Cl$^-$ Surface Concentration	$C_{ST}=$	0 Kg/m^3
	$C_{SW}=$	20 Kg/m^3
	$C_{SS}=$	9 Kg/m^3
Chloride Threshold Parameters		
	$C_{T0}=$	1.78 Kg/m^3
	$E_{T0}=$	-100 mV
	$\beta_{CT} =$	-550 mV/decade (PDT); Variations: -325 mV/decade, -200 mV/decade, -100 mV/decade (all previous ones are PDT),-infinity (PIT).

Polarization Parameters**	E_0 (-V SCE)	i_0 (A/cm^2)	Tafel Slope (V)
Iron Dissolution	-0.78	$3.75\ 10^{-8}$	0.06
Oxygen Reduction	0.16	$1.40\ 10^{-10}$	0.14

Steel Passive Current Density	$i_p = 0.01\ 10^{-6}$ A/cm^2
Critical Corrosion Penetration	
Above water	$P_{CRIT} = 0.01$ cm
Below water	$P_{CRIT} = 0.02$ cm
Activation Zone Size	Corresponding to 1 element of height = L/101 Variations : Corresponding to : 1 element of height = L/51, L/201, L/401, L/801 2 elements of height = L/101, L/201, L/401 and L/801.

*Linear variation of log DO with elevation as shown in Figure 16.
**Potentials are presented in this table and in the results section using the usual electrochemical convention where the rate of anodic reactions increases as the potential becomes more positive. Equations in the text however address potentials in the electrolyte with effectively the opposite convention.

Below the waterline the chloride surface concentration was assumed to be constant and of a value lesser than that just above the waterline, since there is no evaporative concentration effect. For the purpose of the calculations all chloride concentrations were expressed in terms of mass of chloride per unit volume of concrete, for a nominal concrete cement factor of 354 kg/m^3 (600 pounds/cubic yard). Table 3 shows the values of the parameter pivot points E_{T0} and C_{T0} in Figure 1, chosen to be roughly representative of such concrete when placed in a subtropical marine environment.[42]

3.4.2 Threshold Parameters and Variations; Steel Polarization and Concrete Cracking Parameters

The values of E_{T0} and C_{T0} (converted to Kg/m^3) in Equation (1) were chosen as those in the pivot point in Figure 1, per the arguments indicated in the Introduction. As noted there, a value of β_{CT} = -550 mV/decade represents a lower bound estimate for that parameter but considerable uncertainty exists as to its effective value in other conditions; values as low as in the order of -100 mV/decade have been suggested elsewhere.[43] Since C_T depends exponentially on the choice of β_{CT}, this parameter was treated as a variable for examination. For the base case a threshold potential dependence β_{CT} value of -550 mV/decade was assumed, reflecting an extreme suggested by a previous literature compilations and recent data.[9, 10, 17, 18] Variations on the choice of β_{CT} were slopes of -325, -200 and -100 mV/decade reflecting increasingly optimistic but also uncertain scenarios. In addition to those potential-dependent threshold (PDT) cases, a potential-independent threshold (PIT) case was

54

used as reference, implemented by making β_{CT} = -∞ mV/decade so that per Equation (1). C_T is fixed at the value C_{T0} that corresponded to cathodically unpolarized steel. While the above material properties and boundary conditions are loosely representative of some field conditions, it is emphasized that the values were chosen mainly for illustration of the modeling concept and not to match the behavior of a specific actual system.

Polarization kinetic parameters values for the corrosion reactions are similar to those used in previous plausible modeling approaches.[31] See note in Table 3 for sign conventions.

The value of P_{CRIT} was chosen to be a 100 μm for elements above water, representative of typical values for atmospherically exposed concrete, and a nominal amount twice as large for submerged zones to capture the expected greater solubility of corrosion products in water-saturated concrete.[33, 44] As for all the other parameters, these choices are not limiting and can be modified as more precise information becomes available.

3.4.3 Time Period

The calculations cover the period from 0 to 75 years of age, using a 0.25 years time step. The time step value was found to be fine enough to avoid in most instances multiple activation declarations of adjacent elements in a single time step. In those few instances where the chloride content at the steel surface of two or more adjacent elements was found to have exceeded the value of C_T during a single time step, only

55

the element with the greatest excess was allowed to become active. Trial calculations with finer time steps provided essentially the same results.

3.4.4 Activation Zone Size

With uneven surface chloride distribution as in the present example, a similarly uneven C_T-isoconcentration front penetrates into the concrete as time progresses. Ideally, passivity breakdown would occur first at just the point of intersection between that front and the surface of the steel. In reality, passivity breakdown is likely to involve some stabilization delay period, at the end of which the chloride content would exceed C_T over some finite region around the initial point.

Depending on the progression of breakdown stabilizing phenomena such as local pore water acidification and migration of chloride ions, the newly created anodic region may quickly develop a finite size area before the local potential drop is enough to temporarily prevent corrosion initiation in the immediately surrounding, still passive steel surface. That finite size area is named the activation zone size in the following discussion. Its value merits attention because if it is small, the effective electrolytic ohmic resistance for macrocell coupling with the rest of the system becomes high.[45] In such case, the corrosion-preventing influence would extend to only a short distance around the activation zone. Conversely, a larger activation zone size would have a lower associated electrolyte resistance and project its corrosion preventive action over a longer distance.

Given uncertainty regarding what the effective activation zone size is in an actual structure situation, parametric calculations were made to determine trends and

56

sensitivity of the forecasted amount of corrosion damage as function of that value. For the system modeled here, the activation zone size was varied simply by dividing the constant column length into various numbers of equal segments differing from each other by approximate multiples of 2, and taking the activation zone size to be that of the steel element area in one segment.

The resulting activation zone size was 0.38 m^2 for the base case (101 steel elements), and ranged from 0.76 m^2 (51 elements) to 0.0475 m^2 (801 elements) for alternative cases. These values are macroscopic but, as it will be shown later, indicative via extrapolation of the conditions that might be reached at the vanishingly small size limit.

The activation zone size variations just described imply also variations in the computational grid fineness, so the question would linger as to whether any change in the results was due merely to changes in the accuracy of the finite difference representation of the system.

To verify that computational grid fineness changes did not introduce undue artifacts in the analysis, additional computations were made where in some of the element arrays the activation declaration was made to affect two adjacent segments instead of only one at a time. Comparison was then made with the output from the next coarser array, which had elements nearly twice the size but with only one activating at a time. The results, presented later on, showed essentially the same damage progression in both cases indicating that only minor artifacts came from this source.

57

3.5 Results

3.5.1 Polarization Profile Evolution

The computations utilizing the innovative model discussed here resulted in calculated potentials and corrosion current densities for the active and passive portions that generally approximated those encountered in actual corroding marine structures. However, for the methodology demonstration purposes of this investigation no further modification of the selection of kinetic parameters was made for direct simulation of any specific system. Within that generic context, incorporation of potential dependence of the chloride threshold was found to strongly influence the projected corrosion evolution of the system. Figure 18 exemplifies the steel potential- and corrosion current density-elevation profiles obtained by running the model for the base case (β_{CT} = -550 mV/decade) to various ages representative of conditions of interest. Initially the chloride concentration everywhere on the steel surface was zero, so passive conditions prevailed. The rate of the anodic reaction over the entire rebar assembly was thus uniform, per the assumed value of the passive dissolution current density (0.01 $\mu A/cm^2$). As that was everywhere below the limiting current density for oxygen reduction, under the simplifying assumptions used the entire assembly adopted a uniform mixed potential value (~-100 mV) that approached the typical values for passive steel in concrete noted earlier. The corresponding potential profile is shown by the dashed line in Figure 18 a). Since the potential was uniform along the rebar assembly, the value of C_T calculated per Equation (1) was also the same throughout and equal to C_{T0}, 1.78 kg/m^3. The initial condition was maintained until year 12.5 when the waterline steel element was the first to become active as a consequence of the chloride ion surface concentration, being the

58

highest there, having just exceeded the initial value of C_T, consistent with the choice of concrete cover and chloride diffusivity used. Upon activation, the steel element became a net anode, developing a high corrosion current density and a distinctly more negative potential than before. The active steel element and the potential and current density profiles changed into those indicated by the solid line in Figure 18 a).The potential depression extended to the nearby still passive steel elements, reflecting macrocell galvanic coupling. That polarization decreased above water with distance from the active steel element, consistent with macrocell coupling in a resistive electrolyte. At elevations ~>2 m above the waterline the effect vanished for the most part and the potential approached the initial potential. On the submerged side the steel potential shifted and reached a value somewhat more negative than the initial potential, corresponding to the coupling of the large, still passive (effectively nearly equipotential) steel in the submerged zone with the newly activated waterline steel element.

The steel at the newly active spot underwent corrosion at a high rate much as a consequence of the coupling with a locally weak, but overall large cathode. Chloride concentration built up to higher levels in the immediately surrounding passive steel elements, even exceeding the initial C_T value, but activation did not take place in those elements because the C_T values had increased due to the local potential depression. Instead, the next activation event (year 15.75), took place at a higher elevation (~1.5 m above the waterline) where the preventing effect from the polarization induced by the first anodic zone was lower. That second activation event occurred at a later date than the first since C_S was lower at that higher elevation (and C_T had become a greater value) than at the waterline steel element as shown in Figure 18b). The second

59

activation created a second negative peak in the potential profile, with associated potential depression and C_T increase in the nearby passive steel elements. The corrosion current density was somewhat smaller than that of the waterline steel element, as macrocell coupling did not include the relatively large underwater cathode, and as concrete resistivity at higher elevations was higher. The next activation events included several taking place further above the waterline as the increasing chloride ion concentration there exceeded the local C_T value, but always some distance away from elements already active (as those delayed corrosion initiation around them). The result, for the highly simplified one-dimensional approximation used here, was the development of comb-like potential and corrosion current density profiles as in Figure 18 c) for year 37.

The corrosion current density was often greater at the higher elevation elements because, under the assumed parameter profiles, oxygen diffusivity was greater there so diffusional limitation of the cathodic reaction was less prevalent. The entire submerged zone became active at a later date reflecting the lower value of C_S present there and some increase in the value of C_T resulting from the cathodic polarization that had taken place starting with the activation of the waterline steel element in year 12.5. The condition with the zone below water activated is shown in Figure 18 d) for year 75 (end of the simulation). By that time the column potential profile had reached a mature pattern with multiple corroding zones above the waterline, separated by intermediate positions where the cathodic prevention effect delayed activation over a long time frame.

60
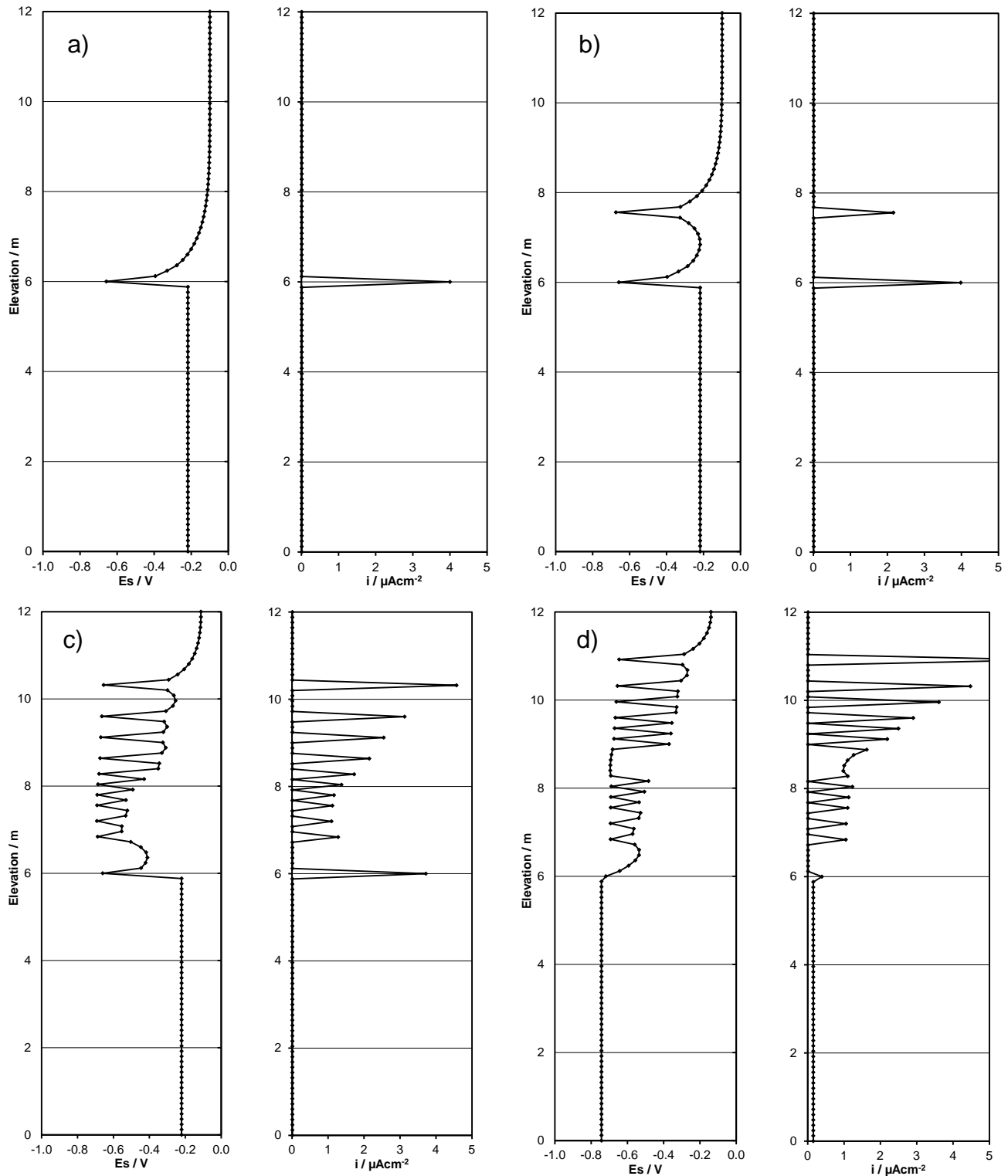
Figure 18 Evolution of potential- and corrosion current density-elevation profile as function of age, base case. Dashed line is initial potential profile of the all-passive assembly. a) 12.5 y: first activation event. b) 15.75 y: second event. c) 37 y: just before activation of submerged portion. d) 75 y: mature pattern. Water level at 6 m elevation

61

The uniform steel activation in the underwater region resulted in the most negative potentials of the system, because the cathodic reaction was fully concentration limited in that zone. Consequently the corrosion rates below the waterline were uniformly very low, at a value equal to that of the limiting current density for oxygen reduction (~0.01 $\mu A/cm^2$), about twice the value of the passive dissolution current density experienced there before activation. Activation underwater also eliminated the large coupled cathodic region that aggravated corrosion in the waterline steel element. Consequently, the corrosion current density at that element dropped to a value commensurate with the low values prevalent where oxygen transport limitation was important, as noted above.

3.5.2 Damage Profile Evolution

3.5.2.1 Base Case: Potential-dependent Threshold (PDT)

In an actual marine structure there would be a tidal zone instead of a fixed waterline, and the evaporative chloride buildup maximum would not take place precisely just above that zone. The first activation occurring at the waterline element in the cases considered here is only a result of the simplified surface chloride profile that was assumed per Figure 16. That assumption is not limiting however. The location for first activation could occur at a higher elevation if a modified profile (using for example field data) was used instead, but the main aspects of the damage evolution discussed here and in the other cases would remain relevant.

Elevations profiles of start and end of the corrosion propagation stage (t_i and t_s, open and filled circles respectively) of the steel elements in the base case that activated

during the modeled period are shown in Figure 19. For steel elements that reached t_s, the symbols are joined by a gray segment of length t_p. Since P_{CRIT} has a constant value above and below the waterline (see Table 3), the length of the gray segment is an inverse indicator of the time-averaged corrosion rate (CR_{AV}) during the propagation stage. For the first element to be activated (that at the waterline) CR_{AV} was ~33 µm/y. This rate is over an order of magnitude higher than the value corresponding to the limiting current density for oxygen reduction there, so the anodic reaction at this element was driven mainly by macrocell coupling with the surrounding passive elements both above and below water. For elements at higher elevations CR_{AV} was in some cases small due to surrounding, earlier-activated elements effectively providing cathodic protection to the newly activated element, after they had earlier provided cathodic prevention by delaying corrosion initiation. The prevention effect is nevertheless dominant in not allowing corrosion initiation altogether in many other elements during the modeled period. On the other hand, CR_{AV} was quite high for some of the elements that had experienced activation at the higher elevations. That outcome reflected the corrosion aggravation that resulted in part from providing beneficial cathodic polarization to the surrounding elements, but also from faster oxygen transport at the higher elevations that supported high corrosion rates there.

It is noted that although the submerged zone experienced activation, no damage declaration occurred up to the end of the modeled period. This behavior is due in part to the very low oxygen diffusion-limited cathodic reaction rate prevalent there. Macrocell coupling that could aggravate corrosion below water is exchanged with the lower part of the above-water portion of the column, but the macrocell current is distributed over a

large submerged steel area with consequently diminished effect there (the situation is the opposite for the first elements above water, where the entire submerged zone effect coupling is concentrated). It is noted that for these simplified simulations the entire submerged region is treated as evolving simultaneously and that significant localized corrosion of small elements could take place if activation below water were not to occur uniformly and simultaneously. Moreover, the extent of corrosion penetration needed to create cracks/spalls in the wetter concrete in the submerged zone could be greater than above water, and the mode of damage there may be different as well. Modeling of that behavior is in progress in follow-up work.[33, 45]
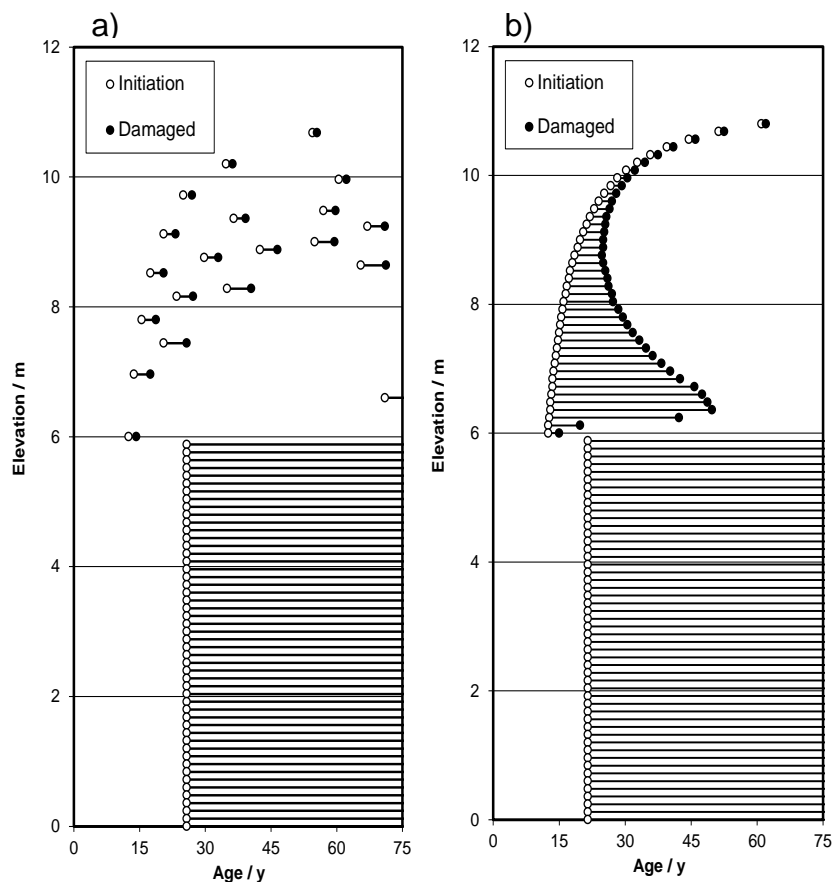
Figure 19 a) Base case (potential-dependent threshold, β_{CT}= -550 mV/decade, elements of height L/101), showing initiation and damage declaration events. Lines joining both events (or extending to 75 years if damage occurs later) are shown for clarity. b) Time-invariant threshold case

64

3.5.2.2 Potential Independent Chloride Threshold Case (PIT)

Further insight is derived from comparison with the behavior with all else as in the base case, but with no threshold dependence on potential. That condition was obtained by making $\beta_{CT}=-\infty$ so $C_T = C_{T0}$, same as the value at age = 0 years in the base case. Results are shown in Figure 19 b).

In this condition the first activation still occurred at the waterline element, and at the same age as in the base case. However, unlike in the base case, activation of the nearby elements that are at increasingly higher elevations occurred very soon as no corrosion prevention was derived from the presence of the first or subsequent active zones. Thus a continuum of active steel tended to form, but with less macrocell action concentration compared with the base case.

The element at the waterline nevertheless experienced efficient macrocell coupling with the still passive region below waterline, and consequently reached the damage condition a relatively short time after activation, at an age comparable to that of the base case. At the other lower elevation elements CR_{AV} tended to become small (and t_p consequently longer) as the cathodic reaction was more diffusion-controlled and less macrocell-enhanced, since activation of nearby elements followed promptly. At the higher elevations CR_{AV} tended to be high and dominated by local cell action, given the high oxygen diffusivity and high concrete resistivity present there. Eventually the much larger number of corroding elements resulted in a greater number of damage declarations than in the PDT cases, as is discussed next.

3.5.3 Cumulative Damage Function Trends

3.5.3.1 Effect of Threshold Potential Dependence and of Value of Cathodic Prevention Slope

The overall damage projection, or damage function of the system, is displayed for selected cases in Figure 20 as the percentage of steel elements in the column that reached the damage declaration point with increasing age. A 75-year evaluation period is covered. Because in the evaluation interval no damage declarations took place in the below-water elements in any of the cases addressed, the damage function had an upper limit of 50%.

There was strikingly greater projected damage development at mature ages in the PIT case, effectively having an infinitely large value of β_{CT}, than in the potential-dependent chloride threshold (PDT) cases where β_{CT} is finite. Furthermore, there was increasingly less projected damage in the aged system as the finite value of β_{CT} decreases. For example, in Figure 20 a) the PIT condition resulted in about 90% of the waterline and above elements reaching damage declaration by age 75 years, while for the PDT cases the corresponding percentage was only 34% (β_{CT} = -550 mV) to 8% (β_{CT} =- 100 mV) . This dependence on β_{CT} is as expected from prior discussion on the form of Equation (1), since the increase in threshold (and consequent prevention of corrosion initiation in regions near an anode) due to a given decrease in potential should be greater the smaller the value of β_{CT}. Also as expected the effect was observed but with a different, much smaller alternative activation zone size as illustrated in Figure 20 b) for the elements of height L/801 simulations. This behavior is summarized in Figure 21

www.manaraa.com

where damage by age 75 years is plotted as function of β_{CT}^{-1} for the two values of the activation zone size considered, showing that proportional behavior was roughly of the same order in both cases.

In the early period shortly following the first damage declarations, the differentiation between PIT and PDT cases was more complicated than in the aged system. As shown in Figures 20 a) and Figure 20 b), damage for the PDT condition in that period tended to progress at a modest rate that was comparable to, and in one instance (β_{CT} = -550 mV, Figure 20 a) even faster than for PDT. Only at a later, intermediate age the rate for PDT began to raise clearly (and quite abruptly) above the PDT cases. There it is noted that in the PDT cases the waterline steel element, which is the one experiencing first activation, provided substantial cathodic prevention for some time to its surrounding steel elements.

Those elements remained passive and acted as cathodes that increased the corrosion rate of the waterline steel element and resulted in earlier damage declaration there. As indicated previously, that macrocell corrosion rate aggravation was not as strong in the PIT case, so the first damage declaration there could be delayed compared with that in the PDT condition. It was not until later at some intermediate age, when the somewhat slower but much more numerous PIT damage declarations began to accumulate, that the long term differences in the corrosion pattern between both cases became well established. This issue has been explored further in work presented elsewhere.[49]
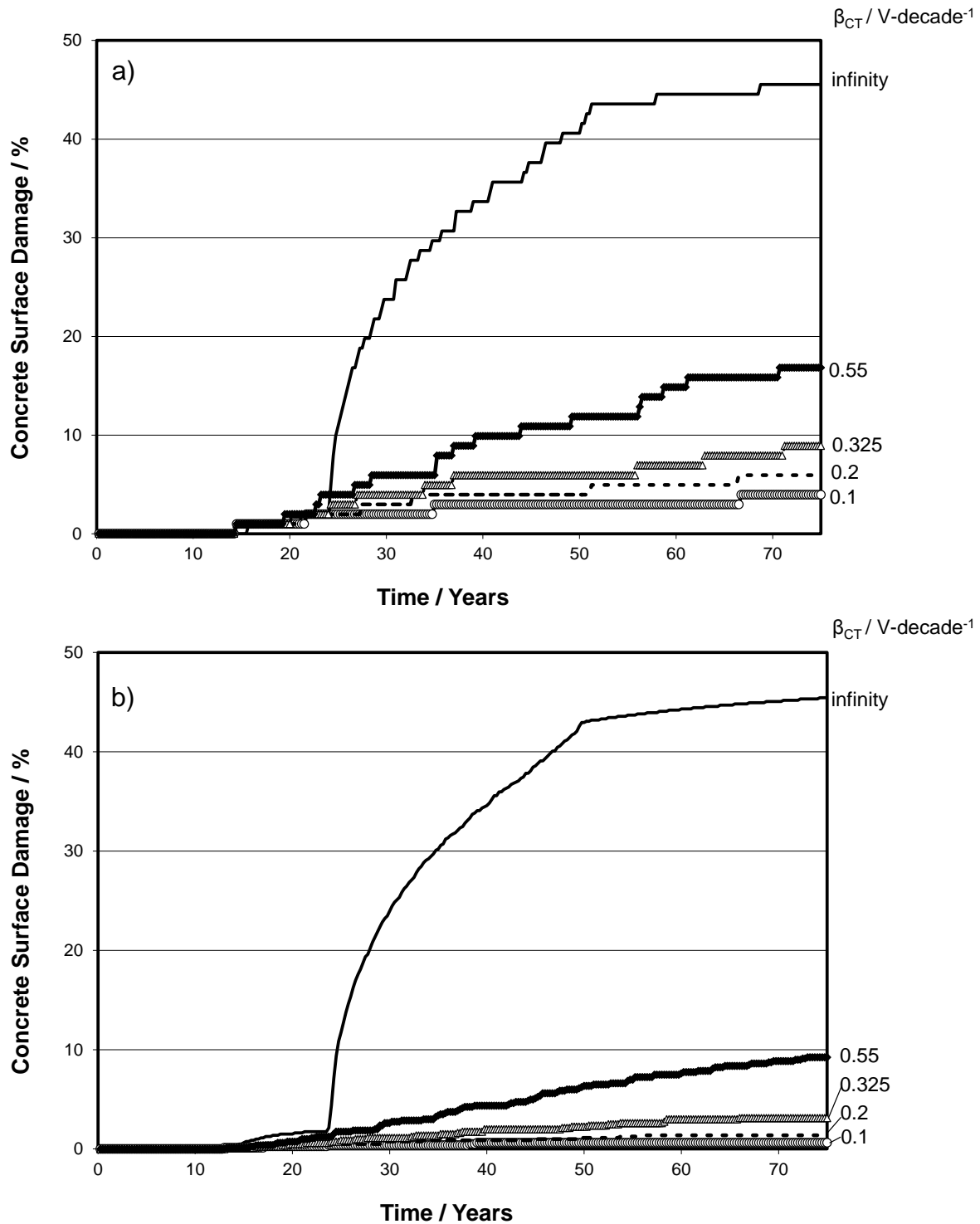
Figure 20 Damage projections for all parameters with β_{CT} slope variations from a) the base case (elements of height L/101) and b) for elements of height L/ 801.
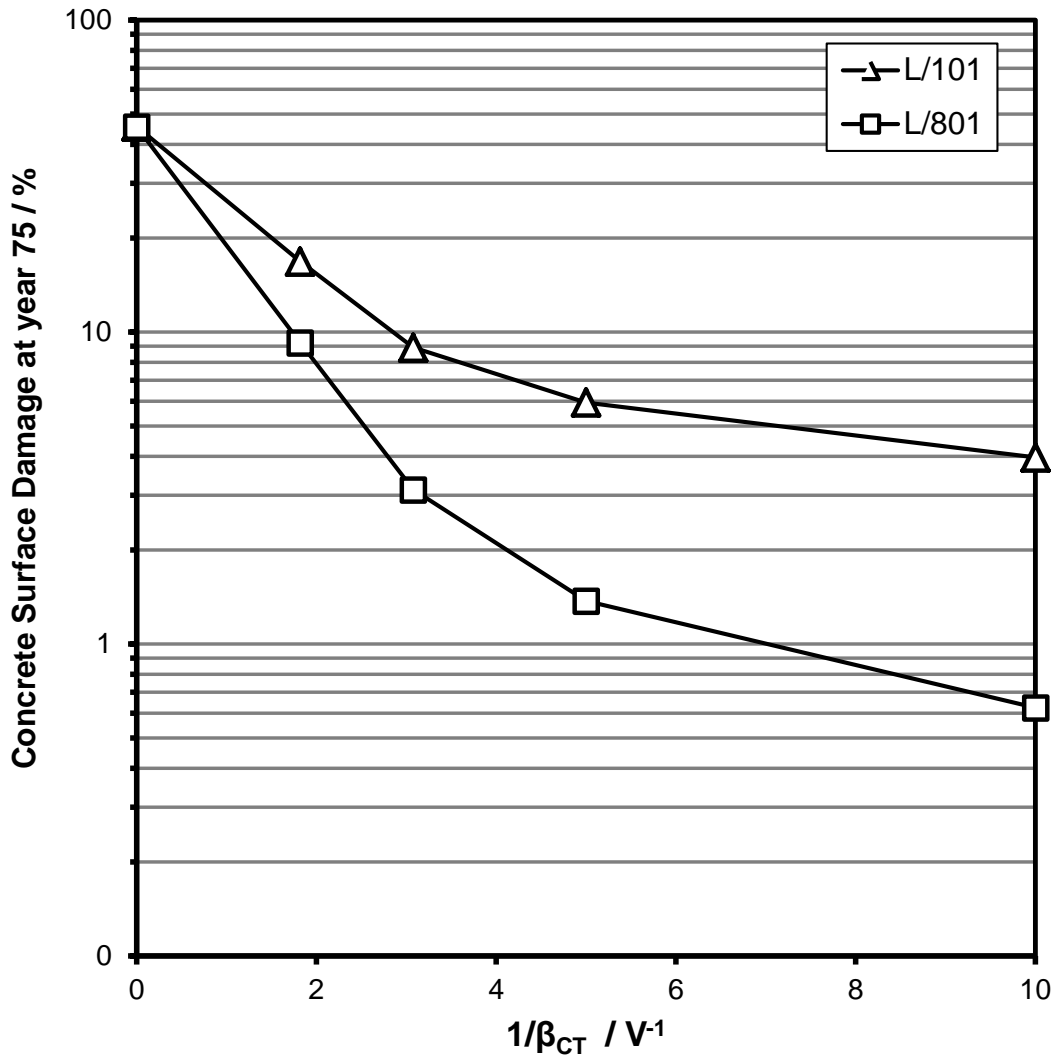
Figure 21 Effect of cathodic prevention slope (β_{CT}) variations on the damage projection for age = 75 years. Results are shown for elements of height L /101 (triangles) and L / 801 (squares).

Further insight in the propagation stage evolution of the system is provided by examination of Figure 22 a) and b), which details the evolution of the corrosion propagation stage for the two cases addressed in Figure 19. The integrated anodic (corrosion) charge density is shown as function of time for each steel element that reaches the active condition, in the form of a line that starts at the moment of activation and increases with a slope that corresponds to the instantaneous corrosion current

density of that element. The damage event is declared when the charge density reaches the Faradaic equivalent of P_{CRIT} (270 C/cm^2 and 539 C/cm^2 for above and below water elements respectively, per Table 3, assuming Fe^{+2} formation). The curves are consistent with the above interpretations, showing that at early ages the fewer PDT activated elements tend to have a greater slope than the more numerous cases for PIT, per the arguments stated in the previous paragraph. At increasing service times, the damage accumulation for PDT overcomes that of PDT with the long-term trend differences noted earlier. The mostly regular propagation stage pattern of lines seen for the PIT case reflects the assumed uniform variation with elevation of parameters such as oxygen diffusivity and surface chloride concentration. Those trends result in gradually increasing corrosion rates and delays in activation times for elements at greater elevations. As discussed later on, the pattern for the PDT case appears at first glance to be random, but it is actually the result of a deterministic sequence dictated by the macrocell coupling and activation rules detailed earlier.

3.5.3.2 Effect of Activation Zone Size

Detailed dependence of projected damage at 75 year age on activation zone size is shown in Figure 23. The results are given as function of activation zone size for the range 1/8 to 2 times relative to that of the base case (0.38 m^2 per element). Activation zone size should not appreciably affect the damage projection for the PIT_T cases, since corrosion initiation in an element does not affect that of the others, and indeed that was the outcome for that condition as evidenced by the nearly constant damage results. That outcome served also as a positive check of the robustness of the calculation procedures, since discretization of the column length in the range examined (51 to 801

elements) did not introduce any major artifacts in the model application for the PIT condition.
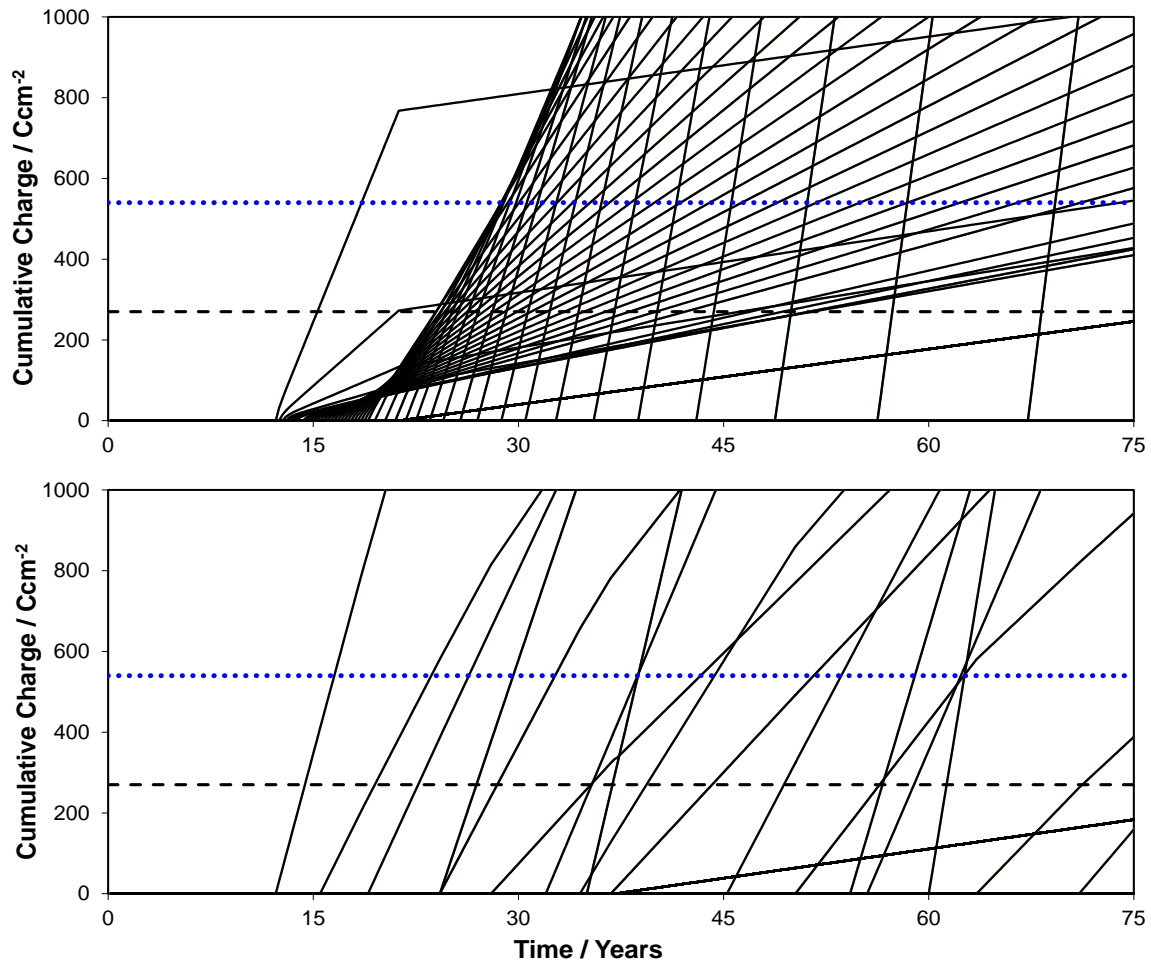
Figure 22 Propagation stage behavior comparison of results for the a) PIT and b) PDT cases addressed in Figure 18. The cumulative corrosion charge density is shown as a function of time. Dotted blue lines and dashed black lines corresponds to the critical penetration conditions above (270 C-cm^{-2}) and below (539 C-cm^{-2}) water, respectively.

In contrast to the time-invariant threshold behavior, activation zone size in PDT cases is expected to influence damage development. Two opposing effects are anticipated. As the activation zone becomes smaller, the amount of active steel created by an activation event is smaller too and so is the extent of later surface damage under the modeling assumptions used here. Simultaneously, as an activation zone becomes

71

smaller, the corrosion preventing effect of that zone tends to becomes less, as the overall polarization of the anode becomes increasingly ohmic due to the local current constriction that develops around a small anode.[31]Hence, the size of the region where effective cathodic prevention takes place around the small anode tends to become smaller as well, enabling the earlier initiation of additional active spots nearby. Consequently, while the amount of corrosion per activation event is smaller for small activation zones, the number of zones is expected to increase concurrently so some kind of terminal behavior is expected under the two opposing effects for the vanishingly small activation zone limit. The modeling results shown in Figure 23 (circles, regular calculations) show that under PDT the damage limit under the terminal behavior is finite. For the system simulated here the 75-year surface damage, which was 18% of the total surface (36% for the portion not submerged) for the base case, tends toward an apparent finite limit of 8% (16% of portion not-submerged) for terminally small activation zone sizes. That outcome, which has been documented in more detail elsewhere, indicates that combined initiation-propagation modeling that incorporates PDT is not overly sensitive to the precise choice of the activation zone size at its low end.[39] Therefore, modeling using this approach could serve to obtain useful insight for a variety of plausible scenarios even in the absence of detailed information on the size of the activation zone for the systems of interest.

As indicated earlier, the dependence of the output on activation zone size should not be confused with response of the calculation results to variations in the fineness of the computational grid. The latter dependence is only minor, as illustrated in Figure 23, where the trend for the PDT regular calculations (circles) is contrasted with the result

72

obtained when the activation declaration was made to affect two adjacent segments instead of only one at a time (crosses) in computational grids that were twice as fine. With the exception of the largest activation zone cases, where discretization is very coarse, the results with both alternative approaches, and the resulting overall trends, are essentially the same.
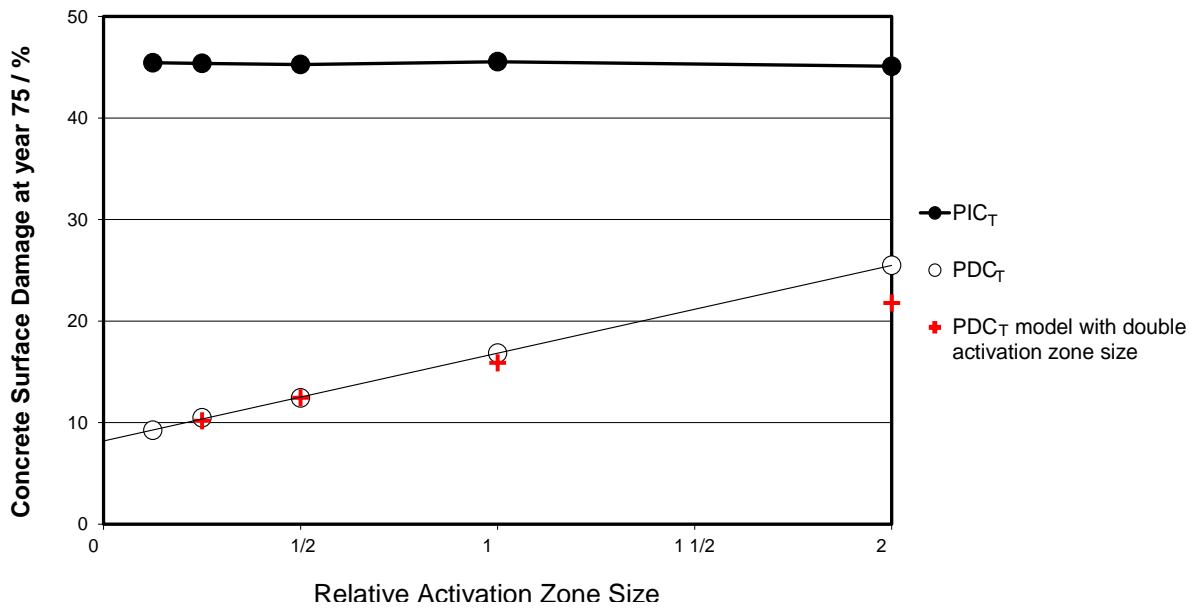
Figure 23 Damage forecast for year 75 as a function of activation zone size. Relativel activation zone size: [elements of height L/101]*[x] with x = 0.125, 0.25, 0.5, 1 and 2. Circles: regular calculations, activation of one element at a time. Crosses: activation of two adjacent elements simultaneously in computational grids twice as fine.

3.6 Summary

This novel work on introducing with proper consideration the threshold dependence on potential in a forecasting model demonstrates feasibility of integrating the corrosion initiation and propagation phases. The calculations were enabled by an iterative approach that updates the system's corrosion distribution when new regions of the rebar assembly become active. The approach successfully accounts for electrochemical interaction between different parts of the rebar assembly, no longer

73

requiring the assumption of independent behavior of those parts. Implementation of that interaction, especially as it concerns the corrosion initiation events, strongly affected the damage projections compared to those obtained with traditional non-interacting element approaches.

For an aged system condition, the innovative model projected dramatically less damage development than when using the traditional PIT assumption. The effect was strongest for hypothetical low values of β_{CT}, but reduction in projected damage was still very substantial even when the cathodic prevention slope β_{CT} was assigned a value of -550 mV, at the lower envelope of known polarization influence on the corrosion threshold.

Conversely, for the earliest stages of corrosion damage manifestations, the model projected intensification of corrosion damage where the first activations occurred (due to delay of corrosion initiation in the surrounding zones and consequent macrocell action), compared to sometimes milder projections by the traditional potential-independent threshold assumption.

Overall, the results indicate that traditional, PIT models may miss features in the damage evolution of a system that are important in decision making and design. Incorporation of a PDT approach may avoid exaggerated long term damage projections and consequently overly conservative cost estimates for the later service stages of a structure. Conversely, the early stages of damage development may be more accurately represented, better guiding design decisions that aim to delay the onset of serviceability limit states set at very low levels.

74

The system and conditions used in this investigation were highly simplified, as the main objective was to demonstrate the PDT modeling concept. The following observations apply noting some of the features that would merit consideration in the development of more realistic models with associated greater complexity.

The damage functions exemplified in Figure 20 have, especially for the large activation zone size cases (elements of height L/101, Figure 20 a), an uneven and stepwise quality. The shape reflects the appearance of successive activation and propagation events at different elevations (see also Figure 22), following systematic trends in Cs and related variables, and the relative corrosion-preventing influence of each newly activated element. That influence is determined according to the local corrosion rate of the element and the effective resistance of the concrete path to nearby elements. Further variability is introduced by the development of different post-activation CR_{AV} values during the individual propagation stages of different elements. However, it is emphasized that while the damage projection may appear to consist of random steps, the projection for the situations simulated here is entirely deterministic and not the result of a probabilistic assignment of corrosion initiation events or propagation rates, as it is used in other forecasting approaches.[3, 46] Ongoing work presented in Chapter 5 and elsewhere [49] explored the effect of random parameter variations superimposed to global trends, showing that the same general approach used here can also be successfully implemented for those more realistic cases.

The simplified, one-dimensional model presented here does not capture the shape of the active zones or any radial variability - the zones might be imagined as being ring-shaped. Hence the comb-like periodicity of the active zones apparent in

75

Figure 18 would be replaced by a mottled pattern in a more realistic multidimensional realization of the model. Likewise, the device of dividing the length into segments of different sizes to represent corresponding active zones was only a rough approximation. It is also important to note that the simultaneous activation for the steel elements below water is a combined result of the simplifying assumption that all elements there share the same potential, and that C_S and D are also the same on that entire zone. Those assumptions are clearly unrealistic, but their effect is minimized by the low limiting current density for oxygen reduction in that zone. Furthermore, the findings presented above are relevant to the zone above water, where the manifestations of corrosion are most evident in actual systems. It is also observed that while concentration of corrosion at submerged regions of the rebar assembly could lead to significant local loss of steel cross section; it does not necessarily cause concrete cracking as accumulation of solid corrosion products may be lessened.[33] Despite those shortcomings, these calculations served to answer key questions regarding the effect of introducing potential-dependence of the corrosion threshold and resulting macrocell effects on durability forecasts. There is no conceptual limitation in implementing more sophisticated models introducing features including, but not limited to, full three dimensional configurations, probabilistic parameter distributions [49], and concrete aging effects.

CHAPTER 4: EFFECT OF VARIATION IN SYSTEM PARAMETERS ON CORROSION DAMAGE FORECAST WITH POTENTIAL DEPENDENT THRESHOLD

4.1 General Approach

An expansion of the forecast model cases developed in Chapter 3 was revisited in this chapter with emphasis on establishing sensitivity of the model output to the choice of model input parameters, primarily to reveal the extent of the macrocell interaction between anodic and cathodic regions under various system conditions. Concrete parameters varied were resistivity ρ, oxygen diffusivity DO and chloride diffusivity D, representing values comparable to those encountered in the field plus some extreme conditions, especially at the low resistivity end. Additionally, the effect of the variations on the value of β_{CT} was also examined, including the comparison PIT condition.

4.2 Cases Examined

The partially submerged reinforced concrete column system was modeled with deterministic profiles of C_S, DO ρ, and D that were variations from those used in Chapter 3. In the cases examined, the only input parameters that remained unchanged with respect to the cases simulated in Chapter 3 were the profiles of X_C and C_S. In the following, the terms ρ_0, DO_0 and D_0 mean the values that the parameters ρ, DO and D had at any given elevation in the cases simulated in Chapter 3.

77

A total of ninety cases were examined as listed in Table 4. Values of the input parameters and the linear elevation-pattern of the resistivity profile remained similar to that of the Chapter 3 base case but variations involved local resistivity ρ_0 values that were three and ten times smaller than the original (base case) resulting in ρ_L (see Table 4).

Cases simulated in Chapter 3 experienced a limited amount of oxygen availability in atmospheric regions near the waterline after activation of the steel elements; hence, the rate of the cathodic reaction was smaller than in the higher elevation regions. As an alternative condition, a system with a much fast DO profile (linear increase with elevation) than the base case (exponential increase with elevation) was evaluated. Those conditions will be referred to in the following as "fast" and "slow" DO respectively.

The chloride diffusion coefficient was assumed to be a time-invariant and constant value throughout the column in the base case. However, data obtained from the field indicates that there is an inversely proportional trend between the values of ρ and D. As a result of that, two linked variations of the diffusion coefficient with the ρ were evaluated: ρ linked D elevation-invariant and ρ linked D elevation-variant. In the former case the base case diffusion coefficient is multiplied by ρ_0/ρ_L and would remain elevation-invariant, and the latter case involved a local variation of the chloride diffusion coefficient that would follow an inverse function of elevation- ρ profile. Variations of the β_{CT} slopes of -550 (base case), -100, -200, -325 and -infinity mV/decade of Cl^- were also evaluated to compared results with those presented in chapter 3.

Table 4 Cases examined (each combination includes 5 alternative values of β_{ct})

ρ	DO	D
ρ_0 $\rho_0/3$ $\rho_0/10$	(Log DO varies linearly with elevation above the waterline as in the Chapter 3 cases)	D_0
ρ_0 $\rho_0/3$ $\rho_0/10$	DO below water and waterline same as DO_S. DO above water varies linearly with elevation from DO_S to DO_T	
ρ_0 $\rho_0/3$ $\rho_0/10$	(Log DO varies linearly with elevation above the waterline as in the Chapter 3 cases)	$D_0 \times \dfrac{\rho}{\rho_L}$
ρ_0 $\rho_0/3$ $\rho_0/10$	DO below water and waterline same as DO_S. DO above water varies linearly with elevation from DO_S to DO_T	
ρ_0 $\rho_0/3$ $\rho_0/10$	(Log DO varies linearly with elevation above the waterline as in the Chapter 3 cases)	$D_0 \times \dfrac{\rho}{\rho_L} \times f(\rho, L)$
ρ_0 $\rho_0/3$ $\rho_0/10$	DO below water and waterline same as DO_S. DO above water varies linearly with elevation from DO_S to DO_T	

4.3 Results and Discussion

The cumulative corrosion-related damage progression (given in logarithmic scale) for a period of 75 years and ρ variations (D not-linked with ρ) with slow (top) and fast (bottom) DO is shown in Figure 24. The red lines indicate the PIT ($\beta_{CT}= -\infty$) condition and the black lines represent the PDT ($\beta_{CT}= -550$) condition. The thick, dotted

and thin lines correspond to the ρ_0, $\rho_0/3$ and $\rho_0/10$ conditions respectively. Similar trends to those presented in Chapter 3 were found. The long-term outcome was, as expected, sensitive to the choice of β_{CT} with a smaller damage progression rate the smaller the slope was. However, for the β_{CT} variations the resulted damage at year 75 is lesser for the case with slow DO than for the case with fast DO.

For the cases with fast DO (Figure 24 b) the damage progression rate was much more pronounced than for the cases with small DO (Figure 24 a).

For the PIT and for the PDT conditions, the activation events of the steel elements near the water line took place at a much faster rate for the fast DO due to the abundant oxygen availability compared to the cases with slow DO. For the PIT case, the activation of the steel elements occurred following a sequential stepwise increase with elevation as a function of time. No preventive effect was developed in the steel elements exposed to the steel since the elements were not macrocell coupled as in the PDT cases.

Not surprisingly, within a given assumed condition (PIT or PDT) the cases with the lower concrete ρ projected earlier damage than in those for the higher ρ, since the latter results in lowered macrocell action and hence slower corrosion at the active spots. It is noted that in all cases the first activation event occurred on the steel element located in the water line. Nonetheless, in some instances damage appearance occurred earlier for the PDT condition than for the corresponding PIT condition. The reason for this behavior is discussed in more detail in the following chapter.
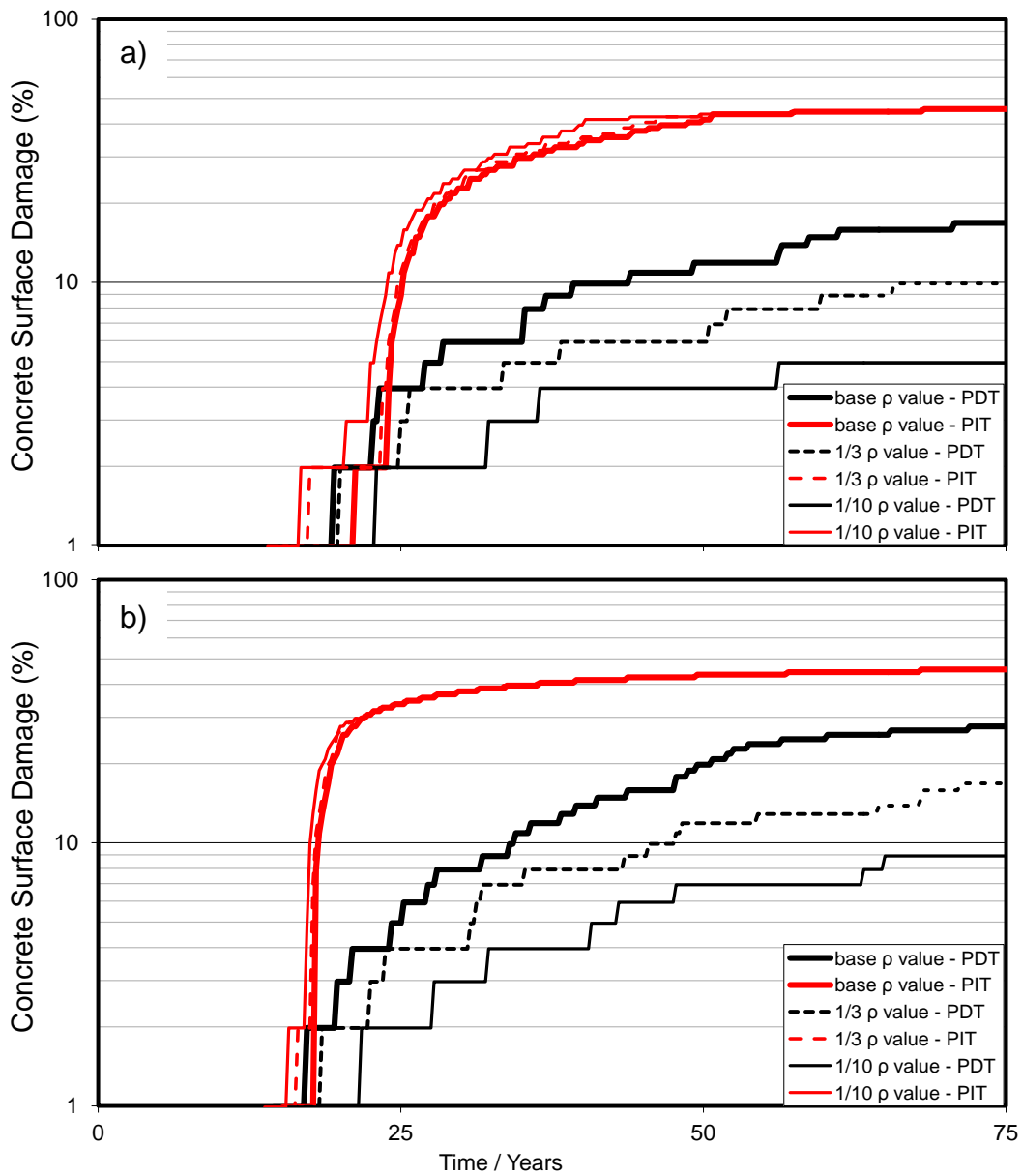
Figure 24 a) Damage projections output for cases with slow DO where ρ at each elevation level was varied from the base case by multiplication factors of 1, 1/3 and 1/10. b) Damage projections output for cases with fast DO where ρ at each elevation level was varied from the base case by multiplication factors of 1, 1/3 and 1/10.

The effect of the oxygen availability and variations of ρ for a long term damage projection at year 75 as a function of the inverse value of β_{CT} is shown in Figure 25. It is noted that the case where $\beta_{CT} = -\infty$ corresponds to the value of zero in the x-axis. A

total of six cases are shown in Figure 25. The two plots at the top (Figure 25 a and b) correspond to the cases were D is not linked with ρ.

The two plots in the middle (Figure 25c and d) are the results of the cases with D elevation-invariant but linked with ρ, and the bottom plots are for D varying with elevation and linked with ρ. The plots placed on the left hand side correspond to the cases with faster DO and plots on the right-hand side correspond to the cases with slower DO. In all six schemes in Figure 25, the damage projection at year 75 diminished as the inverse of the value of β_{CT} increased. Consistent with previous findings, the damage projected with 1/ β_{CT}=0 (PIT) was the largest and long-term results (50% damage) were independent on the value of DO, ρ and D. This outcome is consistent with the entire above-water region having nearly reached the damage declaration condition under PIT relatively early in the life of the structure (with the parameters chosen for these simulations the below-water region did not reach the damage declaration condition before year 75 in any of the cases examined).

For the cases with PDT with higher ρ (open circles) the damage at year 75 was relatively greater than for the rest of the cases. The PDT preventive effect caused by the macrocell coupling became substantially less prominent in concretes with higher ρ, as expected. It is also noted that the projected damage at 75 years was more marked in cases where D elevation-invariant was linked with ρ but (plots c and d). The high values of the chloride diffusion coefficient and the low ρ in these cases resulted in damage projections that were greater than the rest of the cases. The cases with lowest projected damage were those when D varying with elevation was linked with ρ (Figure 25 e and f).

82
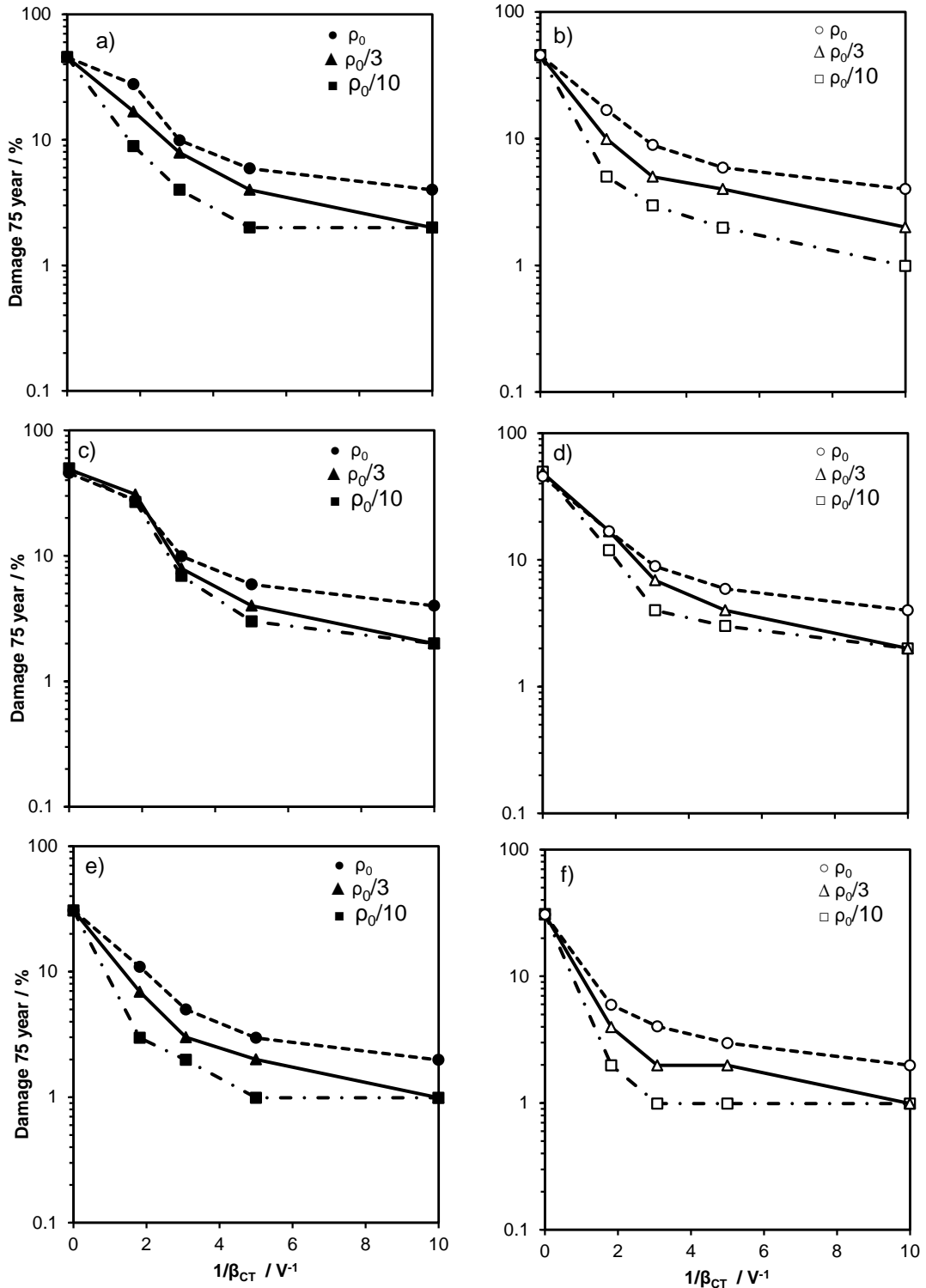
Figure 25 Damage projection for year 75. Effect of oxygen transport and concrete resistivity variations with $1/\beta_{CT}$. Left hand side plots: faster oxygen transport, right hand side plots: slower oxygen transport (a,b) resistivity not linked to D; (c, d) ρ linked D elevation-invariant (e,f) ρ linked D varying with elevation.
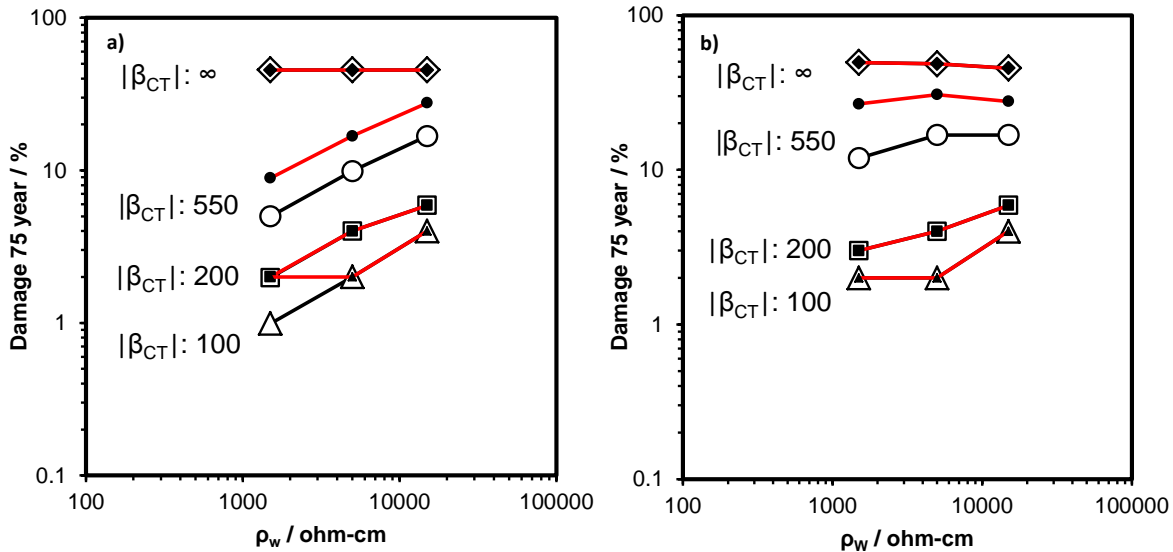
Figure 26 Combined effect on damage projection for age= 75 years of variations of concrete resistivity, threshold dependence slope, and oxygen transport (slower: open symbols, faster: filled symbols). (a): Base case from Chapter 3. (b): ρ linked D varying with elevation.

Figure 26 illustrates the projected damage at 75 years as a function of the choices ρ, DO, D and β_{CT}. The left hand side corresponds to the base case modeled in Chapter 3 and the right hand side corresponds to the case where ρ linked D elevation-invariant. The ρ indicated in Figure 26 corresponds to the base case and variations value of ρ_w listed in Table 3 in Chapter 3. Results are in agreement with those presented in Figure 25, where when the local ρ values become smaller the damage projected under PDT tended to decrease. The macrocell beneficial effect developed to a larger extent in concretes with low ρ at long terms projections.

4.4 Summary

Long-term damage projection with low resistivity concretes resulted in a lesser estimations compared with concrete with higher resistivity. The macrocell interaction between the active and passive steel was much more efficient in concretes with low

84

resistivity. That beneficial effect prevailed in cases where the resistivity was linked with the chloride diffusion coefficient.

The increase in the rate of the oxygen transport accelerated the damage progression during the early stages in PIT and PDT cases and slightly increased the long-term damage projection (year 75) compared with cases with slower diffusion coefficient.

The effect in the amount of oxygen and the value of the concrete resistivity was minor for the long-term projections with PIT, where a near terminal regime for the above water region had already been reached.

CHAPTER 5: PROBABILISTIC CORROSION FORECASTING WITH POTENTIAL DEPENDENT THRESHOLD[3]

5.1 General Approach

The previous chapters demonstrated experimentally and mathematically that PDT leads to slower long term predicted damage development than with traditional potential-independent threshold (PIT) models. However, those introductory calculations were deterministic, with systematic but not random variation of key parameters. The random variation is more likely to be representative of actual systems. This chapter expands the previous modelling approach developed in Chapter 3 and 4 to explore the effect of incorporating PDT on damage projections for a system with randomly distributed profiles of selected corrosion determining parameters. Instances are revealed where PDT can also result in earlier onset of damage compared with PIT predictions, reverting to the previously established long term behavior later on as the system ages.

5.2 Modelled System and Investigated Cases

The system modelled is comparable to that simulating a partially submerged marine column described in Chapter 3 and 4 [4, 7, 39]. However, in this chapter only the atmospheric portion of the column was considered as illustrated in Figure 27. Using a

---

[3] This chapter includes previously published material from publications of which the author of this dissertation is the lead author [49]. Permissions are included in Appendix F

simplified one-dimensional approach, the column is divided into 101 elements along the length L of the column with diameter ϕ. Model parameters and input values are indicated in Table 5. The versions of this modelling approach in Chapter 3 and 4 were deterministic with smoothly elevation-variant concrete resistivity, surface concentration, DO and D. In this chapter, random pattern profiles (Figure 27) without systematic overall trends were implemented for the chloride surface concentration and the concrete cover. The profiles were created using a random number generator and modified to minimize short wavelengths variations. Typical average and standard deviation values found in Florida marine structures were assigned to each profile.[3, 42]
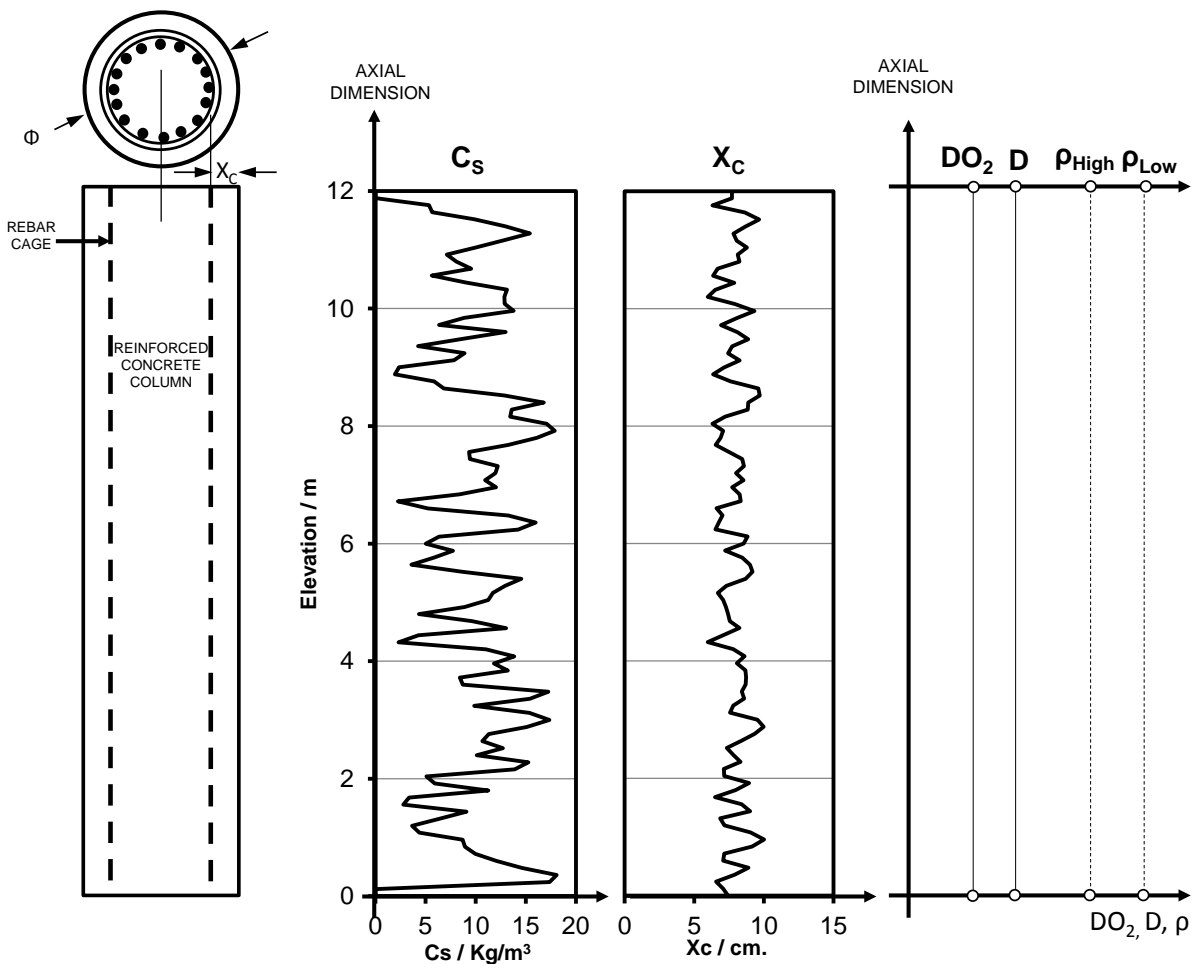
Figure 27 System modeled with representative randomly distributed profiles for the surface concentration and concrete cover.

Similar to the systems modelled in Chapter 3 and 4, the entire structure is passive and the chloride ions ingress through the concrete pore network. Later on, active corrosion starts, first at regions with the most adverse combinations of chloride surface concentration and low cover. The corrosion evolution of the system is calculated at every time step by three modules described in detail Chapter 3.

For this exploratory study random variability was limited to the values of C_S and X_C, in two case classes in which only one of each respectively was varied, and another case class where both varied simultaneously.

All other system parameters were kept constant. Each of those scenarios was implemented to obtain damage functions for low and high uniform concrete resistivity ρ situations (with consequently strong and weak macrocell coupling situations), for a total of six case classes each incorporating PDT, as well as similar set of control calculations with potential-independent threshold (PIT). Each class calculation was replicated with multiple randomizations.

Table 5 Model parameters for the randomly distributed mathematical approach

Column diameter	$\Phi=$	105 cm	
Column Length	$L=$	1,200 cm	
Steel Cover (average)	$X_{Cavg} =$	8 cm	
Steel Cover (standard deviation)	$X_{Cstd} =$	2 cm	
Cl$^-$ Surface Conc. (average)	$C_{Savg}=$	10.4 kg/m^3	
Cl$^-$ Surface Conc.(standard deviation)	$C_{Sstd}=$	4.5 kg/m^3	
Concrete Resistivity	$\rho_{High}=$	7.5×10^4 ohm-cm	(Base); ×1/3, 1/10 (Variations)
	$\rho_{Low}=$	1.5×10^4 ohm-cm	(Base); ×1/3, 1/10 (Variations)
Oxygen Diffusivity	$DO=$	2.5×10^{-5} cm^2/s	
Chloride Diffusivity	$D=$	2.5×10^{-8} cm^2/s	

Table 5 (Continued)

O_2 Surface Concentration	$C_{SO}=$ 2.5×10^{-7} mol/cm^3 (in pore water)		
Chloride Threshold Parameters	$C_{T0}=$ 1.78 kg/m^3		
	$E_{T0}=$ -100 mV		
	$\beta_{CT} =$ - 550 mV/decade of Cl$^-$		
Polarization Parameters	E_0 (-mV SCE)	i_0 (A/cm^2)	Tafel Slope (mV)
Iron Dissolution	-780	1.875×10^{-8}	60
Oxygen Reduction	160	6.25×10^{-10}	160
Steel Passive Current Density	$i_p=$ 0.058×10^{-6} A/cm^2		
Critical Corrosion Penetration	$P_{CRIT}=$ 0.01 cm		

5.3 Results and Discussion

Results presented are from one realization each, but representative of the trends obtained with multiple realizations of the random variable distributions. Figure 28 illustrates a typical output, showing potential and corrosion current elevation profiles for the PDT and PIT cases with randomly distributed X_C and low ρ. The first two activation events occurred at 12.5 years, manifested by local negative potential shifts and the transition from passive current density i_p to a higher active iron dissolution value at each active spot. By year 13.5 the system with PIT had two more active spots, but no new activation was observed in the PDT case. By year 15 twelve activation events already took place for PIT compared to five activations for PDT. As expected, less activation events were present in the PDT case as a result of the increase of the C_T by the negative drop of E in the passive areas adjacent to the active spots.

For the same case described above, the corrosion charge per area of each active element in a 75 year period is shown in Figure 29. The top and the bottom figures correspond to the PIT and PDT scenarios, respectively. The horizontal dashed line indicates the faradaic conversion equivalent to P_{CRIT}, which corresponds to 270 C/cm^2.

89

Concrete damage is declared when the solid lines cross the dashed line. The damage function for the system, expressed as the total count of damaged elements (each corresponding to about 0.39 m^2 of external column surface) as function of time is exemplified for all case classes examined in Figure 30. Multiple realizations with the same averages and variances of the distributed parameters, but with different random assignments, yielded damage functions not deviating much from those exemplified in the figure.
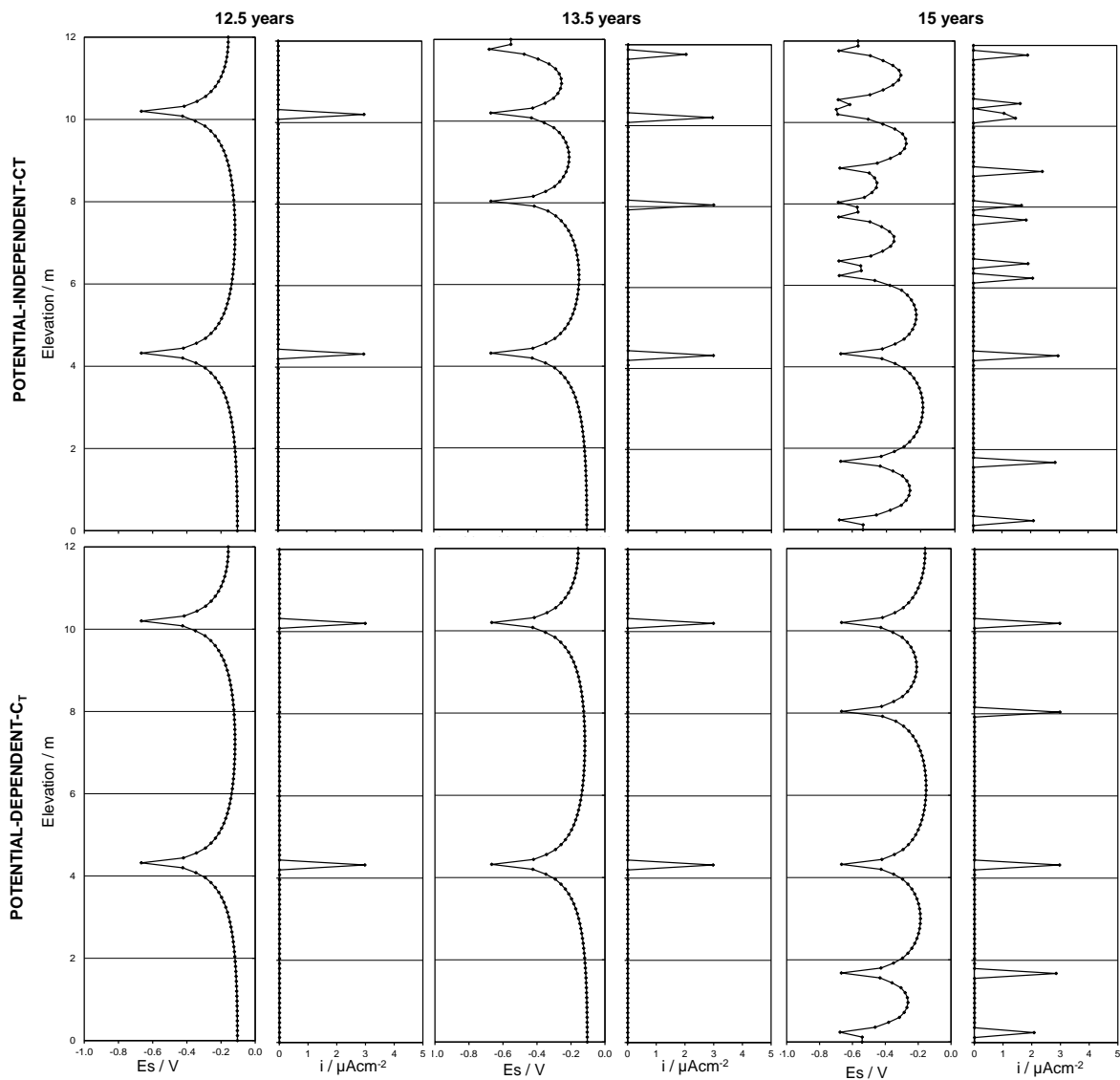
Figure 28 Evolution of the steel potential and corrosion current density with respect to the elevation as a function of time for the random distributed concrete cover with low resistivity

The results share features seen in results from Chapter 4 with systematic instead of random parameter variability. Most noteworthy is the much reduced (by factors ranging from ~2 to ~5) damage projection for the PDT compared to the PIT cases at greater structure ages. That behavior is the direct result of the delay, and sometimes suppression, of new activation events as the potential of the remaining passive part of the steel becomes increasingly more negative with time with consequent elevation of C_T there. That delay/suppression is easily observed in Figure 28, where the initial activation sequence does not vary much between the PDT and PIT scenarios but strong differentiation emerges later with much fewer activation events in the PDT case. That same message over a longer time frame is conveyed in Figure 29. The results further confirm the conclusions of the findings in Chapter 3 and 4 indicating that this differentiation between PIT and PDT, presently ignored in most analyses, should be incorporated in advanced models of damage forecasts for aged structures.

A notable finding in this chapter is that introduction of random parameter fluctuations revealed some instances of significantly greater *early* damage projections in the PDT than in the corresponding PIT cases of the same resistivity. This finding was not readily apparent in the results obtained in Chapter 3 and 4 with systematic and uniform variation of parameters with elevation. As shown in Figure 30, the earlier damage development in PDT sometimes started as much as ~7 years earlier than for PIT. These instances are a propagation stage phenomenon and, paradoxically, a result of the delay in other activation events following the first ones. That delay enables sustained macrocell enhancement of the early active regions with consequent faster local corrosion rates for those few regions, and their early declarations of damage. In

91

contrast, for PIT the rate of appearance of new active regions is not decreased and thus the remaining cathodic portion of the steel assembly has to support an increasing number of anodes, with consequent less enhancement of their corrosion rate and slower arrival of the damage declarations. The corrosion charge curves in Figure 29 are consistent with this interpretation, showing that the fewer PDT propagation events have a greater slope than the more numerous cases for PIT. As time progresses, the extent of macrocell action per active region decreases and the system tends toward smaller, and increasingly diffusion-limited, cathodically controlled regimes in both cases. At longer service times, the damage accumulation for PIT eventually overcomes that of PDT with the long-term trend differences noted earlier.
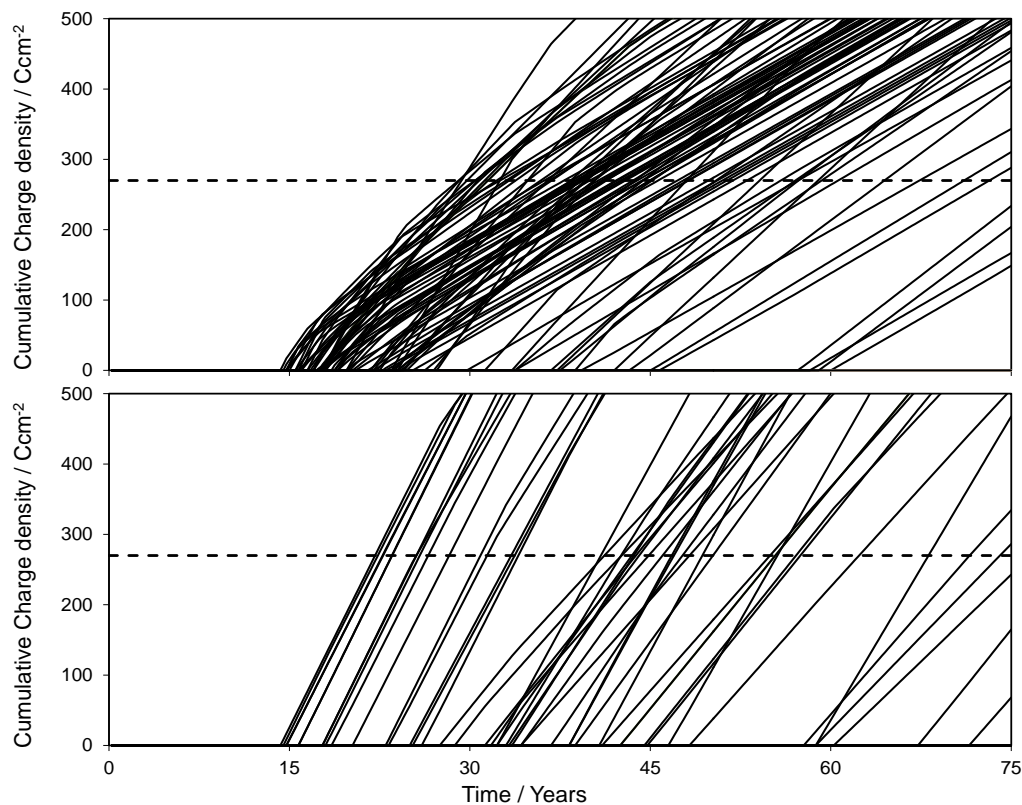
Figure 29 Cumulative corrosion charge density as a function of time for the randomly distributed Cs with high resistivity. Top: Potential-independent-threshold case. Bottom: Potential-dependent-threshold case. Dashed line corresponds to the critical penetration condition.

92

The increased early damage progression for PDT relative to PIT was not observed in all instances, and it is likely to depend on the variability of the parameters chosen to capture the non-uniformity of external aggressive agents and concrete cover and properties. The simulations with uniform systematic parameter profiles used in Chapter 3 tended to mask this outcome through the timing of new activation events. Future work is suggested to determine the sensitivity of that behavior to assumed parameter distributions.
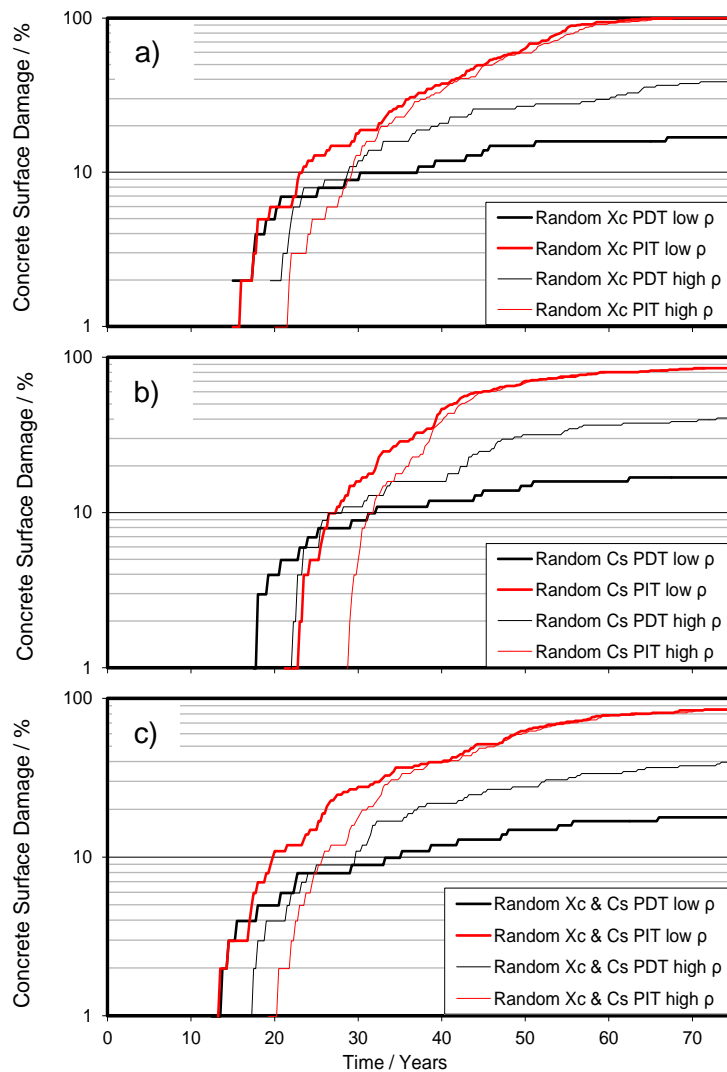
Figure 30 Damage progressions for all cases. a) Randomly distrbuted Xc. b) Randomly distrbuted Cs. c) Combined case

93

5.4 Summary

An expansion of the system modelled in Chapter 3 and 4 was developed by implementing a probabilistically distributed chloride surface concentration and the concrete cover. Traditional potential-independent threshold (PIT) cases were calculated for comparison.

The results were consistent with those obtained in in systems with systematic parameter variations (Chapter 3 and 4), showing that long-term damage was strongly reduced or delayed for PDT cases compared to the PIT controls. The damage reduction is due to the suppression or delay of corrosion initiation events due to the polarization of the remaining steel assembly toward more negative potentials as more active regions develop, thus increasing the value of the corrosion threshold.

The probabilistic calculations revealed situations where accounting for PDT actually resulted in more early damage events than with PIT, with the opposite long term trend noted above developing later on. The finding was ascribed to a propagation stage phenomenon, where the fewer active regions present under PDT experience greater localised macrocell-induced corrosion than the more numerous regions under PIT.

The results underscore the importance of considering PDT in the forecast of corrosion in ageing reinforced concrete structures.

CHAPTER 6: PRACTICAL APPROACH TO INTRODUCE A CORRECTION FOR POTENTIAL DEPENDENT THRESHOLD IN A TRADITIONAL PRACTITIONER-ORIENTED PREDICTIVE MODEL[4]

6.1 Overview of the Model Approach

This chapter illustrates how the PDT feature can be incorporated in an otherwise traditional corrosion-related durability prediction modeling approach (assuming time invariant C_T). The application chosen here is a developmental customized predictive model developed for the needs of the Florida Department of Transportation (FDOT), which involved a large inventory of bridges many of which are exposed to aggressive marine service.

A probabilistic corrosion damage projection was developed based on an earlier model approach with time and space invariant C_T developed elsewhere.[3, 47, 48] Individual probabilistic damage projections were made for each combination of concrete type, structural element type, and exposure conditions (a "Class"[5]) present in the bridge to be analyzed. Each projection used corrosion development parameters that were assigned by the model based on the corresponding FDOT data base for each relevant combination of Classes in the bridge. A correction for dynamic evolution of the chloride corrosion threshold was then applied to the output for each individual relevant Class

---

[4] This chapter includes previously published material from a publication of which the author of this dissertation is the lead author [47].
[5] Not to be confused with a concrete class, which is identified in the following by inserting the word "concrete" first.

combination. After the correction was made, the damage results were multiplied by the number of elements in that Class, yielding an overall damage function for the structure as function of service age. That global outcome is then contrasted with the limit state defined by the practitioner (or user), to establish whether the durability design goal for a new structure (or remaining life for existing structures) is achieved or not. The model output is usable alternatively to establish whether specific portions of the structure can achieve individual goals.

6.2 Probabilistic Damage Projection

The principles of probabilistic corrosion damage projection have been described in detail elsewhere and a brief summary is presented in Appendix D .[3, 47, 48] Each portion of the structure of a given Class is divided into a group of multiple elements of equal surface footprint A_e. Each element has properties and environmental conditions that differ probabilistically from the group average reflecting the natural variability of those parameters. The parameters include the concrete cover X_C, chloride diffusion coefficient D, chloride surface concentration C_S, and the corrosion threshold C_T. All those parameters and their variability are considered to be time-independent. In particular, the C_T values do not vary as different elements become active, so the provisional calculations deal with potential-independent threshold (PIT) values for that parameter. The model then proceeds to calculate the time t_i for corrosion initiation of each element (which varies from element to element depending on the particular values given to it by the probabilistic function assumed), adds to each a globally assumed value of the length of the propagation stage t_p, and reports as $t_s = t_i + t_p$, the time for damage declaration of that element. The fraction of the total number of elements that by

96

an age t satisfy the condition $t_s < t$ is the value of the provisional damage function (PDF) for that Class.

6.3 Correction Function

The basic scenario to develop the correction function was the generic reinforced concrete column system already described in Chapter 3 to Chapter 5. Representative examples of the comparative output of the scenarios explored (systematic parameter distributions, systematic resistivity variations and random X_C, random C_S and combined) were shown there. Examination of the shape and magnitude of the damage functions calculated for PDT-PIT pair combinations from the Table 3 cases showed that the long term (75 year) ratio of PIT to PDT damage percent ranged from ~2 to ~5. For the purposes of practical implementation of this effect, a value of 3 is proposed as being representative of a long term correction ratio C_{LTR}.

It is noted that the behavior differentiation described here as taking place in the long term is actually for an extended but intermediate time period, when chloride levels at the steel depth are substantial, but have not yet became so high so as to exceed the chloride threshold at the zones of greatest potential depression.

At very long structure ages, and if the surface chloride concentration is high enough, the amount of damage in the PDT case may eventually approach the terminal amount of damage for the comparable PIT situation. Hence, the concept of a long term ratio, and the representative value adopted for it are to be considered as working approximations subject to update and refinement in future investigations.

97

At lower ages and lower levels of damage (e.g. a few %) the manifestations of early damage for PDT and PIT tended to appear at comparable times but with some variability, with one or the other taking the lead by a few years over the other. Instances where PDT took the lead at early damage levels appeared to be more evident in cases where the system parameters were subject to random variations, and less so when systematic changes with elevation dominated. As noted elsewhere the instances where PDT takes the lead may be explained as being the result of a propagation stage phenomenon and, paradoxically, a result of the delay in other activation events following the first ones.[49] That delay enables sustained macrocell enhancement of the relatively few early active regions with consequent faster local corrosion rates for those few regions, causing their early declarations of damage. In contrast, for PIT the rate of appearance of new active regions is not decreased and thus the remaining cathodic portion of the steel assembly has to support an increasing number of anodes, with consequent less enhancement of the corrosion rate in those anodes and slower onset of the damage declarations.

It is noted that these simulations have been conducted with parameter choices that tended to result in relatively short times to corrosion initiation, in order to reduce the need for long computational runs while still spanning a large range of total damage development. Hence, the calculations tended to emphasize any effect of propagation period-related differentiation such as the one just discussed. That type of effect is expected to be relatively modest in the overall service life estimate for the structures commonly designed by FDOT (many decades), where highly impermeable concrete is often specified if the environment is aggressive. The chloride diffusion coefficients are

small in those cases and consequently the initiation stage is the dominant period in the service life of the structure and propagation stage-related phenomena tend to be less important. Hence, pending detailed examination in follow-up research, the differentiation between PDT and PIT cases in the early stages of damage is treated here as being of secondary importance. Based on the above and on the results of the simulations conducted, a working approximation is proposed whereby the damage projection for PDT conditions was considered to be the same as that for PIT conditions up to a nominal crossover value C_{CR} = 2%. Further refinement of that value and of its underlying concept is pending on future investigations.

Per the above considerations an adjustable provisional nominal values for the long-term correction ratio C_{LTR} = 3, and for the crossover damage percent C_{CR}= 2 % were adopted. For the entire service life forecast then the corrected damage function DF is obtained from the preliminary damage function PDF by:

$$DF = PDF(t) * \gamma(PDF(t)) \tag{15}$$

with the PDT Partial Factor γ defined by:

$$\gamma = 1 \qquad \text{for PDF(t)} < C_{CR} \tag{16}$$

$$\gamma = \frac{1}{1 + (C_{LTR} - 1) \cdot \dfrac{PDF(t) - C_{CR}}{100\% - C_{CR}}} \qquad \text{for PDF(t)} \geq C_{CR} \tag{17}$$

99

Reflecting the previous discussions, at long ages when PDF approaches 100% in severe environmental exposures, γ approaches $1/C_{LTR}$. At short ages the value of γ becomes increasingly close to unity while approaching the crossover early regime.

Equation (17) presupposes that within a given Class the exposure conditions are severe enough that given a sufficiently long service time, the PDF would reach nearly 100% damage. It also presupposes that the distribution of times to damage declaration within the Class is not distinctly multimodal. It should be noted that the damage evolution of the cases modelled in Chapter 4 was indeed bimodal (with strong above- and below-water differentiation). In that case, the long term damage for the above-water portion dominated during much of time interval investigated, so apparent terminal damage was 50% instead of 100%, and the value of C_{LTR} was evaluated via the PIT-PDT damage ratio during that domain. Clearly for distinctly multimodal cases application of Equation (17) would only serve as a rough approximation. For the general intent of the modeling approach proposed here, where conditions within individual Classes tend to be somewhat regular, Equation (17) represents a working compromise pending the development of more sophisticated approaches in the future.

An example of the application of Equation (17) in a is illustrated in Figure 31, where the preliminary damage function (PDF) and the adjusted damage function (DF) are represented by the red line blue line. After the damage projection exceeds the crossover point (2%), the variation of γ as function (black dotted lines) of time tends to gradually decrease.
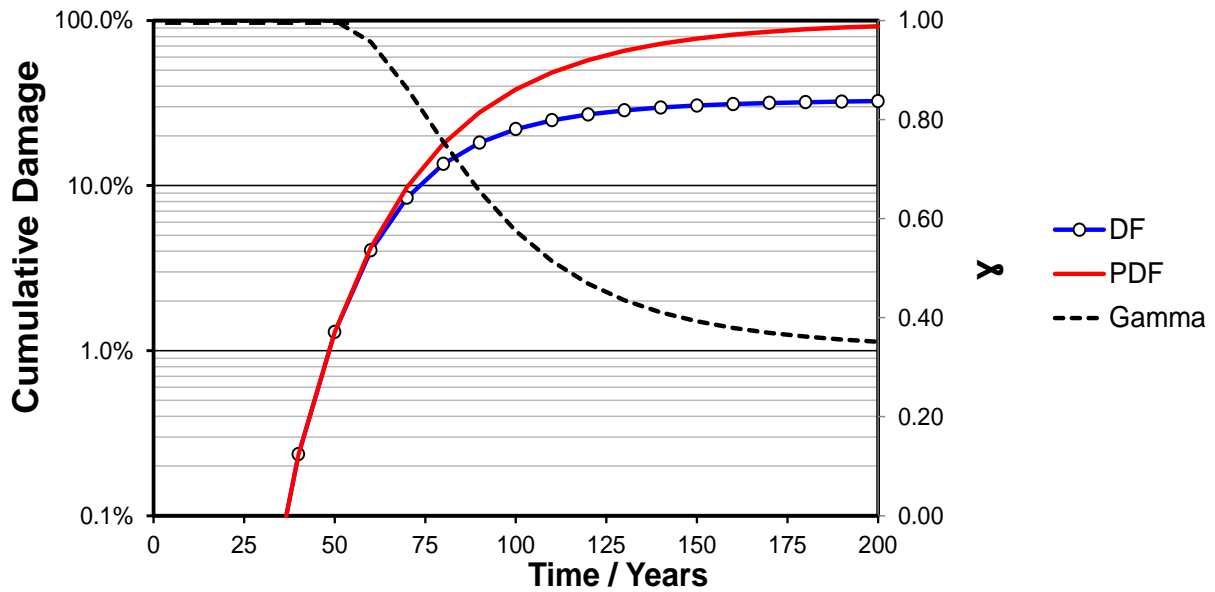
Figure 31 Correction for chloride threshold dependence on steel potential in a traditional forecast approach

6.4 Overall Approach

The information developed from experimental measurements of the dependence of C_T on steel potential (Chapter 2), and from the findings of the dynamic computer models that were built using the experimental results on PDT and combined Initiation-Propagation computations (Chapter 3 - Chapter 5), was employed to refine the output of the main damage prediction model produced by this project.

The modeling approach used was to organize the functioning of the main model in the following steps:

1) Conduct a provisional probabilistic damage projection for a Class. This is done following the overall procedure described in section 6.2, which assumes PIT conditions.

101

2) Apply a correction to the preliminary damage function (PDF), calculated for PIT conditions in the previous step, to account for PDT and obtain the final model output damage function (DF). The correction approach is used instead of a direct model because PDT calculations are highly computer-resource intensive and direct incorporation into a probabilistic model is deemed to be impractical at present. The approach was developed in the following manner:

   a. Computed separate simplified PDT calculations that have been made for a number of scenarios that capture the main characteristics of marine substructure conditions (Chapter 3 - Chapter 5), and a similar set of calculations was made with the same systems, but assuming PIT conditions instead.

   b. Comparison of the PDT and PIT results was then made to formulate a correction function that, when applied to the PDF obtained under PIT, results in a suitable approximation of the corresponding PDT scenario. The correction function was developed as a global abstraction from the result of computing a representative collection of the cases of interest and it is described in section 6.3.

The global correction function is then applied to the PDF obtained in the previous step. The result is the DF that constitutes the final output of the predictive model for that Class. The output thus corrected for all Classes is then tallied to obtain the damage function for the entire system, or for selected parts as desired.

102

This approach has been recently integrated to a developmental next-generation corrosion forecasting model prepared by the author and collaborators for eventual use by the Florida Department of Transportation. The integrated model includes the traditional probabilistic approach as described in Appendix D, and the correction procedure for PDT just described. A more detailed description of the model is presented in Appendix E. It is cautioned that this approach is a working approximation subject to the qualifications noted in the first paragraph of Section 6.3, especially as what pertains to the designation of long term behavior. Follow up work is necessary for the development of a more comprehensive approach to implementation of PDT effects on corrosion induced damage forecasting.

103

CHAPTER 7: CONCLUSIONS

7.1 Experimental Findings

- Shortages in experimental data to characterize the potential-dependent chloride threshold (PDT) behavior were successfully addressed by experiments with specimens in mortar and concrete and with considerably large area of exposed metal.

- The experiments on potential-dependent threshold determinations produced results consistent with the lower bound of that beneficial effect being approximately described by a threshold value in the order of 0.5% by weight of cement at E=-100 mV (SCE), with a negative slope of ~-550 mV per decade of Cl-. That bound was incorporated in the numerical predictive models used in this project. Extrinsic effects, such as an electro kinetic slowdown of chloride buildup at the steel upon cathodic polarization merit consideration in future work.

7.2 Modeling Findings

- A novel approach on corrosion damage progression in a reinforced concrete column by implementing a chloride threshold dependence on steel potential function and integrating macrocell coupling during the initiation and propagation stages in a single model was presented. Findings reveal that neglecting the chloride threshold dependence on steel potential in corrosion-related forecasting models may result in misleading long-term damage projections.

- Calculations supported the validity of the hypothesis that as active zones become smaller their preventive throwing power would be reduced as well, resulting in the development of more numerous active zones that would make up for their individual smaller size in reaching to a finite damage terminal condition. The model improvement over an earlier PDT model stems from a more realistic implementation of the local concrete resistance RS around the reinforcing steel bars.

- The PDT effect in the damage projections was stronger when the cathodic prevention slope was smaller. The damage forecast decreased as the active zone size became smaller, but resulted in the development of more numerous active zones that would make up for their individual smaller size in reaching to a finite damage terminal condition.

- For concretes with low resistivity the long-term damage projection with PDT tended to be much smaller than for comparable PIT cases, which may be ascribed to more efficient macrocell coupling between anodic and cathodic sites.

- In contrast, the probabilistic calculations revealed some situations, less evident in work with the deterministic approach, where accounting for PDT actually resulted in more early damage events than with PIT. The opposite long term trend, noted above, developed only later on. This finding was ascribed to a propagation stage phenomenon (important at relatively young ages), where the fewer active regions present under PDT experience greater localized macrocell-induced corrosion than the more numerous regions under PIT.

105

- Integration of a full probabilistic corrosion forecasting approach and a PDT feature was developed and provisionally achieved via a correction function that links both modalities. The corrosion factor was abstracted from comparative calculations using representative marine corrosion scenarios.

REFERENCES

[1]   K. Tuutti, "Corrosion of Steel in Concrete", Swedish Cement and Concrete Research Institute, Stockholm, 1982.

[2]   C. Andrade, "Probabilistic Treatment of the Reinforcement Corrosion" *Corrosion* In-Press*, vol. 70, pp. 643-651, 2014.

[3]   A. A. Sagüés, "Modeling the Effects of Corrosion on the Lifetime of Extended Reinforced Concrete Structures" *Corrosion,* vol. 59, pp. 854-866, 2003.

[4]   A. A. Sagüés, S. C. Kranc, and K. Lau, "Service Life Forecasting for Reinforced Concrete Incorporating Potential-Dependent Chloride Threshold". Paper No. 09213, presented at the NACE Corrosion 2009, Atlanta, GA. NACE International, Houston, TX., 2009.

[5]   U. Angst, B. Elsener, C. K. Larsen, and Ø. Vennesland, "Critical chloride content in reinforced concrete — A review" *Cement and Concrete Research,* vol. 39, pp. 1122-1138, 2009.

[6]   A. A. Sagüés, S. C. Kranc, and K. Lau, "Modeling of Corrosion of Steel in Concrete with Potential-Dependent Chloride Threshold". Paper No. 4006, presented at the 17th International Corrosion Congress Las Vegas, NV, 2008

[7]   A. A. Sagüés, A. N. Sánchez, K. Lau, and S. C. Kranc, "Service Life Forecasting for Reinforced Concrete Incorporating Potential-Dependent Chloride Threshold" *Corrosion* In Press*, 2014.

[8]   P. Pedeferri, "Cathodic protection and cathodic prevention" *Construction and Building Materials,* vol. 10, pp. 391-402, 1996.

[9]   F. J. Presuel-Moreno, A. A. Sagüés, and S. C. Kranc, "Steel Activation in Concrete Following Interruption of Long-Term Cathodic Polarization" *Corrosion,* vol. 61, pp. 428-436, 2005.

[10]   C. Alonso, M. Castellote, and C. Andrade, "Chloride threshold dependence of pitting potential of reinforcements" *Electrochimica Acta,* vol. 47, pp. 3469-3481, 2002.

[11]   C. Alonso, C. Andrade., M. Castellote, and P. Castro, "Chloride threshold values to depassivate reinforcing bars embedded in a standardized OPC mortar".*Cement and Concrete research*, vol. *30*, pp. 1047-1055.

[12]   F. J. Presuel-Moreno, S. C. Kranc, and A. A. Sagüés, "Cathodic Prevention Distribution in Partially Submerged Reinforced Concrete", *Corrosion,* vol. 61, pp. 548-558, 2005.

[13]   P. Pedeferri, "Cathodic Protection and Cathodic Prevention", *Construction and Building Materials,* vol. 10, pp. 391-402, 1996.

[14]   J. Bockris and A. K. N. Reddy, Volume 1: *Modern Electrochemistry: Ionics*, 2nd ed. Plenum Press, New York, 1998.

[15]   L. Li and A. A. Sagüés, "Chloride Corrosion Threshold of Reinforcing Steel in Alkaline Solutions-Effect of Specimen Size", *Corrosion,* vol. 60, pp. 195-202, 2004.

[16]   L. Basheer, J. Kropp, and D. J. Cleland, "Assessment of the durability of concrete from its permeation properties: a review" *Construction and Building Materials,* vol. 15, pp. 93-103, 2001.

[17]   A. N. Sánchez and A. A. Sagüés, "Chloride Threshold Dependence on Potential in Reinforced Mortar". Paper No. 1728. NACE Corrosion 2012, Salt Lake City, UT. NACE International, Houston, TX., 2012.

[18]   A. N. Sánchez and A. A. Sagüés, "Chloride Corrosion Threshold Dependence on Steel Potential in Reinforced Concrete". Paper No. 4118. NACE Corrosion 2014, San Antonio, TX. NACE International, Houston, TX., 2014.

[19]   R. Weast, *CRC Handbook of Chemistry and Physics*, 54 ed. Chemical Rubber Company, Cleveland, 1973.

[20]   ASTM Standard A615, "Standard Specification for Deformed and Plain Carbon-Steel Bars for Concrete Reinforcement", ASTM International, West Conshohocken, PA, 2005, www.astm.org

[21]   P. P. Castro, A. A. Sagüés, E. I. Moreno, I. Maldonado, and J. Genesca, "Characterization of Activated Titanium Solid Reference Electrodes for Corrosion Testing of Steel in Concrete", *Corrosion,* vol. 52, pp. 609-617, 1996.

[22]   FM5-516, "Florida Method of Test for Determining Low-Levels of Chloride in Concrete and Raw Materials", Florida Department of Transportation, 2009.

[23]   J. Crank, *The Mathematics of Diffusion*, Second ed. Oxford University Press, Oxford, 1975.

[24]   S. C. Kranc, A. A. Sagüés, and F. J. Presuel-Moreno, "Decreased Corrosion Initiation Time of Steel in Concrete due to Reinforcing Bar Obstruction of Diffusional Flow", *ACI Materials Journal,* vol. 99, pp. 51-53, 2002.

[25]   Q. Yuan, C. Shi, G. De Schutter, K. Audenaert, and D. Deng, "Chloride binding of cement-based materials subjected to external chloride environment – A review" *Construction and Building Materials,* vol. 23, pp. 1-13, 2009.

[26]   M. G. Hernández, M. A. G. Izquierdo, A. Ibáñez, J. J. Anaya, and L. G. Ullate, "Porosity estimation of concrete by ultrasonic NDE" *Ultrasonics,* vol. 38, pp. 531-533, 2000.

[27]   T. Oshiro and S. Tanigawa, "Effect of Surface Coating on the Durability of Concrete Exposed to Marine Environment" in *Second International Conference Concrete in Marine Environment Proceedings*, St. Andrews by-the-Sea, Canada, pp. 179-198, 1988.

[28]   T. Luping and L.-O. Nilsson, "Rapid Determination of the Chloride Diffusivity in Concrete by Applying an Electric Field" *Materials Journal,* vol. 89, pp. 49-53, 1993.

[29]   K. Takewaka and S. Mastumoto, "Quality and Cover Thickness of Concrete Based on the Estimation of Chloride Penetration in Marine Environments" in *SP109-17*. vol. 109, pp. 381-400,1988.

[30] ASTM Standard G109-07, "Standard Test Method for Determining Effects of Chemical Admixtures on Corrosion of Embedded Steel Reinforcement in Concrete Exposed to Chloride Environments", ASTM International, West Conshohocken, PA, 2007, www.astm.org

[31] S. C. Kranc and A. A. Sagüés, "Computation of Reinforcing Steel Corrosion Distribution in Concrete Marine Bridge Substructures" *Corrosion,* vol. 50, pp. 50-61, 1994.

[32] S. C. Kranc and A. A. Sagüés, "Advanced Analysis of Chloride Ion Penetration Profiles in Marine Substructure", Final Report Contract No. BB-880", Florida Department of Transportation Research Center, Tallahassee, FL., 2003.

[33] A. A. Torres-Acosta and A. A. Sagüés, "Concrete Cracking by Localized Steel Corrosion - Geometric Effects" *ACI Materials Journal,* vol. 101, pp. 501-507, 2004.

[34] C. Andrade, C. Alonso, J. Rodriguez, and M. Garcia, "Cover Cracking and Amount of Rebar Corrosion: Importance of the Current Applied Accelerated Tests" in *Concrete Repair, Rehabilitation and Protection*, R. Dihr and M. Jones, Eds., ed London: E&FN Spon, pp. 263-273, 1996.

[35] E. Busba and A. A. Sagüés. "Critical Localized Corrosion Penetration of Steel Reinforcement for Concrete Cover Cracking", Paper No.2747., NACE Corrosion 2013,Orlando, FL. NACE International, Houston, TX., 2013

[36] A. A. Sagüés and S. C. Kranc, "Model for a Quantitative Corrosion Damage Function for Reinforced Concrete Marine Substructure" (Summary Paper) in Rehabilitation of Corrosion Damaged Infrastructure, p.268, Proceedings, Symposium 3, 3rd. NACE Latin-American Region Corrosion Congress, P.Castro, O.Troconis and C. Andrade, Eds., ISBN 970-92095-0-7, NACE International, Houston, 1998.

[37] S. C. Kranc and A. A. Sagüés, "Development of Damage Functions to Predict the Durability of Steel Reinforced Concrete Structural Elements" presented at the Corrosion-Conference on Understanding Corrosion Mechanisms in Concrete, M.I.T Cambridge, Massachusetts, 1997.

[38] A. A. Sagüés, M. A. Pech-Canul, and A. K. M. S. Al-Mansur, "Corrosion macrocell behavior of reinforcing steel in partially submerged concrete columns" *Corrosion Science,* vol. 45, pp. 7-32, 2003.

[39] A. N. Sánchez and A. A. Sagüés, "Potential-Dependent Chloride Threshold in Reinforced Concrete Damage Prediction – Effect of Activation Zone Size". Paper No. 2704 presented at the NACE Corrosion 2013, Orlando, FL. NACE International, Houston, TX., 2013.

[40] M. Raupach, " Models for the Propagation Phase of Reinforcement Corrosion – an Overview", Materials and Corrosion, vol. 57, pp. 605-613, 2006

[41] E. Busba, "Effect of Localized Corrosion of Steel on Chloride-Induced Concrete Cover Cracking in Reinforced Concrete Structures" (2013). *Graduate School Theses and Dissertations.* http://scholarcommons.usf.edu/etd/4872

[42] A. A. Sagüés, S. C. Kranc, F. Presuel-Moreno, D. Rey, and A. T.-A. L. Yao, "Corrosion Forecasting for 75-Year Durability Design of Reinforced Concrete", Final Report Contract No. BA502, Florida Department of Transportation Research Center, Tallahassee, FL., 2001.

[43] L. Bertolini, F. Bolzoni, T. Pastore, and P. Pedeferri, "New Experiences on Cathodic Prevention of Reinforced Concrete Structures" in *Corrosion of Reinforcement in Concrete Construction*, C. Page, P. Bamforth, and J. Figg, London: Society for Chemical Industry, pp. 390-398, 1996.

[44] M. T. Walsh and A. A. Sagüés, "Rebar Corrosion in Submerged Concrete Structures - Modeling and Field Results. Paper No. C2014-4118. NACE Corrosion 2014, San Antonio, TX. NACE International, Houston, TX., 2014

[45] R. Oltra and M. Keddam, "Application of impedance technique to localized corrosion" *Corrosion Science,* vol. 28, pp. 1-18, 1988.

[46] E. Bentz, "Probabilistic Modeling of Service Life for Structures Subjected to Chlorides" *ACI Materials Journal,* vol. 100, pp. 391-397, 2003.

[47] A. N. Sánchez and A. A. Sagüés, "Modeling Reinforced Concrete Durability". Final Report Contract No. BDK84 977-09" Florida Department of Transportation Research Center, Tallahassee, FL., 2014.

[48] A. A. Sagüés "Implementation of SHRP Corrosion Diagnosis Projects in Planning Maintenance Strategies for Florida Bridges", Final Report WPI 0510862, Florida Department of Transportation Research Center, Tallahassee, FL., 2002.

111

[49]   A. N. Sánchez and A. A. Sagüés, "Probabilistic Corrosion Forecasting of Steel in Concrete with Potential-dependent Chloride Threshold" pp. 408-415, Proceedings of the 1st International Conference on Ageing of Materials & Structures. Editors: K. van Breugel and E.A.B Koenders. Delft University of Technology. Delft, The Netherlands, 2014.

[50]   L. Bertolini, B. Elsener, P. Pedeferri, and R. Polder, *Corrosion of Steel in Concrete : Prevention, Diagnosis, Repair*. Germany: Weinheim : Wiley-VCH, 2004.

[51]   M. Pourbaix, *Atlas of Electrochemical Equilibria in Aqueos Solutions*, 2nd ed. Houston, TX: NACE International, 1974.

[52]   M. Fontana, *Corrosion Engineering*. McGraw-Hill, New York, NY,1986.

[53]   G. H. Koch, M. Brongers, N. G. Thompson, Y. P. Virmani, and J. H. Payer, "Corrosion Costs and Preventive Strategies in the United States" Report FHWA-RD-01-156, Contract: DTFH61-99-X-00004, 2002.

[54]   ASCE. American Society Civil Engineers. *Report Card for America's Infrastrusture*. Available: http://www.infrastructurereportcard.org/

[55]   S. Lee. Current State of Bridge Deterioration in the U.S. - Part 1. *Materials Performance*. Vol. 51, pp. 62-67, 2012.

[56]   Structural Concrete Textbook on Behaviour, Design and Performance: Design of durable concrete structures, 2 ed. vol. 3: *fédération internationale du béton*, 2009.

[57]   E. Poulsen and L. Mejlbro, *Diffusion of Chloride in Concrete: Theory and Application*. New York: Taylor & Francis Group, 2006.

[58]   C. Evans and M. Richardson, "Service Life of Chloride-Contaminated Concrete Structures". Proceedings from the *Concrete Research in Ireland Colloquium*, pp.131-137, 2005.

[59]   "Chloride Resistance of Concrete" Report prepared by te Cement Concrete & Aggregates Australia. Sydney, Australia. 2009.

[60] G. K. Glass and N. R. Buenfeld, "The influence of chloride binding on the chloride induced corrosion risk in reinforced concrete" *Corrosion Science,* vol. 42, pp. 329-344, 2000.

[61] S. Mindess, J. F. Young, and D. Darwin, *Concrete*, 2nd ed. Prentice Hall, Upper Saddle River, NJ, 2002.

[62] Model Code for Service Life Design, fib Bulletin 34, ISBN: 978-2-88394-074-1, *fédération internationale du béton*, Lausanne, Switzerland, 2006.

[63] C. C. Lim, N. Gowripalan, and V. Sirivivatnanon, "Microcracking and Chloride Permeability of Concrete Under Uniaxial Compression" *Cement and Concrete Composites,* vol. 22, pp. 353-360, 2000.

[64] H. R. Samara and K. C. Hover, "Influence Of Microcracking on the Mass Transport Properties of Concrete" *Materials Journal,* vol. 89, pp. 416-424, 1992.

[65] K. Lau, A. A. Sagüés, and R. G. Powers, "Corrosion of Epoxy-Coated Rebar in Marine Bridges—Part 2: Corrosion in Cracked Concrete" *Corrosion,* vol. 66, pp. 065002-065002-16, 2010.

[66] K. Tuutti, "Service life of structures with regard to corrosion of embedded steel" in *American Concrete Institute Special Publication SP65-13*. vol. 65, pp. 223-236, 1980.

[67] Y. Li and R. E. Weyers, "Modeling the Time-to-Corrosion Cracking in Chloride Contaminated Reinforced Concrete Structures" *ACI Materials Journal,* vol. 95, pp. 675-681, 1983.

[68] P. B. Bamforth, "Enhancing reinforced concrete durability; Guidance on selecting measures for minimising the risk of corrosion of reinforcement in concrete" Technical Report 61:Part 1,The Concrete Society, Camberley, UK, 2004.

[69] G. Williamson, R. Weyers, M. Brown, A. Ramniceanu, and M. Sprinkel, "Validation of Probability-Based Chloride-Induced Corrosion Service-Life Model" *ACI Materials Journal,* vol. 105, p. 375, 2008.

113

[70]   A. A. Sagüés, K. Lau, R. G. Powers, and R. J. Kessler, "Corrosion of Epoxy-Coated Rebar in Marine Bridges—Part 1: A 30-Year Perspective" *Corrosion,* vol. 66, p. 13, 2010.

[71]   ASTM Standard C-1556, " Determining the Apparent Chloride Diffusion Coefficient of Cementitious Mixtures by Bulk Diffusion", ASTM International, West Conshohocken, PA, 2007, www.astm.org

[72]   U. U. Angst, Ø. Vennesland, and R. Myrdal, "Diffusion potentials as source of error in electrochemical measurements in concrete" *Materials and Structures,* vol. 42, pp. 365-375, 2009.

[73]   U. Angst, B. Elsener, R. Myrdal, and Ø. Vennesland, "Diffusion Potentials in Porous Mortar in a Moisture State Below Saturation" *Electrochimica Acta,* vol. 55, pp. 8545-8555, 2010.

[74]   N. R. Buenfeld, G. K. Glass, A. M. Hassanein, and J. Z. Zhang, "Chloride transport in concrete subjected to electric field" *Journal of Materials in Civil Engineering,* vol. 10, pp. 220-228, 1998.

[75]   M. Collepardi, A. Marcialis, and R. Turriziani, "The Kinetics of chloride ions penetration in concrete" *Il Cemento,* vol. 67, pp. 157-164, 1970.

[76]   P. Mangat and B. Molloy, "Prediction of long term chloride concentration in concrete" *Materials and Structures,* vol. 27, pp. 338-346, 1994.

[77]   M. Nokken, A. Boddy, R. D. Hooton, and M. D. A. Thomas, "Time dependent diffusion in concrete—three laboratory studies" *Cement and Concrete Research,* vol. 36, pp. 200-207, 2006.

[78]   T. Luping and J. Gulikers, "On the mathematics of time-dependent apparent chloride diffusion coefficient in concrete" *Cement and Concrete Research,* vol. 37, pp. 589-595, 2007.

[79]   J. Marchand and E. Samson, "Predicting the service-life of concrete structures – Limitations of simplified models" *Cement and Concrete Composites,* vol. 31, pp. 515-521, 2009.

114

[80] B. F. Johannesson, "A theoretical model describing diffusion of a mixture of different types of ions in pore solution of concrete coupled to moisture transport" *Cement and Concrete Research,* vol. 33, pp. 481–488, 2009.

[81] A. V. Saetta, R. V. Scotta, and R. V. Vitaliani, "Analysis of Chloride Diffusion into Partially Saturated Concrete" *ACI Materials Journal,* vol. 90, pp. 441-451, 1993.

[82] E. Samson and J. Marchand, "Modeling the effect of temperature on ionic transport in cementitious materials" *Cement and Concrete Research,* vol. 37, pp 455-468, 2007.

[83] E. Samson and J. Marchand, "Modeling the transport of ions in unsaturated cement- based materials" *Computers and Structures,* vol. 85, pp. 1740–1756, 2007.

[84] K. Y. Ann and H. Song, "Chloride Threshold Level for Corrosion of Steel in Concrete" *Corrosion Science,* vol. 49, pp. 4113-4133, 2007.

[85] G. K. Glass and N. R. Buenfeld, "The presentation of the chloride threshold level for corrosion of steel in concrete" *Corrosion Science,* vol. 39, pp. 1001-1013, 1997.

[86] D. Hausmann.Criteria of cathodic protection of steel in concrete. *Materials Protection*, vol. 8, pp.23-25, 1969

[87] V. K. Gouda, "Corrosion and corrosion inhibition of reinforcing steel; I - Immersion in alkaline solution" *British Corrosion Journal,* vol. 5, pp. 198-209, 1970.

[88] W. Hartt and J. Nam, "Effect of Cement Alkalinity on Chloride Threshold and Time-to-Corrosion of Reinforcing Steel in Concrete" *Corrosion,* vol. 64, pp. 671-680, 2008.

[89] ASTM Standard C-1152, "Standard test method for acid-soluble chloride in mortar and concrete", ASTM International, West Conshohocken, PA, 2007, www.astm.org

[90]   C. Andrade and M. Castellote, "Recommendation of RILEM TC 178-TMC:" Testing and modelling chloride penetration in concrete": Analysis of total chloride content in concrete" *Materials and Structures,* vol. 35, pp. 583-585, 2002.

[91]   K. Clear, "Time-to-Corrosion of Reinforcing Steel in Concrete Slabs: Volume 3: Performance After 830 Daily Salt Applications" Report No. FHWA-RD-76- 70 Federal Highway Administration, Washington, DC, 1976.

[92]   M. Pourbaix, *Lectures on Electrochemical Corrosion*. New York: Plenum Press, 1973.

[93]   K. Ishikawa, I. Cornet, and B. Bresler, "Electrochemical study of the corrosion behaviour of galvanised steel in concrete" *Materials Protection,* vol. 7, p. 44, 1968.

[94]   W. Richartz, "Die Bindung von Chlorid bei der Zementerhärtung" *Zement, Kalk, Gips,* vol. 10, pp. 447-456, 1969.

[95]   V. Gouda and W. Halaka, "Corrosion and corrosion inhibition of reinforcing steel, II. Embedded in concrete", *British Corrosion Journal,* vol. 5, pp. 204-208, 1970.

[96]   A. A. Sagüés, S. C. Kranc, and F. J. Presuel-Moreno, "Applied Modeling for Corrosion protection Design for Marine Bridge Substructures" Final Report: Contract No. B-9119" Florida Department of Transportation, 1997.

[97]   "Life-365 Service Life Prediction Model™ and Computer Program for Predicting the Service Life and Life-Cycle Costs of Reinforced Concrete Exposed to Chlorides", Produced by the Life-365 Consortium II, 2008.

[98]   P. B. Bamforth. The derivation of input data for modelling chloride ingress from eight-year UK coastal exposure trials. *Magazine of Concrete Research*, pp. 87-96, 1999.

[99]   NORDTEST NT BUILD 492: "Concrete, Mortar and Cement-Based Repair Materials: Chloride Migration Coefficient from Non-Steady-State Migration Experiments", P.O. Box 116 FIN–02151, Espoo, Finland, 1999.

[100] F. J. Presuel-Moreno, "Analysis and Estimation of Service Life of Corrosion Prevention Materials Using Diffusion, Resistivity, and Accelerated Curing for New Bridge Structures" Final Report Contract No. BDK79-977-02" Florida Department of Transportation, 2013.

[101] M. F. Hurley and J. R. Scully, "Threshold chloride concentrations of selected corrosion-resistant rebar materials compared to carbon steel" *Corrosion,* vol. 62, pp. 892-904, 2006.

[102] P. F. Marques, A. Costa, and F. Lanata, "Service life of RC structures: chloride induced corrosion: prescriptive versus performance-based methodologies" *Materials and Structures,* vol. 45, pp. 277-296, 2012.

APPENDICES

Appendix A List of Symbols

A	atmospheric zone
Ae	surface area
B	buried sub-exposure
C	chloride concentration at time t and distance x expressed as mass per unit volume of concrete
CE	counter electrode
CF	cement Factor
C_{CR}	nominal PDT-PIT crossover damage percent
C_{LTR}	nominal long-term correction ratio
Cl^-	chloride ion concentration
C_{Sli}	lowest value of chloride surface concentration
C_{Shi}	highest value of chloride surface concentration
C_0	initial chloride concentration of the bulk
C_R	chloride concentration at rebar trace at time t
C_{TA}	chloride concentration at rebar trace at time t_A
C_{TR}	chloride concentration at rebar trace at time t_R
C_S	chloride surface concentration
C_{Savg}	chloride surface concentration – average
C_{SHT}	chloride surface concentration – high tide
C_{ST}	chloride surface concentration – top
C_{Sstd}	chloride surface concentration – standard deviation
C_{SS}	chloride surface concentration – submerged
C_{SO}	oxygen surface concentration or oxygen concentration in the pore water at the external concrete surface
C_T	critical chloride threshold
C_{T0}	baseline chloride threshold value at E_{T0}
c/s	cement-sand ratio
D	apparent diffusion coefficient (cm^2/s)
D_{AVG1}	average diffusion coefficient (cm^2/s) of First Stage specimens 1-3 and 7-8

119

D_{AVG2}	estimated average chloride diffusion coefficient (cm^2/s) of Second Stage specimens 1-6
D_{AVGS1}	estimated chloride diffusion coefficient (cm^2/s) of secondary specimens in First Stage experiment
D_{li}	lowest value of chloride diffusion coefficient
D_{hi}	highest value of chloride diffusion coefficient
DF	damage function (%)
DO	oxygen diffusion coefficient
DO_T	oxygen diffusion coefficient – top
DO_S	oxygen diffusion coefficient – submerged (cm^2/s)
D_{RCM}	rapid chloride ion migration coefficient (cm^2/s)
E	steel electric potential (mV vs. SCE)
E_0	nominal equilibrium potential (mV vs. SCE)
E_{0a}	nominal equilibrium potential for the anodic reaction (mV vs. SCE)
E_{0c}	nominal equilibrium potential for the cathodic reaction (mV vs. SCE)
E_{T0}	baseline steel potential value at C_{T0}
E_{SCE}	steel electric potential vs. SCE
EIS	electrochemical impedance spectroscopy
erf	error function
F	Faraday constant
GS	galvanized steel
i_0	nominal exchange current density ($\mu A/cm^2$)
i_{0a}	nominal exchange current density for the anodic reaction ($\mu A/cm^2$)
i_{0c}	nominal exchange current density for the cathodic reaction ($\mu A/cm^2$)
i_a	anodic current density ($\mu A/cm^2$)
i_{aa}	active dissolution at a potential-dependent current density ($\mu A/cm^2$)
i_c	cathodic current density ($\mu A/cm^2$)
i_{cd}	current density under diffusional control ($\mu A/cm^2$)
i_p	steel passive current density ($\mu A/cm^2$)
i_s	net current density on the steel surface at elevation x ($\mu A/cm^2$)
IS	structural components in soil

120

IW	structural components in water
L	column length
M	molar concentration (mol/L)
$N_d(t)$	number of elements in the entire bridge reaching damage declaration at age t
N	total number of elements in the bridge
Ni	number of elements in Class j
Nj	number of elements within each region j
OCP	OCP
P	dimensionless expression equal to Dt/a^2
P_{cum}	cumulative probability for variable n
P_{CRIT}	critical local corrosion penetration for each steel element
PDF	provisional damage function
PDT	potential-dependent threshold or chloride threshold dependence on steel potential
PIT	potential-independent threshold or chloride threshold independent on steel potential
P_{ki}	probability distribution function for variable V_k
PS	plain steel bar
r	radial direction
RE	reference electrode
R_p	linear polarization resistance
S	submerged zone
S(t)	damaged surface area at age t
SCE	saturated calomel electrode
SE	splash evaporation zone
SF	steel factor
SS	stainless steel
T	tidal zone
t	Time
t_A	time of activation
Tf	correction factor for rebar obstruction effect

t_i	time of initiation
t_p	time of propagation
t_R:	time of removal
t_S:	time to spall
V_1	variable 1
V_2	variable 2
V_3	variable 3
V_4	variable 4
V_s	variable 5
V_k	variable k
V_n	variable n
w/c	water-to-cement ratio
X	distance along the column axis
X_C	concrete cover
X_{Cavg}	concrete cover – average
X_{Cstd}	concrete cover – standard deviation
Y	side dimension of square piles
A	radius of First Stage specimens
β_a	anodic Tafel slope
β_c	cathodic Tafel slope
β_{CT}	slope of the straight line corresponding to Eq.(1) when plotted in an E-$\log C_T$ representation. Also called the cathodic prevention slope
ɣ	PDT partial factor
Φ	column diameter
Φ_r	steel bar or rebar diameter
ρ	concrete resistivity
ρ_T	concrete resistivity – top of the column
ρ_S	concrete resistivity – submerged portion of the column
ρ_{High}	concrete resistivity – highest value
ρ_{Low}	concrete resistivity – lowest

122

Appendix B Review of Corrosion Processes in Concrete and Related Durability Forecasting Issues

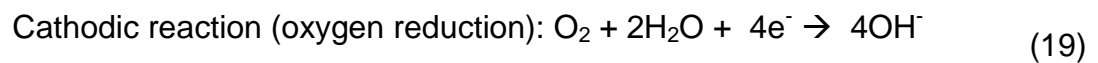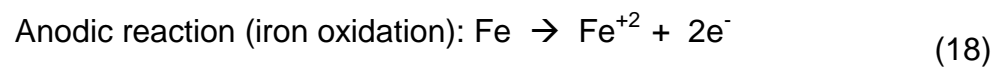**B.1 Chloride-induced Corrosion of Reinforced Concrete**

The high alkalinity of the concrete pore water (typically with a pH greater than 13) develops a protective passive film against corrosion on the surface of the embedded steel. Passive film breakdown of the embedded steel bar in concrete exposed to chloride-laden environments occurs when the chloride ion concentration on the steel surface exceeds the value of chloride corrosion threshold (C_T).

Chloride ions penetrate through the concrete's pore network. Chloride ions build up at the steel bar surface and when chloride concentration reaches a minimum amount, known as the chloride corrosion threshold (C_T), breakdown of the passive film occurs and corrosion initiates. Another factor the causes the breakdown of the passive film on steel is the carbonation of concrete due to the ingress of carbon dioxide (CO_2) and consequent pore water pH decrease. In marine environments chloride-induced depassivation typically occurs earlier so that mechanism receives the most attention, and it is the focus of this dissertation.

B.2 Corrosion Mechanism

Corrosion is defined as the destructive oxidation of metals/alloys as a result of the electrochemical reactions with the exposed environment. The four electrochemical components that are present in the corrosion process are: (i) the anode, where the anodic reaction takes place, (ii) the cathode, where the cathodic reaction occurs, (iii) the electrolyte and (iv) the electronic path.[50] In concrete (where pore water is the

123

electrolyte), iron is dissolved by the anodic reaction, generating cations and electrons as shown in Equation (18). The electrons flow to the cathodic regions through an electronic path (the metal) and are consumed (cathodic reaction, Equation (19) whether by: oxygen (O_2), water (H_2O) and/or hydrogen ions (H^+). The current is also transported by the ions in the pore network of the concrete from the anodic regions to the cathodic regions. High pH and chloride content increases the ion transport.

$$\text{Anodic reaction (iron oxidation): Fe} \rightarrow Fe^{+2} + 2e^- \tag{18}$$

$$\text{Cathodic reaction (oxygen reduction): } O_2 + 2H_2O + 4e^- \rightarrow 4OH^- \tag{19}$$

The electric potential (E)-pH diagram, widely known as the Pourbaix diagram is shown in Figure B 1 .[51] The diagram, based on thermodynamic stability calculations, illustrates the pH and potential regimes where the passive film is stable (passivation region), the solid reduced metal is stable (immunity), and the metal oxidized as ions is the stable form (hence resulting in corrosion). The diagram is calculated for conditions without contamination by chloride ions. If chloride ion concentrations exceeding the value of C_T are present, the passive film experiences breakdown resulting in corrosion even in regions that corresponded to passivity in the Pourbaix diagram.

The process by which the potential change occurs is schematically showed in Figure B 2. The solid black line corresponds to a typical anodic polarization curve of steel (an active-passive metal) in the passive state condition, when embedded in

124

chloride-free concrete. It is assumed that the concrete is exposed to the atmosphere so the cathodic reaction is oxygen reduction, with its polarization function described by the gray line.
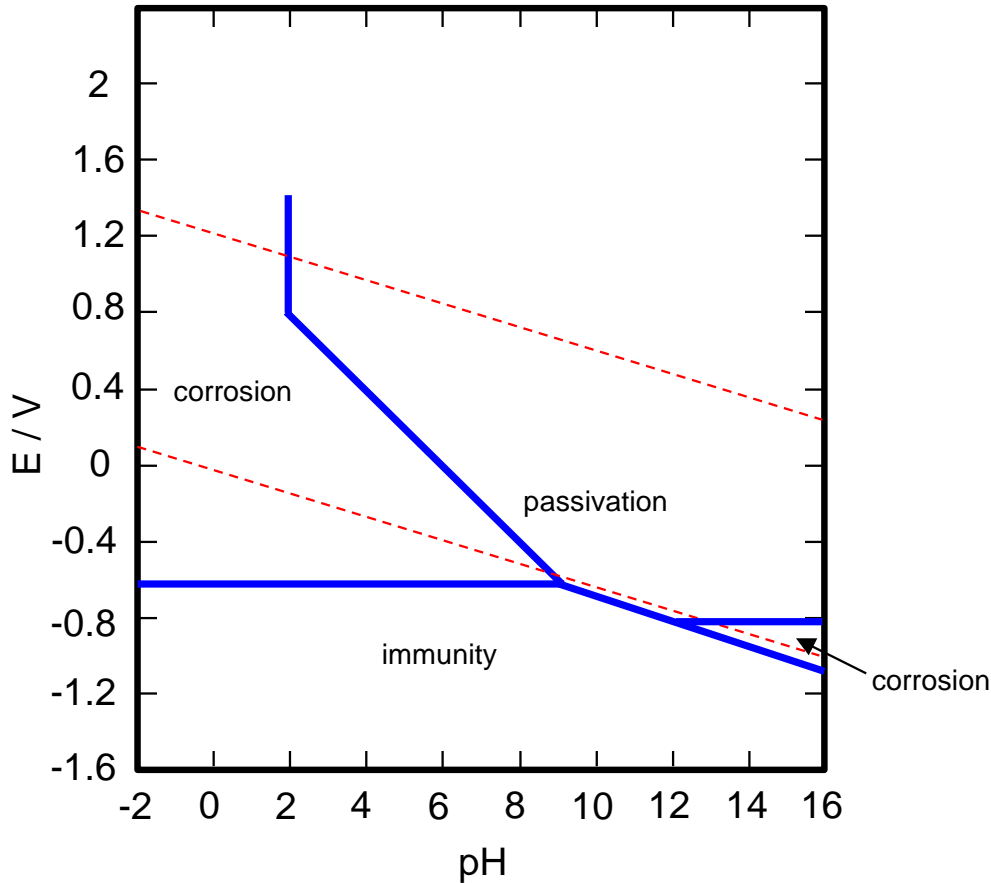

Figure B 1 Theoretical conditions of corrosion, immunity and passivation of iron.

Per the mixed-potential theory the steady state regime is given by the intersection of both lines, where Ep and ip correspond to the electric potential and the anodic current density of the steel, respectively when corroding in the passive state. When the chloride ion content C exceeds C_T, passivity breakdown ensues and in a simplified view the steel polarization curve changes to that corresponding to the active state condition (black-dashed line). A new mixed potential develops to the steady state

potential shifts towards a more negative value (Ea) and the anodic current density increases (ia>>ip), which means a substantially higher value of CR.[50, 52]
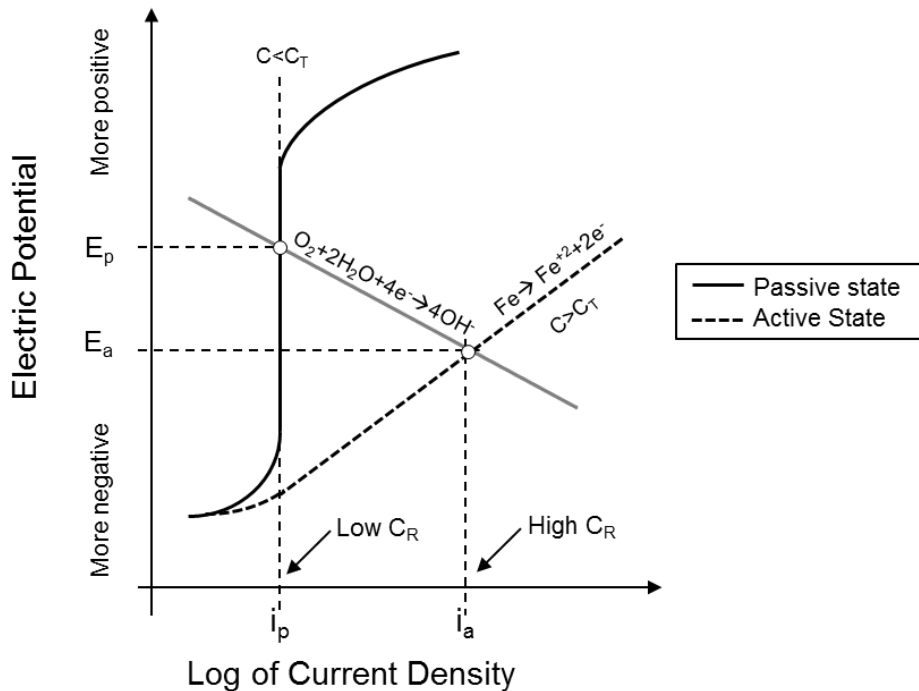
Figure B 2 Potential and current density change of steel embedded in concrete from passive to active condition

B.3 Structural Issues: The Challenge of Long-term Durability

In marine and coastal environments, as in many bridges in the state of Florida, corrosion of reinforced concrete represents a major issue in the infrastructure. FHWA (Federal Highway Administration) requires a minimum bridge design service life of 75 years, representing a challenge when bridges are exposed to severe environments. A recent study from the National Bridge Inventory (NBI) indicates a bridge population of ~600,000 in the U.S., where approximately 15% are categorized as structurally deficient due to corrosion. The direct cost of corrosion for highway bridges in the US represents

126

0.09% ($8.3 billion) of the Gross Domestic Product (GDP); this includes the replacement of structurally deficient bridges. Indirect costs are in the order of 10 times greater. [53-55] In Florida about one half of the state's bridges are exposed to salt water, which highlights the importance of corrosion control in the region.

Long term durability plays a significant role on the design and construction of bridges, since structural reliability, safety and serviceability is needed for extended periods of time.[56] Mathematical predictive models are used to forecast the corrosion damage progression of a structure. Some of the factors that affect the durability of bridges are: 1) chloride presence, relative humidity, and temperature of the site, 2) the quality, permeability, cover, water-to-cement ratio (w/c), types of aggregates, supplementary cementitious materials, presence of chloride ions of the concrete used, and 3) the exposure type (marine, freeze-thaw, de-icing salts, etc.), among others.

Once a structure is placed in service, service life models are still needed to manage maintenance and usage decisions. Quantitative projection of the remaining corrosion-related service life of a structure is necessary for decision making on whether to build a new structure or continue using the existing one. The projections should be sophisticated enough to estimate not only the structure age when substantial damage will appear, but also the rate at which subsequent corrosion damage would develop.

B.4 Chloride Ingress in Reinforced Concrete

Chloride ions accumulate on the surface of the steel to an extent related to the chloride ion build up at the external concrete surface. In structures exposed in marine service, structural elements located near the sea water (tidal zone and splash-

127

evaporation zone) are more susceptible to corrosion. Chloride build up there occurs due to frequent wet and dry event on the concrete surface, during the wet cycle the concrete is moistened and during the dry cycle the sea water evaporates but chloride ions remain and concentrate on the concrete surface.

B.4.1 The Nature of Chloride Ions in Concrete

Chloride ions can be found in concrete due to initial additions to the concrete mix (chloride ions present in mixing water or in aggregates) or by the ingress from an outer and highly concentrated chloride environment such as marine exposure or deicing salts. Chloride ions in concrete are subjected to physical adsorption and chemical binding.[57-59] In the concrete matrix, the total chloride ion content is the sum of the free and bound chloride contents. Free chloride content is that found in the pore water and bound chloride content is that present in the solid phase as a product of the reaction between the chloride ions and some compounds from the cement paste, typically C_3A and C_4AF generating Friedel's salts. [56, 60]

It is noted that only a small portion of the C_3A and C_4AF react with the chloride ions, due to separate reactions such as that of C_3A with gypsum to form ettringite and its transformation to monosulfoaluminate.[61] The relationship between the free chloride and bound chloride content is neither linear nor constant with time, as it depends on factors such as type of cement (content of C_3A and C_4AF), mineral admixtures or cement replacements, curing period, water-to-cement ratio, and use of super-plasticizers, among others.

128

B.4.2 The Transport of Chloride Ions in Concrete

The transport of chloride ions in concrete is governed by various mechanisms. Diffusion occurs due to the presence of a chloride concentration gradient between the outer and the inner parts of the concrete causing an inward transport of the chloride ions through the pore network. Permeation is based on a hydraulic pressure gradient in different parts of the concrete. Migration of chloride is driven by an electric potential gradient from lower to higher electrical potential. Capillary absorption takes place when a moisture content difference in the concrete is present.

Of the above, chloride ingress by diffusion is the most dominant process from the point of view of corrosion progression in major structures where considerably thick clear concrete cover over the steel exists.[50, 57, 62]

Concrete deficiencies at an early stage, such as microcracks, provide paths in which chloride ions can penetrate faster than through bulk diffusion into the concrete. Microcracks are developed by the gradients of temperature and humidity while the concrete is still in the early hydrating stage, generating deformation processes such as shrinkage, bleeding and alkali-silica reactions, which leads to induced stresses into the concrete and intensifies with external loads. Samaha and Hover determined the effect of microcracks in the transport of ions in concrete while applying uniaxial compression loads. [50, 63, 64]Results showed that subjecting concrete to loads lower than 75% of the compressive strength does not have a negative impact in durability. However, drying shrinkage has a greater effect than compressive stress. During a bridge survey Lau et al. found that chloride ingress in minor cracks was most notable in structures with low

permeability concrete, and was relatively less marked in high permeability concrete due to the higher rates of bulk chloride diffusivity, as expected.[65]

B.5 Forecasting the Service Life of Reinforced Concrete Structures

B.5.1 Tuutti's Definition of Service Life

In the early 80's Tuutti divided the length of service life in two stages, initiation and propagation as shown in Figure B 3. [1, 66] The initial stage starts when the structure is placed in service, the steel bar is in its passive state and it ends when the C_T value is exceeded. At this point, the propagation stage takes place and expansive corrosion products (volume typically three times or more than that of the steel that originated them) accumulate at the steel surface, leading to the generation of tensile stresses that cause cracks and spall to the concrete, affecting the durability of the structure.
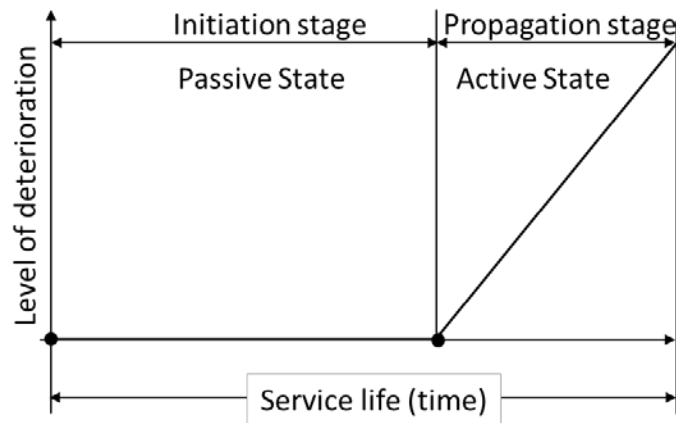
Figure B 3 Service life diagram according to Tuutti

Tuutti's diagram is a simplistic description of the propagation stage, since it assumes a constant corrosion rate, hence other researchers [62, 67, 68] such as Li et

al., have modified the description by adding a more detailed progress of the propagation stage.

B.5.2 Initiation Stage

The stage that has received more attention in the literature is the initiation stage, which in many bridges is found to have longer duration (periods of decades) than the propagation stage, which tends to be much shorter (in the order of only a few years) [69]. Although that situation is not always the case, it is nevertheless common for marine bridges in Florida to be built with plain reinforcing steel in sound concrete of low permeability, so as to maximize the duration of the initiation stage while not explicitly addressing the propagation stage duration.[70]

B.5.2.1 Involved Parameters

Considerable emphasis has therefore been given to the factors that are mainly responsible for the length of the initiation stage in chloride rich environments. Foremost in those factors are the rate of transport of chloride ions in concrete (usually by a predominantly diffusional mechanism, quantified by the chloride diffusion coefficient D) and the value of C_T.

Extensive research work has been conducted on the process of chloride diffusion in concrete and on establishing the chloride threshold value.[5, 71-74] However, the results on the latter are subject to considerable scatter and key issues, such as the dependence of the threshold value on steel potential have remained largely unexplored. The work proposed here focusses on resolving some of those issues.

131

B.5.2.2 Fick's Laws of Diffusion

The phenomenon of diffusion generally follows the mathematical models developed by Adolph E. Fick (1829-1901).[57] The transport of chloride ions in concrete is through the pore water network. Fick's first law of diffusion states that the mass of chloride ions diffusing through a unit area of a section of the concrete per unit time, defined as flux (J), is proportional to the concentration gradient of chloride ions, as it is shown in Equation (20), where the minus sign denotes a mathematical convention since the chloride ingress occurs in the opposite direction (from high concentration to low concentration). The constant of proportionality D, is the chloride diffusion coefficient.

$$J = -D \cdot \nabla C \tag{20}$$

In Equation (21) Fick's second law of diffusion expresses the time-dependent evolution

$$\frac{\partial C}{\partial t} = \nabla \cdot J = \nabla \cdot (D \nabla C) \tag{21}$$

In practice D is obtained from acid-soluble chloride concentration measurements of chloride-exposed laboratory or field samples at different depths, thus yielding a concentration profile that can be mathematically fitted to a solution of Equation (3) using the value of D as a fit parameter. Implicit in that process is the simplifying assumption that D is time- and space-invariant. D is frequently considered to be a material property that is an inverse indicator of the concrete's resistance to the penetration by chloride

132

ions.[50, 71] Fick's second law of diffusion is widely used to model and analyze the chloride transport in concrete. One of the first pioneers in modeling chloride diffusion in concrete was Collepardi et al in 1970, where the model was based on Crank's error function solution of Fick's second law for the one dimensional case with constant chloride surface concentration (C_S), shown in Equation (22).[32, 75] There the diffusion coefficient is considered as a constant parameter, C0 is the initial (native) chloride content in the concrete (also treated as constant) and *erf* is the error function.

$$\frac{C - C_0}{C_s - C_0} = 1 - erf\left(\frac{x}{\sqrt{4Dt}}\right) \tag{22}$$

B.5.2.2.1 Limitations

More sophisticated chloride transport approaches than those considered above exist. Previous investigations have found that concrete evolves with time, often resulting in a less-interconnected pore network as hydration and pozzolanic reactions progress. The diffusion process changes accordingly, becoming slower. Authors including Takewaka, Mangat and Molloy, Tang, [62] and others suggest the incorporation of a time dependent diffusion coefficient to develop less conservative damage forecasts.[29, 76-78].

Some authors disagree with the use of the analytical solution of Fick's second law of diffusion to approximate the chloride transport in concrete, mainly because it neglects the effects of moisture, the presence of other ionic species (eg. Na+, OH-) and of chloride binding. Saetta, Marchand, Samson, Johannesson, along with many other

133

authors, have published models where chloride binding, multi-ionic interaction, temperature, humidity are addressed.[79-83] However, these advanced and sophisticated models reach to a point where they can become impractical due to the complexity and the relative lack of precise input data for the many parameters involved.

B.6 Critical Chloride Corrosion Threshold

B.6.1 General

The selection of the best chloride content expression to quantify the chloride threshold has been the subject of significant discussion in the technical literature. Most authors recognize that C_T should be expressed as a fraction of the cementitious content of the concrete.[84, 85] Some have proposed that only the free chloride content (that in the pore water) represents a corrosion risk to the steel, so that C_T values should be reported in terms of the free chloride content in the concrete. In such cases, the threshold may be alternatively expressed as a ratio of chloride to hydroxide ion content in the pore water.[86, 87] In contrast, Glass and Buenfeld concluded that the effect of the bound chloride content cannot be neglected, since it can be released by local acidification in an incipient corroding region that helps to stabilize the corrosion process there.[85] These authors and others have noted too that free chloride content is subject to variations due to the moisture content of the medium and that the chloride to hydroxide ion ratio is dependent on the pH. Hence, presenting C_T as the total chloride content mass by mass of cement seems at present to be the best approach since it includes free and bound chloride content and the inhibitive nature of cement matrix.

134

B.6.2 Measuring the Value of C_T

Various experimental methods to determine the value of C_T can be found in the literature. These include assessment of mortar, concrete and simulated pore water. The ionic transport may be through diffusion, capillary suction (wet and dry cycles), and migration. In all these methods, it is essential to establish the precise moment in which corrosion initiation has taken place.

Transient electrochemical techniques tend to provide a more accurate detection of the moment of corrosion initiation than half-cell potential transitions. The most common techniques of this type are linear polarization resistance (LPR) and electrochemical impedance spectroscopy (EIS). These techniques are essentially non-disruptive as they involve only small potential deviations from the steady state condition. The techniques allow for highly sensitive estimation of the corrosion rate (CR) increase associated with the corrosion initiation event. Typically a steel specimen is declared to be in the actively corroding condition when CR > 0.2µA/cm^2.[10]

Time of corrosion initiation can be also detected by measuring macro-cell currents. ASTM (American Society for Testing Materials) G109 "Standard Test Method for Determining Effects of Chemical Admixtures on Corrosion of Embedded Steel Reinforcement in Concrete Exposed to Chloride Environments" is a test method that uses concrete slabs exposed to saltwater wet and dry cycles near the top with one embedded steel bar near the top surface and two steel bars embedded near the bottom (in a chloride-free region). The bars are interconnected and the corrosion macro-cell current is monitored as function of time.[30] A sharp increase in the current indicates

that the bar near the top has experienced passivity breakdown and entered active corrosion. In an investigation by Hartt et al. where G-109 specimens were assessed, active corrosion was deemed to have occurred when the macrocell current exceeded 10µA. The concurrent drop of potential (to < -280 mV versus saturated calomel electrode (SCE)) served as a parallel indicator of activation.[88]

Another method to detect corrosion initiation is through monitoring the impressed current between the steel bar and an auxiliary electrode, a method mostly used to determine the onset of active corrosion when the steel embedded in concrete is under potentiostatic control, meaning that the steel bar is polarized at a fixed potential. This method is used in research aimed to determine the extent to which C_T varies with steel potential. When the steel is in its passive state and cathodically polarized (more negative potential), the impressed current density is found to shift upon activation to a lesser cathodic amount or to a distinct anodic regime, clearly defining the activation event in either case.

As soon as the onset of active corrosion has been confirmed by the methods mentioned above, the next step is demolition of the specimen for a visual inspection to confirm the existence of corrosion. Immediately afterwards, concrete powder collection is made, by grinding, drilling or crushing the trace of the rebar on the surrounding concrete to depths < 1 to 2 mm.[10] Since concrete is a heterogeneous medium (hydrated cement paste, fine and coarse aggregate), it is important to ensure that of the proportion of cement paste to aggregate in all samples collected is nearly the same.[10]

136

The final step is to perform the determination of the chloride content by a suitable assaying method depending on the desired form of expressing the value of C_T. Since this investigation will focus on total chloride content by weight of cement, the focus will be on chloride analysis methods applicable for that expression.

Standardized procedures to determine the total chloride content developed by ASTM and RILEM (International Union of Laboratories and Experts in Construction Materials, Systems and Structures, acronym in French) can be found in the literature FDOT (Florida Department of Transportation) follows its own method based on potentiometric titration using ion selective electrodes.[22, 89, 90]. This later methodology was chosen for much of the research proposed here.

B.6.3 Chloride Corrosion Threshold: Influencing Parameters

In the literature there is wide scatter of data on values of reported C_T. In some cases that variation is by more than two orders of magnitude. Part of that scatter reflects that the experimental work regarding C_T has been neither systematic nor consistent, with most of the experimental assessments following methodology that departs to some extent from the others. Consequently much uncertainty exists when attempting to comparing data from different studies. Hence nominal, conservative values of C_T tend to be adopted for design purposes. For example, a C_T value of 0.2% by weight of cement for carbon steel bars was proposed in a study performed by Clear in 1976, for the design phase and for durability forecast of reinforced structures [91], but the range of 0.2% to 0.5% is also often considered. Despite the scatter, some general trends have been identified indicating that the value of C_T depends on many parameters. In addition

137

to the type and amount of cement in the mix such parameters include: condition of the steel surface, exposed area of the steel, concrete properties, oxygen availability at the steel surface temperature, pore solution composition, w/c ratio, type of chloride salt and chloride source, as well as the potential of the steel while in the passive state.[5] This last factor in particular has received little attention in the literature. As it is shown elsewhere in this Dissertation consideration of that dependence can strongly affect the projected extent of damage in a structure, and has been chosen for detailed study in the proposed dissertation work.

B.6.3.1 The Dependence of C_T on Steel Potential While in Passive State

There is increasing evidence that the chloride corrosion threshold increases substantially when the still passive steel is polarized to potential values more cathodic than the typical open circuit potential in atmospherically exposed concrete. The latter is in the order of ~-100 mV (SCE).[83] As a result of that increase, when corrosion starts at a given location in a reinforced concrete structure and the potential of the steel drops towards more negative values, macrocell coupling with nearby steel lowers the potential there as well. Consequently the local value of C_T increases in adjacent regions which delays corrosion initiation of the passive steel there.

Previous investigators have shown that a negative polarization of several hundred mV may be needed to attain an increase in corrosion initiation threshold of about one order of magnitude. However, much of the available data in the literature shows a large scatter on the values of C_T since experimental assessment was not conducted specifically to investigate the chloride threshold dependence on potential in

138

steel embedded in concrete, instead, other issues were investigated such as: stability of the passive layer in alkaline solutions, [86] C_T of the steel submerged in alkaline solutions with salt (NaCl or KCl), [92, 93] C_T of steel embedded in concrete with ordinary Portland cement (OPC) varying the potential to determine depassivation, among others.[94, 95] Consequently, the functional relationship between C_T and potential was affected by much uncertainty.

An experimental investigation that focused on determining the chloride corrosion threshold dependence on potential was first made by Alonso et al. Their results indicated that C_T increased when potentials were more cathodic than -200±50 mV (SCE) and was relatively independent of the potential when it is more anodic than that value.[9, 10]. They identified a functional relationship (see Equation (1)) with tentatively identified parameters. However, the trends from Alonso et al. were obtained from limited test conditions involving a small area of steel (6 cm^2) beneath a thin mortar cover (0.5 cm.), conditions that tend to add uncertainty to the values of C_T obtained.[10] A systematic investigation that addresses the issues and uncertainties of the latter investigation was needed to confirm and validate the dependence of C_T on steel potential, resulting in some of the work presented here.

139

Appendix C Modeling Equations for the Corrosion Distribution Module

As introduced in Chapter 2 the modeling process involves several key tasks that can be stated as follows:

- Build a model that determines the time dependent ingress of chloride ions, the locations and times where the chloride threshold is exceeded, and the resulting distribution of potentials and corrosion currents over an entire structure.

- At each time step, the model needs to recalculate the potential pattern based on which regions just became active, and reevaluate the local chloride threshold of the adjacent passive regions. This task effectively addresses a moving target.

- With that reevaluated chloride threshold, determine which new locations will become active in the next time step, and what will be the new potential pattern for the subsequent step.

- The model also has to keep track of the accumulated degree of corrosion at each location to establish where and when the propagation stage of corrosion has been completed, so that a damage function tally is updated as the structure ages.

The tasks were addressed in three modules that are described in Chapter 2 and summarized in Figure C 1. The chloride concentration at the rebar surface, determined at every time step, is denoted by C_{Cl}. As mentioned in Chapter 3, each module determines the system's conditions at each time step.

Chloride transport /activation module

C_{Cl} at each node compared with previous time step	If $C_{Cl} > C_T$, node is declared active for next time step	Anodic dissolution is assumed to occur at active node

Corrosion distribution module

Compute E_s and corrosion rate of steel at each element	Based on passive/active characteristics of steel in previous time step	Results in E_s for next time step, calculated new value of C_T at each node

Surface damage evaluation module

Local corrosion rate at the element for each node is integrated $f(t)$	Converted into local corrosion penetration (P)	When $P > P_{critical}$, external concrete surface is declared damaged

Figure C 1 System model modules

The chloride transport part of the transport/activation module is straightforward with the simple conditions indicated in Section 3.2.2 so no it will not be addressed here, other than noting that more refined versions of the model could include the effect of changes in the electric field within the concrete (from the corrosion distribution module) as an additional term. The Surface damage evaluation module was described in Section 3.2.3.

This Appendix presents additional details on the Corrosion Distribution Module. For this module the potential distribution within the concrete was evaluated as follows under a 1-dimensional scheme. A simple rectangular section system with a single lateral flat steel surface is considered first. Per Figure C 2, using the principles of conservation of charge and assuming that the corrosion macrocell current travels through the area of concrete Ac along axis z and is progressively increased or

decreased as it sinks or is sourced at area of steel As, the net current density on the steel surface at elevation z is expressed in Equation (23).

$$i_S \, As = -Ac \left.\frac{dE}{dz}\right|_z \sigma_z + Ac \left.\frac{dE}{dz}\sigma\right|_{z+dz} \sigma_{z+dz}$$
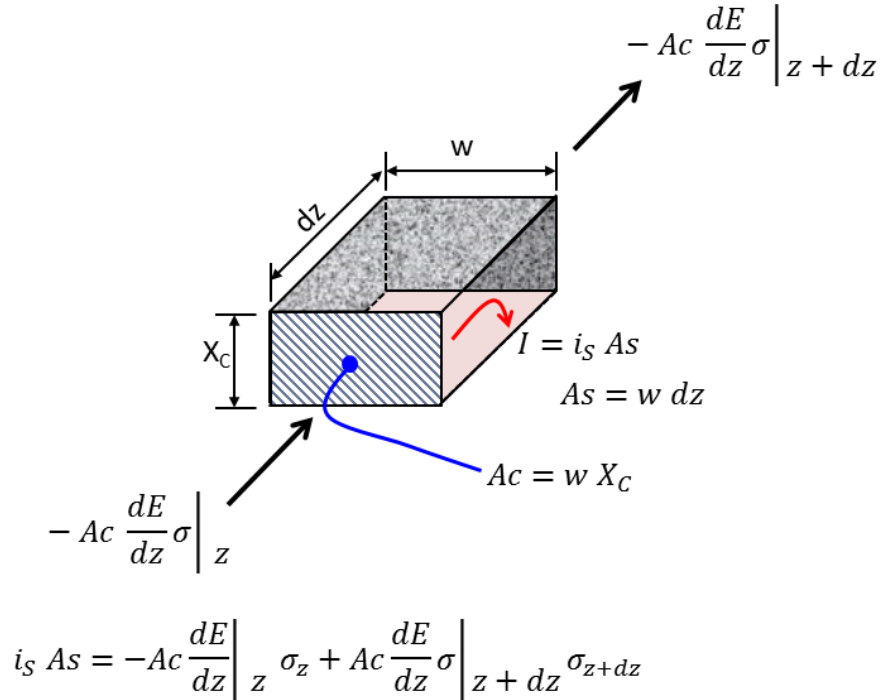
Figure C 2 Idealized current flow and potential relationship in a concrete slab with steel as a flat plate on the side

$$i_S \; = \frac{Ac}{w}\left(\sigma \frac{d^2E}{dz^2} + \frac{dE}{dz}\cdot\frac{d\sigma}{dz}\right) \tag{23}$$

where σ: electric conductivity of the concrete.

Extending the concept to the case of a concrete column where the steel is no longer a flat plate but instead is the external surface of a rebar assembly yields the situation described in Figure C 3 and resulting in Equation (24).

$$i_S \; = \frac{\varphi}{4 \, SF}\left(\sigma \frac{d^2E}{dz^2} + \frac{dE}{dz}\cdot\frac{d\sigma}{dz}\right) \tag{24}$$

142
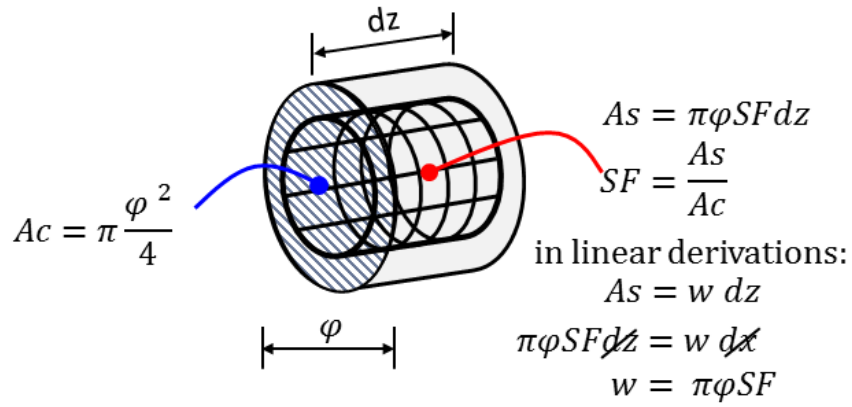
Figure C 3 Idealized current flow in a reinforced concrete column

The equation for i_S was solved using finite difference method with the following formulations:

$$\frac{d^2E}{dz^2} = \frac{1}{\Delta z^2}\left(E_{\gamma+1} - 2E_\gamma + E_{\gamma-1}\right) \tag{25}$$

$$\frac{dE}{dz} = \frac{E_{\gamma+1} - E_{\gamma-1}}{2\Delta z} \tag{26}$$

$$\frac{d\sigma}{dz} = \frac{\sigma_{\gamma+1} - \sigma_{\gamma-1}}{2\Delta z} \tag{27}$$

143

Equations,(29), (30), (31) were then implemented by relating i_S to the local potential (with additional accounting for local resistance polarization) as described under sections 3.2.2 of the main body of this dissertation.

Appendix D Probabilistic Damage Projection[6]

D.1 Principles of Probabilistic Corrosion Damage Projection

As a preamble to this Appendix, the reader is referred to the introductory remarks given in Section 6.2 prior to the start of Section 6.3.

As detailed in Ref [3] from which part of the following is extracted, t_s for a given element in a Class may be viewed as a function of parameters such as X_C, D, C_S, C_T, etc.:

$$t_s = f(X_C, D, C_S, C_T \dots) \tag{28}$$

If the values of all the parameters other than X_C were kept the same, then the value $X_{C'}$ of X_C that results in damage appearing at time $t_s \leq t_p$ could be expressed as a function of the other parameters such as:

$$X_{C'} = f(t_s, D, C_S, C_T \dots) \tag{29}$$

For generality, a series of variables $X_C, V_2 \dots V_n$ can be considered where $V_2, \dots, V_n$ represent all the relevant factors other than X_C. Thus a more general form of Equations. (34) and (35) is:

$$t_s = f(X_{C'}, V_2, \dots, V_n) \tag{30}$$

---

[6] This appendix includes previously published material from a publication of which the author of this dissertation is the lead author [47].

145

$$X_{C'} = f(t_s, V_2, ..., V_n) \tag{31}$$

In an actual structure these parameters are subject to variability that can be both systematic (for example changes with elevation) and probabilistic (such as changes in batch-to-batch of concrete). It will be assumed that the structure can be divided into separate Classes such that within each range the values of variables $X_{C'}$, $V_2...V_n$ obey independent probability distributions. In the following, Classes will be numbered 1,2,...i....N_r, and elements within each region will be numbered 1,2,...j...N_i.

Calling P_{ki} the probability distribution function for variable V_k in region i and $P_{cum1i}(X_{Cs})$, the cumulative probability for X_{Cs}, the PDF takes the form

$$Nd(t)/N = (1/\textstyle\sum_i N_i) \sum_i N_i \int_{V2} \cdots \int_{Vn} P_{cum1i}(F(t, V_2,..V_n)) P_{2i}(V_2)...P_{ni}(V_n)\, dV_2...dV_n \tag{32}$$

where $Nd(t)$ is the number of elements in the entire bridge reaching damage declaration at age t, N is the total number of elements in the bridge, and N_i is the number of element in Class i.

For the model implementation addressed in this report, the relevant variables have been chosen as $V_2= C_S$; $V_3=D$; $V_4=C_T$; $V_5=t_p$, of which only X_C, V_2 and V_3 are distributed while V_4 and V_5 are constants within each Class. Variability in C_T, however will be implemented explicitly via the dynamic evolution models, and implicitly via variability in C_S as noted later (Appendix E). Because in the cases of interest t_p tends to be small compared with t_i, variability in t_p will not be addressed but that choice is

146

deemed to be of little impact on the model output. Assuming simple Fickian chloride diffusion, time-invariant chloride diffusion coefficient and surface concentration results in t_s being given by

$$ts = \frac{x^2}{4D\left(\operatorname{erf}^{-1}\left(1-\frac{C_T}{C_S}\right)\right)^2} + tp \tag{33}$$

and

$$\frac{Nd(t)}{N} = \frac{1}{\sum_i N_i} \sum_i N_i \int_{Dli}^{Dhi} \int_{Csli}^{Cshi} P_{cumxi}\left(2\sqrt{D(t-tp_i)}\operatorname{erf}^{-1}\left(1-\frac{C_T}{C_S}\right)\right) P_{csi}(Cs)\, P_{Di}(D)\, dCs\, dD \tag{34}$$

where Dl_i, C_Sl_i and Dh_i, C_Sh_i represent the lowest and highest values, respectively, of D and C_S, in Class i. The total projected damaged surface area S(t) in the substructure at age t is then:

$$S(t) = Nd(t) \cdot A_e \tag{35}$$

The choice of parameters defining the probability distributions of X_C, C_S and D as well as the integration limits for each Class is addressed in Appendix E.

147

Appendix E Integrated Predictive Model[7]

An Integrated Predictive Model was developed as part of a project conducted for the Florida Department of Transportation (FDOT) to create a prototype next-generation model that incorporates both probabilistic parameter distributions, the effect of PDT, and other advanced features reflecting the state of the art in this type of application.[47]

The model version is intended to serve as a working prototype for evaluation and subsequent adaptation by FDOT into user-compatible platforms that may include versions for internal FDOT use, and versions for incorporation in the Structures Design Manual and related documentation for a broader audience. Internal default values for parameters in the alpha model include provisional entries (see Table 6) that are updatable as new information or improved interpretation of existing data becomes available.

Eventual use of the model for decision making purposes is contingent on subsequent finalized adoption of an appropriate set of parameter values as well as updated simplifying assumptions as needed. The model receives user input on the makeup of a bridge substructure (highest corrosion risk region) including for each type of component, the structural configuration, materials of construction and service environment, and develops an output consisting of the corrosion-related damage function for a long period (e.g. 100 years) for each Class of structural/environmental combinations and for the structure as a whole. The following functionalities are incorporated.

---

[7] This chapter includes previously published material from a publication of which the author of this dissertation is the lead author [47].

148

E.1 Structural Components

The model addresses three types of structural components: square piles, rectangular footings, and round columns, each having type-specific external dimensions and steel clear cover. The clear cover can be either as prescribed by the SDG according to the environmental classification of the service environment (see next item), or user-selected if the effect of variations from prescribed values is to be explored. The rebar size is selectable as well. Based on the type and size of the component, a fraction of its surface is assigned to one of four chloride penetration regimes: flat wall, 2-way corner, 3-way corner and round.[96] For square piles of side dimension Y the perimeter of the cross section is 4Y, of which a fraction $8*(X_C)/4Y$ (where X_C is the steel cover) is deemed to correspond to the length of the perimeter representative of a 2-way corner exposure geometry, and the rest $(4Y-8*(X_C))/4Y$ to the flat wall exposure geometry. A comparable assignment based on rebar cover and dimensions is made for the parallelepiped footing geometry to assign fractions representative of flat wall, 2-way and 3-way corners. For round columns, the entire surface is assigned a round condition.

E.2 Exposure Conditions

Each component type can be distributed (by specifying number of components in each) into two main types of exposure conditions: in water (IW), and in soil (IS). For the IW type there are 4 sub-exposure types: submerged near surface, tidal zone, splash-evaporation, and atmospheric (S, T, SE and A, respectively). The model does not require user entry for the total absolute elevation range at-corrosion-risk, which has been internally set at 16 ft starting 2 ft below the bottom of the T condition region, as a

149

placeholder to represent typical conditions in marine substructure. However, user input for that range size as well as for the fraction assignations given next can be easily implemented in new model versions if desired. The sub-exposure type fractions of the total elevation range are assigned as 1/8, 1/8, 3/8 and 3/8 of the total for S, T, SE and A, respectively. Square piles and columns are assumed to be of uniform cross section and exposed laterally to the entire range, so the corresponding at-corrosion-risk area fractions are given by the same values. Footings are assumed to be exposed only to the S,T and SE regimes, laterally as well as on the top surface for the SE regime, with the corresponding surface area fractions calculated accordingly by simple geometry. For the IS type there are two sub-exposures types: buried and atmospheric (B and A, respectively), each spanning a nominal height of 8 ft for piles and columns and assigning each ½ of the at-risk area. For the footings the B and A elevation ranges are assumed to be 5 ft each, with area fractions obtained by appropriate calculations. More complicated structural member geometries, including for example columns on top of footings can be incorporated for each of the exposure condition types at the discretion of the Florida Department of Transportation following the same procedures.

For the IW and IS components, three environmental classifications (Extremely Aggressive, Moderately Aggressive and Slightly Aggressive) can be selected by the user. By selecting an environmental aggressiveness, default values for the chloride concentration in water, chloride concentration in soil, and concrete cover are assigned in accordance to the SDG. Those default values can be modified by the user as well.

E.3 Concrete Properties

Each component type is assigned an FDOT concrete class ranging from concrete class I to concrete class VI. In the present model implementation, for simplified generic calculations each concrete class is assigned a time- and space-invariant value of chloride ion diffusion coefficient, with a baseline provisionally abstracted from the present body of properties information from FDOT reports and related data. The baseline values for the concrete classes are listed in Table 6. As a first alternative to default values, user-selected values of the diffusion coefficient can be directly entered in the worksheet to replace the baseline value. As a second alternative, the user can have the program obtain an estimate of the diffusion coefficient based on concrete cement factor, percentage of pozzolanic or slag cement replacement and water-to cement ratio. The calculation is performed using the relationship developed under FDOT project BA502 [39] to estimate concrete chloride diffusion coefficients, based on regression of field data from a group of bridges about 10-years old and built with modern concrete formulations. That estimate is best applicable to the higher concrete class types.

Once the diffusion coefficient is set, a multiplier is assigned based on the ratio of rebar diameter Φ_r to concrete cover X_C to reflect the increased rate of chloride accumulation due to the obstruction presented by the rebar. The value of that multiplier ($1/Tf$), related to the ratios of Φ/X_C and the C_T/C_S, has been abstracted from work developed in prior FDOT projects assuming a flat wall regime with the presence of a single rebar. [24,32] Additionally, the value of the chloride diffusion coefficient is further conditioned (to obtain a fictitious equivalent value) by adopting a multiplying factor to correct for the geometric regime effects (2-way corner, 3-way corner and round) based

151

on characteristic correction factors developed in an earlier FDOT project.[38] For the case of the round columns, the factor is a function of the ratio C_T/C_S and the ratio of the radius r of the column to concrete cover X_{Cobs} corrected for the rebar obstruction effect. Reference [39] reported values only for X_{Cobs}/r = to 0.1, 0.2, and 0.3; therefore the correction in the present version is constrained to those values. Cases with X_{Cobs}/r values less than 0.1 or greater than 0.3, are approximated as having a value of 0.1 or 0.3, respectively. All these geometric adjustments are slated for more refined treatment in future versions of the model.

The same FDOT project that developed a Tf adjustment to correct for rebar presence in a flat wall also investigated the case of a 2-way corner with a single rebar presence.[32] Results were comparable with those obtained assuming a 2-way corner geometry without correction for rebar obstruction effect, likely because the corner geometry already incorporated a strong multi-dimensional aggravation of chloride ingress. Therefore, in the present model chloride penetration in a 2-way corner geometry regime was not adjusted for rebar presence. For the case of a 3-way corner there is no available information at present on the effect of rebar presence, but by analogy with the 2-way case no correction for rebar presence was made in this situation either, it is suggested that the rebar presence effect in 3-way corner geometry should be examined in follow-up investigations.

Following practice from previous probabilistic model realizations in FDOT-sponsored modeling efforts, the chloride diffusion coefficient distribution was represented by a normal distribution with an average value equal to the baseline after

152

being modified for the appropriate adaptations indicated above, and with a coefficient of variation and upper and lower limits values as listed in Table 6.

Notably, the present modeling approach does not include time-variability of the chloride diffusion coefficient, whereby some reduction in value would be projected as the structure ages.[98] That feature is not included because much on the information on chloride diffusion coefficient developed by FDOT has been obtained from cores extracted from its structures at mature ages (e.g. typically >10 years [42]), in the form of effective long-term diffusion coefficient values. It is those diffusion coefficient values, rather than values extrapolated from very short term laboratory tests, that are primarily intended to be used in the model developed under this investigation. This choice of time-independent diffusion coefficient is somewhat conservative, especially for concrete with pozzolanic and slag additions where the most pronounced further decreases in the diffusion coefficient might be expected as a structure ages [76, 97, 98].

It is noted that scarcity of long term data introduces uncertainty in the validity of expecting a sustained decline in diffusion coefficient in the long term. Indeed, in the Life-365 program [97] credit for beneficial aging is suspended for that reason for periods beyond about 3 decades of service. Hence, the extent of conservativeness introduced by using the present approach is limited as it concerns a relatively short relative time period before other uncertainty sets in. The potential beneficial reduction in diffusion coefficient would be limited as well due to its dependence being expected to follow only a fractional power law.[97]

153

Nonetheless, additional features for future development have been included in the model as placeholders. These include: a) the use of the rapid chloride migration coefficient (D_{RCM}) obtained through the Nordtest NT Build 492 procedure [99] to convert it into an effective chloride diffusion coefficient, and b) the expansion to admit user input to obtain chloride diffusion coefficient based on concrete resistivity or laboratory permeability data, which can potentially be incorporated with the availability of the output just published from FDOT Project BDK79-977-02.[100] In those cases, provision to account for an age factor in the value of the chloride diffusion coefficient will be necessary in future versions of the model.

At present, the model assigns for simplicity the same chloride diffusion coefficient (representative of the more severe conditions prevalent at the lowest elevations) to all the elevations within a structural element. The resulting conservativeness may be reduced as more data documenting lower diffusion coefficients at higher elevations [42] become available, by implementing user entry for elevation-dependent values. That implementation is in principle straightforward in new model versions. Likewise, the model does not make provision for input on local average temperature. Should precise enough data on chloride diffusion coefficient variation with temperature (within the relatively limited range existing in Florida) become available, a temperature correction factor can also be included in future versions.

E.4 Surface Conditions

Each of the exposure types and sub-exposure types noted above has been assigned a specific value of C_S as listed in Table 6. Those values are provisionally

154

abstracted from the present body of properties information from FDOT reports and related data and capture trends of decreasing chloride accumulation with elevation for evaporative regimes, and chloride concentration below water. Similar to the treatment of concrete properties, following practice from previous probabilistic model realizations in FDOT-sponsored modeling effort, the surface chloride distribution was represented by a normal distribution with a standard deviation (conservatively selected as noted below) and upper and lower limits values listed in Table 6. As an alternative, the user can enter a preferred value of C_S for each sub-exposure condition.

E.5 Chloride Threshold and Rebar Type

For its PDF calculations described in Appendix C, the program has plain steel (PS) as the default rebar material, and as alternatives options: galvanized steel (GS), "MMFX" (ASTM A1035) and a generic austenitic stainless steel (SS). The assumed value of C_T for PS is a value equal to 0.04% of the nominal CF of each of the concrete classes, which is listed in Table 6. For the other materials the default value of C_T is adjusted by a respective multiplier also listed on Table 6. All those values have been provisionally abstracted from the information available from FDOT previous investigations and other literature sources, but are included primarily as placeholders for future development and do not constitute an endorsement of specific products and materials.

The defaults can be overridden by the user if alternative scenarios are to be explored. Variability in C_T for the PDF calculation is implemented implicitly to some degree via the amount of variability conservatively assumed for C_S, since the time to

155

corrosion initiation is not a function of C_T by itself but, per Equation (33), of the ratio C_T/C_S, so variability in C_S results in variability in the ratio even if C_T is constant. The program introduced additional, time-variable dispersion in C_T via the subsequent conversion of the PDF into the PF by the procedures described in Chapter 6.

E.6 Propagation Time

A default flat value of 5 years has been assigned to the value of propagation time tp, representative of the choice used in previous FDOT projects for the development of predictive models, and per the arguments for limited need to capture variability of this parameter. However, the default can be overridden by the user if alternative scenarios are to be explored, especially for the case of SS rebar, where there are indications in the literature that much longer corrosion propagation times may develop.[101]

E.7 Limit State

A corrosion related damage limit state of 2.3% surface damage (that may be viewed as being comparable to the limit value adopted by LNEC, an European agency [102]) has been incorporated as a default for rapid informal contrasting of results against an assumed durability goal, either for specific structural/environmental Classes or for the entire bridge. That default value is presented only as an example, as the development of a corrosion related damage limit state, which may have different values for specific Classes and a different meaning if applied to the entire structure, is an open issue to be decided by FDOT in future discussions. The default value can be overridden by the user to explore alternative scenarios.

156

Table 6 Concrete and steel bar properties for modeling parameters

Notice: These values are provisional selections intended primarily to establish model functionality. Subject to update and modification pending subsequent data evaluation, and decision on implementation of the program

Chloride Diffusion Coefficient, D						
D / in^2 y^{-1}	1	0.3	0.1	0.025	0.01	0.0075
Concrete class	I	II	III	IV	V	VI
Distribution formulation	mean μ	standard deviation sd	lower limit	upper limit		
	D	25%	3 × sd	10 × sd		

Chloride Surface Concentration, Cs					
			C_S / pcy		
Cl⁻ Concentration in Water / ppm:	>6000		Sq. Piles	Footings	Columns
		Submerged	15	15	15
		Tidal	40	40	40
		Splash-Evap.	40	40	40
		Atmospheric	15		15
Cl⁻ Concentration in Water / ppm:	≤6000				
		Submerged	7.5	7.5	7.5
		Tidal	20	20	20
		Splash-Evap.	40	40	40
		Atmospheric	10		10
Cl⁻ Concentration in Soil / ppm:	>2000				
		Buried	10	10	10
		Atmospheric	10	10	10
Cl⁻ Concentration in Soil / ppm:	>2000				
		Buried	7.5	7.5	7.5
		Atmospheric	7.5	7.5	7.5
Distribution formulation	mean μ	standard deviation sd	lower limit	upper limit	
	C_S	25%	3 × sd	3 × sd	

Chloride Threshold, C_T					
Type of rebar	Plain Steel	Galvanized	MMFX	316L	316L-clad	-
Multiplier	1	2	4	10	10	-
Concrete class	1	2	3	4	5	6
CF / pcy	544	575	600	650	700	752
C_T / pcy	2.18	2.30	2.40	2.60	2.80	3.01

Appendix F Copyright Permissions

F.1 Permissions to Publish Contents in Chapter 2

Reproduced with permission from NACE International, Houston, TX. All rights reserved. Paper 1728 presented at CORROSION/2012, Salt Lake City, UT. © NACE International 2012.

PURPOSE OR CONDITIONS OF ACCURACY, COMPLETENESS OR QUALITY AND THOSE ARISING BY STATUTE OR OTHERWISE IN LAW, ARE HEREBY DISCLAIMED.

IN NO EVENT WILL NACE BE LIABLE FOR ANY DIRECT, INDIRECT, PUNITIVE, SPECIAL, INCIDENTAL OR CONSEQUENTIAL DAMAGES IN CONNECTION WITH OR RELATED TO THIS AGREEMENT (INCLUDING LOSS OF PROFITS, USE, DATA, OR OTHER ECONOMIC ADVANTAGE), HOWSOEVER ARISING.

This Agreement and the rights granted herein may be terminated immediately by NACE upon breach of this Agreement by Publisher. Unless earlier terminated, this Agreement and the rights granted herein will automatically terminate 6 months from the Date set forth above. If the Work has not been published within that time period, a new Agreement must be obtained.

Publisher may not, directly or indirectly, sell, assign, sublicense, lease, rent, distribute, or otherwise transfer this Agreement or any rights granted herein, without the prior written consent of NACE.

If any provision of this Agreement is found to be unenforceable, then this Agreement shall be deemed to be amended by modifying such provision to the extent necessary to make it legal and enforceable while preserving its intent. The remainder of this Agreement shall not be affected by such modification.

This Agreement does not create, and shall not be construed to create, any employer-employee, joint venture or partnership relationship between the parties. No officer, employee, agent, servant or independent contractor of either party shall at any time be deemed to be an employee, servant, agent or contractor of any other party for any purpose whatsoever.

This Agreement shall be governed by, and construed and enforced in accordance with, the laws of the State of Texas, without regard to the choice of law provisions of that State.

This Agreement shall only be effective if signed by authorized representatives of both parties. This Agreement constitutes the entire Agreement between the parties with respect to the subject matter of this Agreement. Any change, modification or waiver hereto must be in writing and signed by authorized representatives of both parties.

Other Terms & Conditions: _____
_____

Publisher hereby requests permission to publish the paper/article described above and agrees to comply with all Terms and Conditions listed above.

Request submitted by:

Andrea N. Sánchez
Printed Name

Graduate Research Assistant
Title

Signature

5 | 8 | 2014
Date

Request approved by NACE:

Daniela Freeman
Printed Name

Audience Development Manager
Title

Signature

7/7/14
Date

Request agreed to by:

Andrea N. Sánchez
Lead Author Printed Name

Graduate Research Assistant
Lead Author Title

Lead Author Signature

5 | 8 | 2014
Date

PermissiontoPublishNACECopy

159

Permission to Publish
NACE International
Copyrighted Paper/Article .

NACE International
1440 South Creek Drive
Houston, TX 77084
Tel: 281-228-6219
Fax: 281-228-6318

Date: 5/8/2014

Name: Andrea N. Sánchez   Title: Graduate Research Assistant

Company ("Publisher"): University of South Florida

Address: 4202 E Fowler Ave, ENB 118, Tampa, FL, 33647

Tel: ▮▮▮▮▮▮▮   Fax: _____

Email: asanchez1@mail.usf.edu

Publication Media: Check the applicable Box:

☐ Magazine/Journal ("Periodical"): _____ Issue: _____

☐ Web Site URL ("Web Site"): _____

Circle the source: Materials Performance   CORROSION   (Conference Paper)   Standards

Paper/Article Title: Chloride Corrosion Threshold Dependence on Steel Potential in Reinforced Concrete   ("Work") Conference Paper No./Year: 4118/2014

Authors: Andrea N. Sánchez and Alberto A. Sagüés

NACE International ("NACE") hereby grants to "Publisher" the right to publish the Work utilizing the Publication Media elected above. To the extent the Publication Media is a Periodical, the publication right is limited to publication in the specific issue identified above of the Periodical identified above and this right shall automatically terminate upon the date of issue of the particular issue of the Periodical, whether or not such Work is actually published. To the extent the Publication Media is a Web Site, the publication right is limited to publication at the specific Web Site identified above. Any right granted herein is a limited, non-transferable, non-exclusive right. No other rights in the Work are granted herein. The Publisher agrees to hold NACE harmless and indemnify NACE against any and all legal action and expenses arising out of the Publisher's use and editing of NACE material.

Notwithstanding the foregoing, Publisher may edit or otherwise modify the Work as reasonably necessary to accommodate the style and size requirements of the specific publication so long as the published Work that will appear in the Publication remains substantially similar to the original Work. Any such permitted edit or modification shall maintain the integrity of the overall original Work.

Publisher shall obtain a copy of the original Work directly from NACE International and shall not utilize copies of the Work from other sources, including the author(s). Publisher shall include on the published version of the Work the names of all authors listed on the original Work.

The Publisher shall include the following applicable Copyright notation with any publication of the Work:*

A. Conference Paper
    Reproduced with permission from NACE International, Houston, TX. All rights reserved. Paper NUMBER presented at CORROSION/YEAR, City, State. © NACE International YEAR.
B. Magazine/Journal Article
    Reproduced with permission from NACE International, Houston, TX. All rights reserved. Published in the MONTH, YEAR issue of JOURNAL. © NACE International YEAR.
C. Standards
    STANDARDS/TECHNICAL COMMITTEE REPORT NAME. © NACE International YEAR. All rights reserved by NACE. Reprinted with permission. NACE standards are revised periodically. Users are cautioned to obtain the latest edition; information in an outdated version of the standard may not be accurate.
    * Modifications to Notations: Other reference wording can be used, but must be approved by NACE in writing in advance.

As between NACE and Publisher, Publisher acknowledges that NACE owns all rights in the Works. Publisher shall not be entitled to any compensation for its efforts in promoting the Work.

THE WORK IS PROVIDED "AS IS." ALL EXPRESS OR IMPLIED COVENANTS, CONDITIONS, REPRESENTATIONS OR WARRANTIES, INCLUDING ANY IMPLIED WARRANTY OF MERCHANTABILITY OR FITNESS FOR A PARTICULAR

PermissiontoPublishNACECopy

PURPOSE OR CONDITIONS OF ACCURACY, COMPLETENESS OR QUALITY AND THOSE ARISING BY STATUTE OR OTHERWISE IN LAW, ARE HEREBY DISCLAIMED.

IN NO EVENT WILL NACE BE LIABLE FOR ANY DIRECT, INDIRECT, PUNITIVE, SPECIAL, INCIDENTAL OR CONSEQUENTIAL DAMAGES IN CONNECTION WITH OR RELATED TO THIS AGREEMENT (INCLUDING LOSS OF PROFITS, USE, DATA, OR OTHER ECONOMIC ADVANTAGE), HOWSOEVER ARISING.

This Agreement and the rights granted herein may be terminated immediately by NACE upon breach of this Agreement by Publisher. Unless earlier terminated, this Agreement and the rights granted herein will automatically terminate 6 months from the Date set forth above. If the Work has not been published within that time period, a new Agreement must be obtained.

Publisher may not, directly or indirectly, sell, assign, sublicense, lease, rent, distribute, or otherwise transfer this Agreement or any rights granted herein, without the prior written consent of NACE.

If any provision of this Agreement is found to be unenforceable, then this Agreement shall be deemed to be amended by modifying such provision to the extent necessary to make it legal and enforceable while preserving its intent. The remainder of this Agreement shall not be affected by such modification.

This Agreement does not create, and shall not be construed to create, any employer-employee, joint venture or partnership relationship between the parties. No officer, employee, agent, servant or independent contractor of either party shall at any time be deemed to be an employee, servant, agent or contractor of any other party for any purpose whatsoever.

This Agreement shall be governed by, and construed and enforced in accordance with, the laws of the State of Texas, without regard to the choice of law provisions of that State.

This Agreement shall only be effective if signed by authorized representatives of both parties. This Agreement constitutes the entire Agreement between the parties with respect to the subject matter of this Agreement. Any change, modification or waiver hereto must be in writing and signed by authorized representatives of both parties.

Other Terms & Conditions: _____

_____

Publisher hereby requests permission to publish the paper/article described above and agrees to comply with all Terms and Conditions listed above.

Request submitted by:

Andres Sanchez
Printed Name

Graduate Research Assistant
Title , M

S_____

5/8/2014
Date

Request agreed to by:

Andres Sanchez
Lead Author Printed Name

Graduate Research Assistant

Lead Author Signature

5/8/2014
Date

Request approved by NACE:

Daniele Freeman
Printed Name

Audience Development Manager
Title

Signature

7/7/14
Date

PermissiontoPublishNACECopy

161

F.2 Permissions to Publish Contents in Chapter 3

Reproduced with permission from NACE International, Houston, TX. All rights reserved. Paper 2704 presented at CORROSION/2013, Orlando, FL. © NACE International 2013

PURPOSE OR CONDITIONS OF ACCURACY, COMPLETENESS OR QUALITY AND THOSE ARISING BY STATUTE OR OTHERWISE IN LAW, ARE HEREBY DISCLAIMED.

IN NO EVENT WILL NACE BE LIABLE FOR ANY DIRECT, INDIRECT, PUNITIVE, SPECIAL, INCIDENTAL OR CONSEQUENTIAL DAMAGES IN CONNECTION WITH OR RELATED TO THIS AGREEMENT (INCLUDING LOSS OF PROFITS, USE, DATA, OR OTHER ECONOMIC ADVANTAGE), HOWSOEVER ARISING.

This Agreement and the rights granted herein may be terminated immediately by NACE upon breach of this Agreement by Publisher. Unless earlier terminated, this Agreement and the rights granted herein will automatically terminate 6 months from the Date set forth above. If the Work has not been published within that time period, a new Agreement must be obtained.

Publisher may not, directly or indirectly, sell, assign, sublicense, lease, rent, distribute, or otherwise transfer this Agreement or any rights granted herein, without the prior written consent of NACE.

If any provision of this Agreement is found to be unenforceable, then this Agreement shall be deemed to be amended by modifying such provision to the extent necessary to make it legal and enforceable while preserving its intent. The remainder of this Agreement shall not be affected by such modification.

This Agreement does not create, and shall not be construed to create, any employer-employee, joint venture or partnership relationship between the parties. No officer, employee, agent, servant or independent contractor of either party shall at any time be deemed to be an employee, servant, agent or contractor of any other party for any purpose whatsoever.

This Agreement shall be governed by, and construed and enforced in accordance with, the laws of the State of Texas, without regard to the choice of law provisions of that State.

This Agreement shall only be effective if signed by authorized representatives of both parties. This Agreement constitutes the entire Agreement between the parties with respect to the subject matter of this Agreement. Any change, modification or waiver hereto must be in writing and signed by authorized representatives of both parties.

Other Terms & Conditions: _____

_____

Publisher hereby requests permission to publish the paper/article described above and agrees to comply with all Terms and Conditions listed above.

Request submitted by:

Andres N. Sanchez
Printed Name

Graduate Research Assistant
Title

Signature

5/8/2014
Date

Request agreed to by:

Andres N. Sanchez
Lead Author Printed Name

Graduate Research Assistant
Lead Author Title

Lead Author Signature

5/8/2014
Date

Request approved by NACE:

Daniela Freeman
Printed Name

Science Development Manager
Title

Signature

7/7/14
Date

PermissiontoPublishNACECopy

NACE
INTERNATIONAL

**Permission to Publish
NACE International
Copyrighted Paper/Article**

NACE International
1440 South Creek Drive
Houston, TX 77084
Tel: 281-228-6219
Fax: 281-228-6319

Date: 5/8/2014

Name: Andrea Sánchez   Title: Graduate Research Assistant

Company ("Publisher"): University of South Florida

Address: 4202 E Fowler Ave, ENB 118, Tampa, FL 33620

Tel: (8_____)   Fax: _____

Email: asanchez1@mail.usf.edu

Publication Media: Check the applicable Box:

☐ Magazine/Journal ("Periodical"): _____   Issue: _____

☑ Web Site URL ("Web Site"): Corrosion journal.org/doi/abs/10.5006/1286

Circle the source: Materials Performance   CORROSION   Conference Paper   Standards

Paper/Article Title: Service Life Forecasting for Reinforced Concrete Incorporating Potential-Dependent Chloride Threshold ("Work") Conference Paper No./Year: 2014

Authors: A.A. Sagüés, A.N. Sánchez, K. Lau, S.C. Kranc

NACE International ("NACE") hereby grants to "Publisher" the right to publish the Work utilizing the Publication Media elected above. To the extent the Publication Media is a Periodical, the publication right is limited to publication in the specific Issue identified above of the Periodical identified above and this right shall automatically terminate upon the date of issue of the particular Issue of the Periodical, whether or not such Work is actually published. To the extent the Publication Media is a Web Site, the publication right is limited to publication at the specific Web Site identified above. Any right granted herein is a limited, non-transferable, non-exclusive right. No other rights in the Work are granted herein. The Publisher agrees to hold NACE harmless and indemnify NACE against any and all legal action and expenses arising out of the Publisher's use and editing of NACE material.

Notwithstanding the foregoing, Publisher may edit or otherwise modify the Work as reasonably necessary to accommodate the style and size requirements of the specific publication so long as the published Work that will appear in the Publication remains substantially similar to the original Work. Any such permitted edit or modification shall maintain the integrity of the overall original Work.

Publisher shall obtain a copy of the original Work directly from NACE International and shall not utilize copies of the Work from other sources, including the author(s). Publisher shall include on the published version of the Work the names of all authors listed on the original Work.

The Publisher shall include the following applicable Copyright notation with any publication of the Work:*

    A. Conference Paper
        Reproduced with permission from NACE International, Houston, TX. All rights reserved. Paper NUMBER presented at CORROSION/YEAR, City, State. © NACE International YEAR.
    B. Magazine/Journal Article
        Reproduced with permission from NACE International, Houston, TX. All rights reserved. Published in the MONTH, YEAR issue of JOURNAL. © NACE International YEAR.
    C. Standards
        STANDARDS/TECHNICAL COMMITTEE REPORT NAME. © NACE International YEAR. All rights reserved by NACE. Reprinted with permission. NACE standards are revised periodically. Users are cautioned to obtain the latest edition; information in an outdated version of the standard may not be accurate.
    * Modifications to Notations: Other reference wording can be used, but must be approved by NACE in writing in advance.

As between NACE and Publisher, Publisher acknowledges that NACE owns all rights in the Works. Publisher shall not be entitled to any compensation for its efforts in promoting the Work.

THE WORK IS PROVIDED "AS IS." ALL EXPRESS OR IMPLIED COVENANTS, CONDITIONS, REPRESENTATIONS OR WARRANTIES, INCLUDING ANY IMPLIED WARRANTY OF MERCHANTABILITY OR FITNESS FOR A PARTICULAR

PermissiontoPublishNACECopy.doc

PURPOSE OR CONDITIONS OF ACCURACY, COMPLETENESS OR QUALITY AND THOSE ARISING BY STATUTE OR OTHERWISE IN LAW, ARE HEREBY DISCLAIMED.

IN NO EVENT WILL NACE BE LIABLE FOR ANY DIRECT, INDIRECT, PUNITIVE, SPECIAL, INCIDENTAL OR CONSEQUENTIAL DAMAGES IN CONNECTION WITH OR RELATED TO THIS AGREEMENT (INCLUDING LOSS OF PROFITS, USE, DATA, OR OTHER ECONOMIC ADVANTAGE), HOWSOEVER ARISING.

This Agreement and the rights granted herein may be terminated immediately by NACE upon breach of this Agreement by Publisher. Unless earlier terminated, this Agreement and the rights granted herein will automatically terminate 6 months from the Date set forth above. If the Work has not been published within that time period, a new Agreement must be obtained.

Publisher may not, directly or indirectly, sell, assign, sublicense, lease, rent, distribute, or otherwise transfer this Agreement or any rights granted herein, without the prior written consent of NACE.

If any provision of this Agreement is found to be unenforceable, then this Agreement shall be deemed to be amended by modifying such provision to the extent necessary to make it legal and enforceable while preserving its intent. The remainder of this Agreement shall not be affected by such modification.

This Agreement does not create, and shall not be construed to create, any employer-employee, joint venture or partnership relationship between the parties. No officer, employee, agent, servant or independent contractor of either party shall at any time be deemed to be an employee, servant, agent or contractor of any other party for any purpose whatsoever.

This Agreement shall be governed by, and construed and enforced in accordance with, the laws of the State of Texas, without regard to the choice of law provisions of that State.

This Agreement shall only be effective if signed by authorized representatives of both parties. This Agreement constitutes the entire Agreement between the parties with respect to the subject matter of this Agreement. Any change, modification or waiver hereto must be in writing and signed by authorized representatives of both parties.

Other Terms & Conditions: _____

_____

Publisher hereby requests permission to publish the paper/article described above and agrees to comply with all Terms and Conditions listed above.

Request submitted by:

Andres N. Sanchez
Printed Name

Graduate Research Assistant
Title

5/8/2014
Date

Request agreed to by:

Alberto Sagüés
Lead Author Printed Name

Distinguished Professor
Lead Author Title

Lead Author Signature

5/23/2014
Date

Request approved by NACE:

Printed Name

Audience Development Manager
Title

Signature

7/7/14
Date

PermissiontoPublishNACECopy.doc

Permission to Publish
NACE International
Copyrighted Paper/Article

NACE International
1440 South Creek Drive
Houston, TX 77084
Tel: 281-228-6219
Fax: 281-228-6319

Date: 07/08/2014

Name: Andrea Sánchez   Title: Graduate Research Assistant

Company ("Publisher"): University of South Florida

Address: 4202 E Fowler Ave ENB 118, Tampa, FL 33620

Tel: _____   Fax: _____

Email: asanchez1@mail.usf.edu

Publication Media: Check the applicable Box:

☐ Magazine/Journal ("Periodical"): _____ Issue: _____

☐ Web Site URL ("Web Site"): _____

Circle the source: *Materials Performance*   CORROSION   (Conference Paper)   Standards

Paper/Article Title: Service Life Forecasting for Reinforced Concrete Incorporating Potential - Dependent Chloride Threshold _____ ("Work") Conference Paper No./Year: 09213 / 2009

Authors: A.A. Sagüés, S.C. Kranc and K. Lau

NACE International ("NACE") hereby grants to "Publisher" the right to publish the Work utilizing the Publication Media elected above. To the extent the Publication Media is a Periodical, the publication right is limited to publication in the specific Issue identified above of the Periodical identified above and this right shall automatically terminate upon the date of issue of the particular Issue of the Periodical, whether or not such Work is actually published. To the extent the Publication Media is a Web Site, the publication right is limited to publication at the specific Web Site identified above. Any right granted herein is a limited, non-transferable, non-exclusive right. No other rights in the Work are granted herein. The Publisher agrees to hold NACE harmless and indemnify NACE against any and all legal action and expenses arising out of the Publisher's use and editing of NACE material.

Notwithstanding the foregoing, Publisher may edit or otherwise modify the Work as reasonably necessary to accommodate the style and size requirements of the specific publication so long as the published Work that will appear in the Publication remains substantially similar to the original Work. Any such permitted edit or modification shall maintain the integrity of the overall original Work.

Publisher shall obtain a copy of the original Work directly from NACE International and shall not utilize copies of the Work from other sources, including the author(s). Publisher shall include on the published version of the Work the names of all authors listed on the original Work.

The Publisher shall include the following applicable Copyright notation with any publication of the Work:*

    A. Conference Paper
       Reproduced with permission from NACE International, Houston, TX. All rights reserved. Paper NUMBER presented at CORROSION/YEAR, City, State. © NACE International YEAR.
    B. Magazine/Journal Article
       Reproduced with permission from NACE International, Houston, TX. All rights reserved. Published in the MONTH, YEAR issue of JOURNAL. © NACE International YEAR.
    C. Standards
       STANDARDS/TECHNICAL COMMITTEE REPORT NAME. © NACE International YEAR. All rights reserved by NACE. Reprinted with permission. NACE standards are revised periodically. Users are cautioned to obtain the latest edition; information in an outdated version of the standard may not be accurate.
    * Modifications to Notations: Other reference wording can be used, but must be approved by NACE in writing *in advance.*

As between NACE and Publisher, Publisher acknowledges that NACE owns all rights in the Works. Publisher shall not be entitled to any compensation for its efforts in promoting the Work.

THE WORK IS PROVIDED "AS IS." ALL EXPRESS OR IMPLIED COVENANTS, CONDITIONS, REPRESENTATIONS OR WARRANTIES, INCLUDING ANY IMPLIED WARRANTY OF MERCHANTABILITY OR FITNESS FOR A PARTICULAR

PermissiontoPublishNACECopy

166

www.manaraa.com

PURPOSE OR CONDITIONS OF ACCURACY, COMPLETENESS OR QUALITY AND THOSE ARISING BY STATUTE OR OTHERWISE IN LAW, ARE HEREBY DISCLAIMED.

IN NO EVENT WILL NACE BE LIABLE FOR ANY DIRECT, INDIRECT, PUNITIVE, SPECIAL, INCIDENTAL OR CONSEQUENTIAL DAMAGES IN CONNECTION WITH OR RELATED TO THIS AGREEMENT (INCLUDING LOSS OF PROFITS, USE, DATA, OR OTHER ECONOMIC ADVANTAGE), HOWSOEVER ARISING.

This Agreement and the rights granted herein may be terminated immediately by NACE upon breach of this Agreement by Publisher. Unless earlier terminated, this Agreement and the rights granted herein will automatically terminate 6 months from the Date set forth above. If the Work has not been published within that time period, a new Agreement must be obtained.

Publisher may not, directly or indirectly, sell, assign, sublicense, lease, rent, distribute, or otherwise transfer this Agreement or any rights granted herein, without the prior written consent of NACE.

If any provision of this Agreement is found to be unenforceable, then this Agreement shall be deemed to be amended by modifying such provision to the extent necessary to make it legal and enforceable while preserving its intent. The remainder of this Agreement shall not be affected by such modification.

This Agreement does not create, and shall not be construed to create, any employer-employee, joint venture or partnership relationship between the parties. No officer, employee, agent, servant or independent contractor of either party shall at any time be deemed to be an employee, servant, agent or contractor of any other party for any purpose whatsoever.

This Agreement shall be governed by, and construed and enforced in accordance with, the laws of the State of Texas, without regard to the choice of law provisions of that State.

This Agreement shall only be effective if signed by authorized representatives of both parties. This Agreement constitutes the entire Agreement between the parties with respect to the subject matter of this Agreement. Any change, modification or waiver hereto must be in writing and signed by authorized representatives of both parties.

Other Terms & Conditions: _____

_____

Publisher hereby requests permission to publish the paper/article described above and agrees to comply with all Terms and Conditions listed above.

Request submitted by:

Andrea N. Sánchez
Printed Name

Graduate Research Assistant
Title

[redacted]

_07/08/2014_
Date

Request agreed to by:

Alberto Sagüés
Lead Author Printed Name

Distinguished Professor
Lead Author Title

[redacted]

_07/08/2014_
Date

Request approved by NACE:

_____
Printed Name

_____
Title

_____
Signature

_____
Date

PermissiontoPublishNACECopy

167

AMS'14

1st International Conference on Ageing of Materials & Structures
Delft 26 – 28 May 2014, The Netherlands

AMS'14 PUBLISHING RIGHTS FORM

Prior to publication of the proceedings it is required that Authors provide their formal written consent to publish their paper. The signed form ensures that the AMS'14 organization has the Authors' authorization to publish the manuscript and contributions.

Conference: 1st International conference on Ageing of Materials and Structures (AMS'14)
Place/Date: Delft. The Netherlands, 26-28 May 2014
Proceedings title (CD): Proceedings of AMS'14
Extended abstracts book title: Ageing of Materials and Structures – AMS'14 – Delft. The Netherlands
Publisher: Selected by AMS'14

Paper No: 219814

Title of the manuscript: Probabilistic corrosion forecasting of steel in concrete with potential-dependent
      chloride threshold
Author: Andrea N. Sánchez (asanchez1@mail.usf.edu), Alberto A. Sagüés (sagues@usf.edu)

It is herein agreed that:
-     The publishing rights of the manuscript identified above is transferred from the Author to AMS'14 organization. This transfer covers the rights to reproduce and distribute the manuscript (full paper and extended abstract), including reprints, photographic reproductions, electronic form (online and offline), or any other reproduction of similar nature, including publication in the proceedings and storage in the TU Delft Repository.
-     The Author certifies that his/her contribution is original in this (as submitted) form, except for excerpts from copyrighted works which might be included with the permission of the copyright holder and respective Authors. The Author certifies that this manuscript contains no groundless statements and does not breach any copyright, patent, trademark, right or property right of others. The Author signs for and accepts responsibility for releasing this material on behalf of any and all co-Authors.
-     The Author retains the rights to publish the contribution in his/her own web site, in his/her employer's web site, or any scientific Journals, as long as it is clearly stated that the contribution was presented at AMS'14 and add a link to the AMS'14 web-site (www.ams.tudelft.nl).

In return for these rights:
The publisher agrees to have the identified manuscript published in the digital conference proceedings and a two-page extended abstract of the manuscript in a printed book format on its own cost and expense.

For jointly Authored manuscripts, all authors or the corresponding author on their behalf should sign this agreement. The undersigned hereby gives permission to AMS'14 to have the above contribution published. If the representative author is not able to maintain a digital signature, please print, sign, and scan the document after filling out all other fields. The signed form should be uploaded together with the full paper on the conference webpage (www.ams.tudelft.nl).

Date (02/25/2014)   Author's signature (on behave of all co-authors):

_____

The organising team of AMS'14, Delft, NL

Publishing rights   -1-   AMS'14

ABOUT THE AUTHOR

Andrea Nathalie Sánchez was a born and raised in Venezuela. She received a Bachelor of Science in Chemical Engineering from University Rafael Urdaneta in 2009, ranking as the number one of her class. Shortly after, in January of 2010, Andrea started the Ph.D. in Civil Engineering program at the University of South Florida working under Dr. Alberto Sagüés.

During her time in graduate school, Andrea was the recipient of a scholarship funded by the Florida Department of Transportation (FDOT). Her research project consisted on developing a next-generation modeling approach for projecting the extent of reinforced concrete corrosion-related damage, customized for new and existing FDOT bridges and suitable for adapting to broader use within the FDOT. That work involved experimental and computational work that enabled Andrea to publish five peer-reviewed conference proceedings in prestigious international conferences organized by NACE International, RILEM and the Technical University of Delft, and authored peer-reviewed papers for the journal Corrosion (one in press, the other under review). Additionally, Andrea participated in six poster competitions, where in one of them she was recognized by the "Honorable Mention Award" by the University of South Florida for her work in the field of engineering. Andrea's aspirations are to join a research and innovation company that develops the next generation technology on corrosion assessment, monitoring and mitigation in oil and gas pipelines.